Identification and characterization of putative cancer stem cells from adenocarcinoma of the lung

submitted by

Verena Tiran, BSc. MSc.

for the Academic Degree of

Doctor of Medical Science

(Dr. scient. med)

at the

Medical University of Graz

Doctoral School of Molecular Medicine and Inflammation

under the supervision of

Assoz. Prof. Priv.-Doz. Dr.med.univ.et scient.med. Marija Balic

Assoz. Prof. Priv.-Doz. Mag. Dr.rer.nat Nadia Dandachi

carried out at the

Department of Internal Medicine

Division of Oncology

2017

Statutory Declaration and Disclosures

I hereby declare that this thesis is my own original work and that I have fully acknowledged by name all of those individuals and organizations that have contributed to the research for this thesis. Due acknowledgement has been made in the text to all other material used. Throughout this thesis and in all related publications I followed the “Standards of Good Scientific Practice and Ombuds Committee at the Medical University of Graz“.

Date and Place
Signature

Part of this thesis has been published in

Tiran V, Stanzer S, Heitzer E, Meilinger M, Rossmann C, Lax S, Tsybrovskyy O, Dandachi N, Balic M; Genetic profiling of putative breast cancer stem cells from malignant pleural effusions; PLoS ONE (2017); 12 (4)

Tiran V, Lindenmann J, Brcic L, Heitzer E, Stanzer S, Ghaffari Tabrizi-Wizsy N, Stacher E, Stoeger H, Popper H, Balic M, Dandachi N; Primary patient-derived lung adenocarcinoma cell culture challenges the association of cancer stem cells with epithelial-to-mesenchymal transition; Scientific Reports 7 (2017); Article number: 10040

Contribution

Project planning, funding, supervision, stimulating discussions and supportive dialogs

Prof. Marija Balic (Division of Oncology)

Prof. Nadia Dandachi (Division of Oncology)

Patient recruitment:

Prof. Jörg Lindenmann (Division of Thoracic and Hyperbaric Surgery)

Prof. Nicole Fink-Neuböck (Division of Thoracic and Hyperbaric Surgery)

Assistance with flow cytometry and cell sorting

Dr. Stefanie Stanzer (Division of Oncology)

Primary tumor diagnostics

Dr. Luka Brcic (Institute of Pathology)

Help with primary cell isolation and cell culture

Nina Treitler, BSc.

Theresa Benezeder, BSc. MSc.

Providing materials and support for CAM Assays

Dr. Nassim Ghaffari Tabrizi-Wizsy (Institute of Pathophysiology and Immunology)

Implementation of CNV sequencing

Prof. Ellen Heitzer (Institute of Human Genetics)

Data analysis of mtDNA analysis

Peter Ulz (Institute of Human Genetics)

Documentation of patient information

Prof. Nadia Dandachi

Aaron Nadig c.m.

Sharing educational and practical knowledge

Prof. Helmuth Popper (Institute of Pathology)

All contributing authors have agreed to the use of their knowledge and data for this thesis.

Acknowledgements

This thesis was financially supported from supervisor Marija Balic through the Österreichischen Nationalbank (14246). Doctoral student Verena Tiran received funding from the Forschungsförderungspreis of the OeGHO and the Medical University of Graz through the Doctoral School Molecular Medicine and Inflammation. I would like to thank all.

Herewith, I would like to express my cordial gratitude for the opportunity of working at the Division of Oncology under the supervision of Marija Balic. It was a pleasure to work as her PhD student, where I was inspired by her ideas and visions. With her “patients first” mentality, she led our research to the next level.

I would also like to express my very great appreciation to Nadia Dandachi, who has mentored me throughout my thesis. With her accuracy, she updated all the patient information and data and thereby I was forced to keep myself organized. I really appreciated our scientific and non-scientific discussions, during which she provided me with new perspectives on the subject through approaches and opinions completely different to mine. She also introduced me to administrative work to promote and strengthen my independence and individual responsibility.

I am particularly grateful for the assistance by Stefanie Stanzer, our flow cytometry specialist. She helped me even during her maternity leave and put all her effort and ideas into our joint work, which resulted in excellent data acquisition.

My gratitude also goes to Ellen Heitzer, Nassim Ghaffari Tabrizi-Wizsy and Luka Brcic, who also added pieces of the puzzle, whether by providing special techniques or technical support in order to make this thesis a comprehensive piece.

Past members of the Balic/Dandachi group also contributed to this thesis. In particular, I would like to thank Theresa Benezeder, Nina Treitler, Theresa Hirschböck and Magdalena Rausch for assisting me with the experiments. Some of them had only spent a few weeks in our lab, but their motivation and skills were outstanding.

I am highly indebted to my parents, who have supported and encouraged me throughout my whole life. Their values to me grow with age.

Last but not least I would like to express my gratitude to my boyfriend Thomas, who had to deal with me, when the lab lights were off. I expected that it was not always as sweet as a piece of a cake, especially during the final phase.

Table of contents

Abbreviations

AC	adenocarcinoma	FFPE	Formalin fixed paraffin embedded
ALDH1	aldehyde dehydrogenase 1	gDNA	genomic DNA
ALK	anaplastic lymphoma kinase	GAPDH	glyceraldehyde-3-phosphate dehydrogenase
B2M	beta-2 microglobulin	IHC	immunohistochemistry
bFGF	basic fibroblast growth factor	IF	immunofluorescence
BSA	bovine serum albumin	KRAS	Kirsten rat sarcoma viral oncogene homolog
CAM	chorio allantoic membrane	LCA	Lens culinaris agglutinin
CD	cluster of differentiation	mRNA	messenger RNA
cDNA	complementary DNA	NAC	non-amplification control
CK	cytokeratin	N-Cad	N-Cadherin
CSC	cancer stem cell(s)	NSCLC	non-small cell lung cancer
CTC	circulating tumor cell(s)	NTC	Non-template control
DMEM/F12	Dulbecco´s modified eagle media/Ham´s F12	PBS	phosphate buffer saline
DMSO	Dimethylsulfoxid	PCR	polymerase chain reaction
DNA	deoxyribonucleic acid	PDMS	polydimethylsulfoxide
ECad	E-Cadherin	qRT-PCR	quantitative real time PCR
EGF	epidermal growth factor receptor (human)	RNA	ribonucleic acid
EGFR	epithelial growth factor receptor	RT	room temperature
EMT	epithelial to mesenchymal transition	SCC	squamous cell carcinoma
EpCAM	epithelial cell adhesion molecule	SCLC	small cell lung cancer
FACS	fluorescence-activated cell sorting	TBP	TATA-Box binding protein
FBS	fetal bovine serum	ULA	ultra-low attachment

Abstract:

Every year, more than 1,800,000 people worldwide are diagnosed with lung cancer, and approximately 1,600,000 people die each year of this disease. Despite advances in diagnosis and treatment, lung cancer remains a fatal disease with a dismal 5-year overall survival rate of around 10%. During the past decade, technological advances have facilitated in-depth analyses of lung cancer genomes, and this knowledge has further defined the remarkable molecular and cellular heterogeneity of this disease. Specifically, intratumoral heterogeneity has been associated with therapeutic failure and drug resistance, which pose considerable clinical obstacles in finding effective treatment modalities. In this context, the cancer stem cell model has attracted a significant amount of attention in recent years as an appealing explanation for the tumor heterogeneity, drug resistance, dormancy and metastasis. The aim of the present study was to isolate, culture and characterize cancer stem cells (CSCs) in order to add new aspects to CSC biology and find new biomarkers.

At the Medical University of Graz 95 patients with an adenocarcinoma of the lung were recruited. Peripheral preoperative blood and a piece of the primary tumor after resection was collected. The primary tumor was processed to isolate and enrich CSCs in cultures. Tumor cells were characterized with immunofluorescence and qRT-PCR and, subsequently, functional assays were performed. CTCs were enriched with a size-based method by filtering blood through a novel parylene microfilter system.

We could establish 3 cell lines from patients with lung adenocarcinomas and 1 cell line of a squamous cell carcinoma. In the spheroid culture of each cell line we could enrich CSCs of each tumor, which could be observed as an increase of CSC markers ALDH1 and CD133, respectively. In one established cell culture, further biological evaluation was performed in a mouse model. In addition, common aberrations of lung adenocarcinomas and squamous cell carcinomas were detected with copy number variation analysis. Grown on a chorioallantoic membrane, the LT8s, LT22s and LT67s cells demonstrated invasive behavior and recapitulated the primary tumor.

Our data demonstrate low efficiency of primary cell culture. However, the established primary cell cultures provide an important basis for the study of disease biology and further molecular characterization. Although these cell cultures were heterogeneous, we were able to challenge the established hypothesis and add existing knowledge on CSC biology, metastasis and resistance.

Zusammenfassung

Weltweit erkranken 1,8 Millionen Menschen jährlich an Lungenkrebs und ungefähr 1,6 Millionen sterben daran. Auf Grund von mangelnder Symptome ist bei einem Großteil der Patienten nur eine späte Diagnose möglich. Mit einer geringen 5-Jahres Überlebensrate von circa 10%, ist Lungenkrebs einer der tödlichsten Krebsarten. Durch eine Verbesserung der Sequenziertechnologie war es möglich Veränderungen des Genoms der Tumorzellen im Detail zu analysieren und es konnte ein hoher Grad an Heterogenität in den unterschiedlichen Tumorzellen festgestellt werden. Die intra-tumor Heterogenität ist verantwortlich für die Resistenz von Therapien, deshalb gilt es neue Möglichkeiten für therapeutische Ansätze zu schaffen. Als Ansatz um Heterogenität und Folgen daraus, wie Therapieresistenz zu beschreiben, wurde das Krebsstammzellmodell formuliert. Dieser spezielle Zelltyp scheint Basis allen Übels zu sein, deshalb wollten wir in dieser Studie die Krebsstammzelle (CSC) charakterisieren und eventuelle Biomarker finden.

Um dieser Vorstellung ein wenig näher zu kommen wurden an der Medizinischen Universität Graz 95 Patienten mit einem Adenokarzinom der Lunge rekrutiert. Von diesen Patienten wurde peripheres Blut vor der Operation und ein Stück vom Primärtumor nach chirurgischem Eingriff gesammelt. Aus dem Primärtumor wurden Tumorzellen isoliert und unter speziellen Kulturbedingungen wurden CSCs angereichert. Die CSCs wurden weiters mittels FACS, IF und qRT-PCR charakterisiert und ihre Funktionalität mit unterschiedlichen Experimenten getestet. Das Blut wurde mittels Größenausschlussbasierender Methode filtriert um zirkulierende Tumorzellen zu isolieren und zu charakterisieren.

Aus 3 Adenokarzinomen und 1 Plattenepithelkarzinom konnten Langzeitkulturen etabliert werden. In der Spheroidkultur konnten die Zellen mit CSC Charakter angereicht werden, dass sich auch in der zunehmenden Expression von ALDH1 und CD133 wiederspiegelt. Eine der Langzeitkulturen wurde näher in einem Mausmodell untersucht. Zusätzlich wurden auch genetische Profile mittels Copy-number-variations erstellt, welche bereits bekannte Aberrationen von Lungen Adenokarzinomen bzw. Plattenepithelkarzinomen detektierten. Migration und Invasion ins Gewebe konnte auf der chorio-allantoic Membran bei LT8s, LT22s und LT67s deutlich beobachtet werden.

Unsere Ergebnisse zeigten, dass es eine große Schwierigkeit darstellte primäre Zelllinien zu kultivieren. Trotzdem stellen primären Zelllinien einen wichtigen Grundpfeiler dar, um die Tumorbiologie zu studieren und neue Therapieformen auszutesten. Alle 4 Zelllinien waren sehr heterogen aufgebaut, aber wichtige Hypothesen wurden uniform bestätigt und somit können wir neue Aspekte der Tumorbiologie beleuchten.

1. Introduction

1.1 Lung Cancer

Nowadays, lung cancer is one of the deadliest cancer types in the Western world. It is the most frequently diagnosed cancer in the male population and the third most common in women. In 2012, more than 1.8 million new incidences world-wide were attributed to lung cancer. (1) Also, in Austria, one in 2,000 Austrians is diagnosed with lung cancer every year. According to table 1 from Statistik Austria, the 10-year survival rate is around 10%. The main reason for this low survival rate is the late stage of diagnosis, since one third of the patients already have peripheral metastasis at initial diagnosis. (2)

Table 1. Relative survival rate of tracheal bronchial and lung cancer incidences in Austria. Data provided by Statistik Austria (3)

		Survival after diagnosis (years)			
Period of diagnosis	**Risk population (N)**	**1 (%)**	**3 (%)**	**5 (%)**	**10 (%)**
			Total		
1985-1989	13.191	28,4	13,0	10,5	8,6
1990-1994	13.737	33,5	16,2	13,3	10,3
1995-1999	15.782	39,0	18,3	14,4	11,2
2000-2004	17.588	41,8	19,9	15,7	11,0
2005-2009	19.225	45,9	23,2	18,0	-
2010-2012	12.035	48,1	24,9	-	-
			Men		
1985-1989	10.225	28,5	12,6	10,2	8,2
1990-1994	10.328	33,4	15,6	12,8	9,9
1995-1999	11.349	38,1	17,2	13,4	10,1
2000-2004	12.135	40,3	18,2	14,0	9,7
2005-2009	12.648	43,7	20,9	15,9	-
2010-2012	7.547	45,5	21,6	-	-
			Women		
1985-1989	2.966	27,9	14,5	11,8	9,7
1990-1994	3.409	33,8	18,0	14,8	11,4
1995-1999	4.433	41,1	21,0	16,9	13,7
2000-2004	5.453	45,2	23,7	19,5	13,7
2005-2009	6.577	50,1	27,6	21,8	-
2010-2012	4.488	52,3	30,4	-	-

While new lung cancer incidences have declined among the male population in Austria, an increase in female population has been observed since 1987. (3) This trend might reflect past smoking patterns and the change of social norms in the Western world. The rise in lung cancer rates is predominantly (>80%) caused by tobacco abuse; the correlation between smoking habits and lung cancer incidences has been confirmed in many ways in the literature. Smoking tobacco generates more than 8,000 compounds which are

responsible for aberrations in the nuclear DNA and mitochondrial DNA, hemoglobin adducts, alterations in micro RNA, transcriptome and proteome and abnormal cell growth. (4) Besides smoking, other etiological factors such as passive smoking, contact with asbestos, as well as indoor and outdoor air pollution may induce lung cancer. The risk of developing lung cancer can be minimized simply by avoiding exposure to the above-mentioned substances. When the link between smoking and lung cancer was discovered (1964) and tobacco control initiated, smoking-related lung cancer mortalities decreased. This fact clearly shows that lung cancer is a type of cancer that is preventable. (5)

1.1.1. Histopathological classification of lung cancer

Lung cancers can be divided into two major histological groups: small cell lung cancer (SCLC) and non-small cell lung cancer (NSCLC). SCLC accounts for 10-15% of lung cancer incidences and is a very aggressive type. With its rapid proliferation and early spread to distant organs, this neuroendocrine tumor can be fatal within a few weeks without treatment. (6) The second and larger group is NSCLC which accounts for about 85% of all lung cancers and comprises the subtypes adenocarcinoma (AC), squamous cell carcinoma (SCC) and large cell carcinoma (LCC). AC is the most common of the three subtypes and is in the focus of this study. AC originates in glandular or secretary structures in the periphery of the lung, whereas SCC originates in cells of the lining of the lungs. LCC is a heterogeneous group of tumors diagnosed, if the tumor does not belong to any other category. (7) Genetic dysfunctions that result in deregulation of signaling pathways are involved in lung cancer development. On a molecular level, even this subtype can be further categorized. (8) The risk for current smokers of getting SCLC or SCC is very high, whereas AC is the most prevalent among non-smokers or former smokers. (9)

1.1.2. Detection and Treatment

Most early stage lung cancers are detected as incidental findings during spiral-computed tomography (CT) or x-ray scans. The occurrence of symptoms indicates late stage lung cancers, when tumor invasion into the lung tissue and spread into surrounding tissue already results in shortness of breath, cough, chest pain, changes in the voice, hoarseness or coughing up of bloody sputum. After the first diagnosis, a specific classification of tumor stage will be obtained by sampling the tumor biopsy via bronchoscopy. Treatment depends on the subtype of lung cancer and its current stage. The criteria for staging are primary tumor size (T), lymph node infiltration (N) and peripheral metastasis (M), which are summarized in the TNM classification according to the International Association for the Study of Lung Cancer (IASLC). (10) Traditional methods of treating lung cancer comprise surgery, chemotherapy, and radiotherapy in the early stages, and chemotherapy, targeted therapies and immunotherapy at the advanced stages of disease. In the early stages, these

being stages I, II or IIIA (IIIB), surgery is attempted with curative intent and if a tumor sample is >3-4 cm, and surgery is usually followed by adjuvant chemotherapy to lower the risk of recurrence. (11) Nevertheless, in two thirds of NSCLC cases, patients are first diagnosed in advanced stage III or IV due to the late onset of symptoms and limited possibilities for early detection. In advanced disease (stage IIIB, regionally advanced with lymph node metastases, and stage IV, with distant metastases), platinum-based chemotherapy is still the backbone of the treatment and provides superior response rates when compared with the best supportive care (20-40% objective response rate) and survival benefit. Additionally, local radiotherapy is an effective method of relieving symptoms such as cough, pain and dyspnea. (12) Recently, progress has been achieved with regards to systemic therapy and includes targeted therapies and immunotherapies with immune check inhibitors. (13, 14)

Unsatisfactory survival rates resulting from therapy resistance change the trend towards targeted therapy and personalized medicine. Besides routine diagnosis, in the case of AC the work up includes the analysis of the mutational status of genes like the epithelial growth factor receptor (EGFR), echinoderm microtubule-associated protein-like 4 and anaplastic lymphoma kinase (EML4-ALK), ROS proto-oncogene 1 (ROS1) and also v-Ki-ras2 Kirsten rat sarcoma viral oncogene homolog (KRAS). (15) The EGFR pathway is a recognized therapeutic target. While the EGFR is responsible for proliferation, invasion and metastasis in NSCLC, the EGFR tyrosine kinase hyperactivates the downstream signal for the pro-survival pathway. (16) In lung tumors, a frequent mutation or amplification of the EGFR is present in 20-50% of AC. (17, 18) Drugs such as Erlotinib, Afatinib and Gefitinib, are able to block the EGFR receptor and to shrink the tumor. (19) The definition of the mutation status influences the choice of treatment in metastatic patients. Besides EGFR, the diagnosis may also include KRAS, (20) rearrangements such as the one described for the ALK gene and further mutations including ROS1. (21) Unfortunately, response to the targeted drug only lasts a few months before the disease progresses. By accumulating additional mutations in other oncogenes or tumor suppressor genes, resistance to the therapy occurs.

Considering the poor prognosis of lung cancer and the fact that a relatively limited number of treatment options exists for real-time disease monitoring, leads to the necessity of new therapeutic targets for defining further biomarkers.

1.2. Heterogeneity in tumors

1.2.1 Intertumoral heterogeneity

The tumor's individual features depend on its localization and on the cells involved in tumor formation, which is why lung tumors cannot be generalized. On a cellular level, pathologists

classify the tumor biopsy into different subtypes. Not only do these subtypes differ according to their cellular landscape, but also in their prognosis and treatment regimes. The classification into subtypes is an approach to categorizing and organizing intertumoral heterogeneity which focuses on phenotypic and genotypic differences of cancer from various sites in the body to different locations of the tumor within an organ. (22) The frequency of mutations in tumor suppressor genes or oncogenes varies between different types of tumors. Besides EGFR mutation, EML4-ALK translocation and ROS1 mutation are typically found in lung cancers, particularly in AC. EML4-ALK is a fusion protein that is the result of an abnormal fusion of two gene regions, which promotes tumor malignancy. The kinase inhibitor Crizotinib specifically targets EML4-ALK activity and shrinks tumor size. (23) However, this effect does not last long; the ALK inhibitor sensitivity decreases which can be observed by the progress of the cancer disease. The underlying mechanism behind this decreased sensitivity is acquired therapy resistance due to genomic heterogeneity among tumor cells. (24)

1.2.2. Intratumoral heterogeneity

Unfortunately, none of the available systemic therapies are able to eliminate all cancer cells and cure the patient. As considerable efforts have been made to characterize lung cancers by whole genome sequencing of primary tumors or single cell sequencing, evidence has been gathered for genomic alterations of individual cells in the tumor and awareness with respect to intratumor heterogeneity was raised. It describes the genotypic and phenotypic differences found between cells of different subclones within a tumor. (25) Such mutations and aberrations can be caused by cigarette smoke or other etiological factors. Not all mutations are relevant for tumor formation. However, so-called driver mutations are important for abnormal proliferation and for tumor growth. Interestingly, driver mutations depend on the type of tissue and more than one mutation is needed for the initiation of tumor formation. (26) Different subclonal cell populations develop through intercellular genetic variation with sequential selective pressure. Some clones have a phenotypic advantage that helps them prevail over others in the special milieu. (27) As tumor size increases, the variety of milieus does so as well, because factors such as nutrient supply, oxygen, space and presence of immune cells differ among the micro-environmental niches. (28) Every niche is occupied by subclones and they evolve independently from each other, carrying different somatic mutations. The evolution of intratumor heterogeneity is rather controversial. In 1976, Nowell was the first to postulate the clonal evolution model, based on the Darwinian principals that all mutated cells can divide and accumulate further mutations over time. (29) Depending on the environment, some subclones are more dominant than others. However, the cancer stem cell (CSC) theory suggests that a specific subset of cells is able to differentiate in every cell that is needed in order for the disease to

progress, and these CSCs are also capable of self-renewing to secure their continued existence. In the next chapter, more details about the CSC theory will be provided. Both theories, these being the clonal evolution and the cancer stem cell theory, seem to not be exclusive but more a mixture of both depending on the type of cancer. (30) Furthermore, to highlight its importance, intratumor heterogeneity generates different genetic and epigenetic clones that are biologically and phenotypically distinct. Each of these clones contributes to the malignant behavior of the tumor with their own specific functions such as migration and invasion.

1.3. Cancer stem cells (CSCs)

Stem cells are characterized by their pluripotency and self-renewing capacity, both of which are important functions for the supplementation of additional cells for cellular structures and maintenance of their functions. The following characteristics were also found in a subset of cancer cells. (31) Researchers initially found evidence for cells with stem-like behavior in leukemia, and these cells were capable of reinitializing and propagating the disease. Based on these findings, this phenomenon was also found in solid tumors such as tumors of the breast, colon, lung and so on. (32, 33) Due to the similar characteristics, these cells were also called cancer stem cells (CSCs). The term CSCs is heavily debated, due to its misinterpretation and generalization. First of all, the cell responsible for tumor initiation is not automatically a CSC. The tumor origins from a normal cell that acquires mutations which promotes oncogenes involved in uncontrolled proliferation; this is reflected in the term cancer-initiating cell. (34) The link between a cancer-initiating cell and cancer stem cell is thought to be at very early tumor onset involving the β-catenin pathway, but this has not been fully described yet. (35) The CSC is the important cell for tumor propagation, which is attributed to their self-renewal capacity. Due to the essential property of self-renewal, the CSC generates one stem cell and one differentiated cell via asymmetric cell division or 2 daughter cells via symmetric division. Both mechanisms ensure that the CSC population remains preserved and that cell diversity is guaranteed. (36) Self-renewal can be tested as sphere formation assay, whereby single-cell suspensions at low density are typically placed in non-differentiating serum-free media in non-adherent culture flasks. Further cell divisions of CSCs, both symmetric and asymmetric finally result in heterogeneity of the tumor. Therefore, the tumor is hierarchically organized with the CSC at the top. A small population of cells is characterized as pluripotent and able to generate differentiated progeny. (37) If we link the hierarchical CSC model with the clonal evolution model, there is evidence that the immunophenotype of CSCs varies within the tumor, which makes it very difficult to pin down only one universal biomarker. (36, 38) Furthermore, the exclusiveness of CSCs has no impact on their frequency. Studies with high numbers of CSCs have been intensively

discussed, because CSCs were assumed to be rare. (39) Depending on the microenvironment and local conditions, in some niches of the tumor, you may find higher CSC distributions. No matter what the quantity of CSCs is, the important feature is the quiescent state, which explains the chemoresistance of these cells. (40) Rycaj et al. introduce two experimental setups for the detection of the cell-of-origin on the one hand and the cancer propagating cell the other hand, to clarify this mistakenly interchangeably used term. (41)

1.3.1. Biomarkers in CSCs

Intensive research in the field of CSCs has already revealed surface markers which can be used to isolate CSCs from the tumor bulk. Some markers are clearly linked to CSCs because they are involved in mechanisms that genuinely benefit CSCs. (42) An example is aldehyde dehydrogenase 1 (ALDH1), a cytoplasmic protein that is known to be involved in the process of oxidation of aldehydes to the according acids. (43) Cytotoxic aldehydes produced by the cancer cell under the influence of chemotherapeutics are eliminated by an ALDH1 mediated process. While ALDH1 is known as a general CSC marker, CD133 is more specific for lung, brain and colorectal cancers. CD133 has been found in slow-growing cells that are able to generate the original tumor in mouse xenografts. (32) Although the biological function of this five-transmembrane glycoprotein is unknown, the aggressiveness of cells is correlated with high $CD133^+$ expression in various studies. (44, 45)

Another biomarker that has already been characterized well in breast CSCs has recently been shown to also have influence in lung CSCs. The hyaluronic acid receptor CD44 is involved in the regulation of proliferation, motility and migration, which are crucial properties of CSCs. (46) Universal expression of CD44 in different types of cells requires a combination with other CSC markers to ensure enrichment of a proper CSC population. Feasible biomarkers can be tested in mice for their quality. In that case, positive and negative subpopulations defined by certain markers are injected into immunodeficient mice at low density and obtained xenografts are investigated. In these models, only cells with ideal biomarkers should be able to reinitiate the tumor. (36)

1.3.2. Therapeutic approaches for CSCs

CSCs, with their distinct characteristics, have been associated with tumor initiation, maintenance, drug resistance and formation of metastasis. Accordingly, CSCs seem to be the ideal target for anticancer drugs, but rare occurrences and sophisticated survival mechanisms make them a rather difficult target.

Some signaling pathways crucial for the maintenance of stemness features have already been characterized. Furthermore, inhibitors or antagonists which can be used to target the

NF-κB, Wnt or Hedghog pathways are already available and there is evidence of reduced aggressive behavior. (47) To suppress chemoresistance, strategies to target ATP-driven efflux pumps are already known.

Another potential target are cell membrane proteins, also known as biomarkers, such as CD133 or CD44, for which antibodies are already available. While these strategies seem to be promising, no break-through in fighting cancer by CSC targeted therapies could be accomplished yet. Minor selectivity is one of the largest drawbacks of these approaches. Furthermore, the influence of the tumor stroma and immune cells has yet to be understood. More insight into CSC biology such as CSC evolution, CSC communication with the microenvironment, or CSC plasticity can give rise to more strategies in order to successfully target CSCs.

1.4. EMT

An AC arises from cells of the epithelial compartment. For the formation of metastasis, elastic and deformable cells need to squeeze through membranes and migrate through the mesenchyme. (48) Subsequently, they infiltrate a blood vessel and use the flow to travel to distant organs and establish a new malignant site. According to the characteristics of an epithelial cell, this process would be a “mission impossible” due to tight cell-cell contact to neighbouring cells through adhesion proteins and tight junction. Furthermore, the apical basal polarity of the cytoskeleton would inhibit the motility of the cells. (49) In contrast, mesenchymal cells are able to move within the extra cellular matrix due to their flexible filamentous actin and the front-back polarity. Scientists have described one way to eliminate the limitations for the formation of metastasis in the form of epithelial to mesenchymal transition. (50)

This process is already described during early embryonic development, whereby the epithelium has to internalize to give rise to mesodermal tissue. (51) The development of all organs relies on EMT during embryonic development. (52) In adults, EMT also plays a key role in wound healing. (53) During cancer progression, the heterogenic structure of the tumor contains cells that accumulate genetic mutations and alterations. According to Kalluri et al., there must be a subset of cells which have undergone genetic and epigenetic changes within the tumor mass and are capable to enter the EMT regulatory circuitry. (54) During this multistep process, the cell detaches and escapes from the primary tumor site. Therefore, the cell has to decrease its E-cadherin (ECad) expression to lose cell contact to neighboring cells. (55) Regulatory transcription factors involved are ZEB1/2, Snail, Slug (56) and Twist (57), which bind to the ECad promoter to block ECad expression. Subsequently, mesenchymal-associated proteins such as Vimentin and Fibronectin are expressed. These

proteins replace cytokeratin, which changes the polarity of the cells. Not only EMT transcription factors, but also upstream pathways that are already known are important. Crucial pathways in the activation EMT are Wnt, Notch, TGF-β, NF-κB and tyrosin kinase receptors. (58-60) The final step of metastasis is the mesenchymal to epithelial transition, by which the tumor cells re-establish the tumor at a distant site.

1.4.1 EMT linked to CSC

Metastasis, tumor recurrence and therapy resistance can be attributed to both CSCs and EMT. This links both characteristics, resulting in the assumption that EMT is triggered by CSCs. Examples of cells undergoing EMT and expressing cancer stem cell-related proteins are found in the literature. For example, Mani et al. induced EMT via Twist and Snail activation and were able to trigger a $CD44^{high}/CD24^{low}$ phenotype that is linked to breast CSCs and, furthermore, an increase in mammosphere formation. (61) Although it seems like a trivial process, evidence in patients is still missing. Importantly, the first breakthrough for EMT was only shown in cell lines or mice experiments. Recent research reveals that the escape from the primary tumor site might be a more complicated process than originally expected. (62)

1.5. Circulating tumor cells (CTCs)

Formation of metastasis is a major step in cancer progression because it is responsible for the vast majority of cancer-related deaths. Cancer cells found in the blood circulation, so-called circulating tumor cells (CTCs), indicate that seeds for metastasis use the circulatory system to travel to distant organs. This effect has already been observed during early development of the tumor. (63) A huge variety of clinical studies aim to use CTCs as biomarkers for real-time monitoring of disease progression or for the determination of the risk of relapse and for monitoring of the treatment response.

1.5.1. CTC enrichment

The isolation of CTCs represents a major challenge because of their rare occurrence. Usually, 1 mL of blood contains $5*10^6$ white blood cells and $5*10^9$ red blood cells, compared to only a few events of CTCs. (64) Therefore, specific enrichment methods are necessary to successfully isolate and identify CTCs.

CTCs enrichment methods isolate cells based on their biological or physical properties. Biological methods rely on the expression of protein markers on the cell surface. These affinity-based methods use either positive selection via the expression of epithelial cell adhesion molecules (EpCAM) on CTCs or negative selection by targeting common antigens of blood cells, like for example CD45. Until now several methods have been used, but only the CellSearch® (Veridex LLC) technology has been approved by the FDA for certain tumor

types. (65) This method uses antibodies against EpCAM, which are attached to immunomagnetic beads. By applying an electric field, the CTC linked to the beads can be separated from the remaining blood cells. (66)

Intensive research about CTCs as biomarkers revealed that EpCAM is not an ideal surface marker because it results in a false low CTC count and therefore may lead to false-negative results. The problem with label-dependent methods is that EpCAM expression depends on the type of cancer because in some types, low or no expression of EpCAM can be detected. Another reason is based on the epithelial to mesenchymal transition (EMT), which is associated with the formation of metastasis. (67) During this process, the cell loses epithelial features such as EpCAM in order to detach and escape from the primary tumor. (68) Strong evidence of insufficient EpCAM reliability, led to the development of more efficient enrichment techniques. Surface marker-independent methods make use of physical characteristics of cancer cells such as size, density, stiffness and electric charge. Corresponding methods are density gradient centrifugation, filtration through filter devices and dielectrophoresis. (69)

In this study, we used a size-based method which captures CTCs that are distinctly larger and lets the majority of blood cells pass through the microfilter. (70) This microfilter was designed with 8 µm pores which allow for marker free enumeration of CTCs from whole blood and the potential capture of heterogeneous subpopulations of CTCs. (71)

1.5.2. CTC relevance in the clinics

The prognostic value of CTCs has been demonstrated in several studies, where the amount of CTCs is correlated with worse outcome of the disease. (72) State of the art tumor characterization is done via tumor biopsies. Besides being a very cost-intensive procedure, only one moment of disease evolution can be analyzed. The use of biopsies for disease monitoring has been proven unfeasible. Furthermore, with regards to tumor heterogeneity, whether the biopsy is representative of the whole tumor is questionable. In contrast, a minor-invasive blood draw would allow to be taken for real-time monitoring of disease progression and therapy response. (73) Not only can simple CTC counts be used, but with the advances of technology, it is becoming increasingly possible to carry out genetic characterization of these cells. Therefore, single CTC may be profiled, and on this level, the complexity of cancer disease becomes even more prominent. The mutational status varies among the CTCs of the same patient and highlights the heterogeneity at the single cell level. De Luca et al. demonstrated the advantage of monitoring CTCs after therapy. The mutation profile of CTCs after therapy changed compared to the first blood draw. Mutation p.V777L in exon 20 of the ERBB2 gene was common among all CTCs after therapy, suggesting a resistant clone. (74) This is another example that demonstrates the importance of CTCs as

biomarkers for individual therapy strategies. CTC´s potential of serving as a platform for liquid biopsy has been demonstrated in several studies. (73, 75)

2. Rationale

At the moment, EGFR, EML4-ALK and ROS1 are the only recognized predictive and prognostic biomarkers of NSCLC, and particularly adenocarcinoma, which underlines the necessity for more intensive research on lung cancer. More detailed and comprehensive profiling of NSCLC adenocarcinoma may allow for definition of other novel biomarkers. Bringing them into the concept of stem cells may allow better understanding of this disease.

Tumor heterogeneity is still the Achilles heel in the move towards curing lung cancer and cancer in general. Heterogeneity is the key player from the evolution of cancer to metastasis. The real-time tracing of tumor heterogeneity in clinics is still in its infancy. Tumor biopsies are still the state-of-the-art when determining the change in the biology and heterogeneity, but due to low amount of the obtained tissue it is sometimes not feasible to recapitulate all molecular changes and mutations of the primary tumor. There is hardly any possibility of regular non-invasive therapeutic monitoring on a low-cost basis, except in expensive CT scans. Resistance to ongoing tyrosine kinase-inhibiting therapies is diagnosed by clinical progress of the disease. The resistance mechanisms (i.e. changes in EGFR mutation status) are only known through case reports from retrospective data analysis. (76) The opportunity to test EGFR mutations on CTCs could allow for minimization of invasive diagnostic steps prior to systemic treatment. For example, the T790M mutation has been shown to confer resistance on EGFR tyrosine kinase inhibitors, and the introduction of next generation tyrosine kinase inhibitors is dependent on its detection in rebiopsies or on liquid biopsies such as CTCs and circulating cell-free DNA. (77) Furthermore, either CTC detection of circulating cell-free DNA may facilitate monitoring of treatment response.

Another factor within primary tumor tissue particularly associated with CSCs is the likelihood of chemoresistance due to their presence and the risk of disease recurrence. (78, 79) Current therapies are mostly ineffective against CSCs and therefore new approaches for personalized treatment options based on genetic profiling of CSCs and prediction of CSC associated chemosensitivity are needed urgently. For this purpose, characterization of CSCs from the primary tumor is required. An important step towards this would be the isolation of CSCs from primary tumor tissue. So far, most tumor research was performed on cell lines. While the advantages of easy handling and highly proliferative cells are very convenient, the application of the results to physiological conditions still poses a challenge. Some cell lines have been around for decades and are used as a monolayer culture;

consequently, comparing results from cells grown as monolayer to cells that are three-dimensionally arranged and under constant influence of a microenvironment is only of limited value. Our first focus was to enrich CSCs from pleural effusion aspirates and culture them under spheroid conditions, since ultimately, the probability to find CSCs in these is considered to be high. (80, 81) These experiments were performed in breast cancer patients, since these patients frequently develop pleural carcinoids and pleural effusions. As a next step, we extended our successfully established protocols to lung cancer cell lines and subsequently to lung cancer tumor samples. Furthermore, enumeration and characterization of CTCs is gaining more and more importance, and may help to elucidate the role of heterogeneity and CSCs in metastasis and the actual biology of the disease. (82, 83) Liquid biopsy, including CTCs and cell-free DNA may represent a platform to study the metastatic process, particularly with respect to the CSC hypothesis.

The objectives of this study were the analysis of primary tumors in order to isolate and characterize CSCs from primary lung tumor tissues. The secondary objective was to refine methods for CTCs capture and characterization. A comparison of patient-derived cancer cell lines along with CTCs may add to existing knowledge and better understanding of the metastatic cascade. Based on that, selected biomarkers may be generated from the surrogate representatives of early metastatic spread.

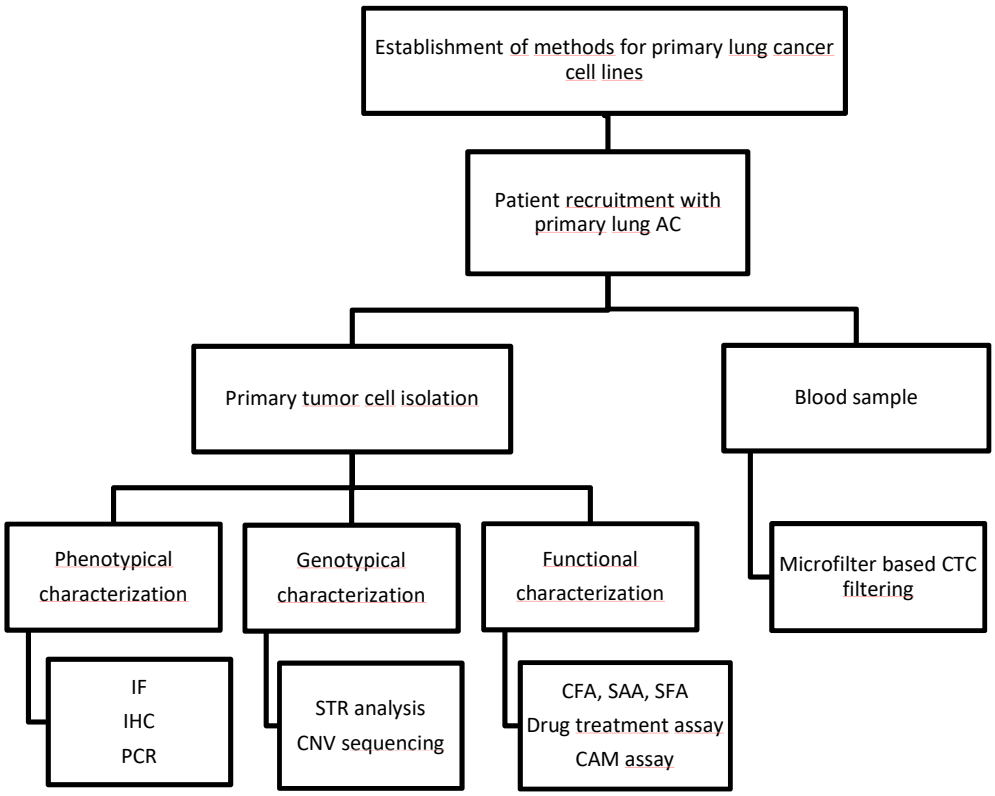

Figure 1: Workplan for the identification of new biomarkers in adenocarcinoma of the lung.

3. Methodology

3.1. Lung cancer cell lines

For method establishment, assay planning and optimization of model systems different types of NSCLC cell lines were used.

Cell lines:

- A549: These human lung adenocarcinoma alveolar basal epithelial cells were derived from a Caucasian male.
- NCI-H1299: These cells were derived from a lymph node metastasis from a Caucasian male with a non-small cell lung carcinoma. Their characteristic is a homozygote p53 deletion.
- NCI-H23: This is a cell line established from a human lung adenocarcinoma of a black male patient.
- NCI-H441: These epithelial cells were isolated from the pericardial fluid of a male patient with a papillary adenocarcinoma of the lung.

All four cell lines were purchased from the in-house cell culture facility, which routinely test cell lines for mycoplasma contamination and authenticate cells by DNA short-tandem repeat analysis.

The same culture conditions were used for all cell lines, to allow comparable results among them. Cell lines were cultured in RPMI 1640 media (Gibco by life technologies, Carlsberg, CA, USA) with 10% fetal bovine serum superior (FBS) (Biochrom, Berlin, Germany) and 1% ABAM (Gibco) and incubated at 37°C and 5% CO_2. Media was changed twice a week.

3.1.1. Splitting of adherent cells

Confluency is an important term in cell culture work, because cells can change their behavior under 100% confluency. Therefore, cells were split to provide them with sufficient space. Media was removed and cells were washed with phosphate buffer saline (PBS). In a T75 flask 2 mL of TrypLE (Gibco by life technologies) were added and incubated for 5 minutes at 37°C. The digestion was stopped with the addition of 5 mL of PBS and cells were centrifuged. The cells were then counted with the Cellometer Auto 1000 (Nexcelom Bioscience LLC, Laurence MA USA) and seeded in new flasks with a specific cell amount depending on growth behavior.

3.2. Patient samples

3.2.1. Patient recruitment for pleural effusion aspirate sample

Malignant pleural effusions were collected from breast cancer patients undergoing thoracentesis for treatment of symptomatic dyspnea at the Division of Pulmonology, Department of Internal Medicine, Medical University of Graz, Austria between September 2011 and April 2013. Patients with histologically verified malignant breast cancer and between the ages 18 and 90 years were eligible for the study. The study was approved by the local ethics committee of the Medical University of Graz (EK Nr. 20–309 ex 08/09) and signed written informed consent was obtained from all patients. This study was of explorative design and thus no statistical power analysis was performed. Altogether, 20 patients were included in this study, from 17 of which had confirmed breast cancer, and 3 were diagnosed with concomitant second metastatic cancer. (81)

3.2.2. Patient recruitment for lung adenocarcinoma samples

Patients were eligible for this study if they were ≥ 18 years old and newly diagnosed with NSCLC AC (verified histologically and/or cytologically). All patients with stage II and III NSCLC who were presented at the Division of Thoracic Surgery at the Medical University of Graz for the planned surgery of the primary tumor were potentially eligible and were included in the study by Assoc. Prof. Dr. Joerg Lindenmann and Ass. Dr. Nicole Fink-Neuboeck. After obtaining written informed consent, primary tumor and peripheral blood samples were collected at the time of surgery (peripheral blood was collected prior to actual surgical removal of the primary tumor). Inclusion criterion was a resectable AC of the lung (cT1-3, cN0-2) prior to adjuvant therapy or after induction (neoadjuvant) chemotherapy has been performed. Exclusion criteria were as followed: preoperative radiotherapy, increased risk of bleeding and anticoagulation. This study has been approved by the local ethics committee of the Medical University of Graz (EK Nr. 25-003 ex 12/13). This research, as well as the study of breast cancer pleural effusions, and the collection and analysis of patient data, were handled according to good scientific practice guidelines, which are required from the Medical University of Graz. (84)

3.3. Single cell isolation from various materials and CSC culturing

3.3.1. Cell isolation from pleural effusions aspirates

The first 8 pleural effusion samples were diluted 1:1 with Dulbecco's modified eagle media (DMEM) low glucose (PAA Laboratories GmbH, Pasching, Austria), 10 % fetal bovine serum (FBS gold PAA Laboratories GmbH, Pasching, Austria) and 2 % antibiotic-antimycotic (ABAM Gibco, Thermo Fischer Scientific, MA, USA). The isolation procedure for samples PL13-25 was optimized, whereby the pleural effusion aspirates were filtered

through a wide-meshed strainer at the beginning. The processed volume varied between 10 mL and 1500 mL, depending on the amount of obtained material. After a centrifugation step at 400xg for 15 min, the cells were washed with PBS and centrifuged at 800xg for 15 min. The cell suspension was treated with an ammonia lysis buffer for 5 minutes. After the lysis step, the cell suspension was filtrated through a 70 µm filter. The cells were counted, and a median number of $40.3*10^7$ cells were transferred to culture (range: $4.3*10^6$–$3*10^9$). Cells were seeded in ultra-low attachment flasks (Corning, New York, USA) and sphere formation assay was initiated. Alternatively, cells were seeded in adherent cell culture with DMEM low glucose, 10% FBS and 2% ABAM. The cells were grown at 37°C and 5% CO_2 conditions. (81, 84)

3.3.2. Single cell isolation from primary lung tumors

The evaluation of the resected tissue was performed by the pathologists of the Medical University of Graz, who identified a piece of the tumor portion for further analysis. The received tumor pieces had an average size of 1 cm^3. The isolation of tumor cells was performed as previously described by Singh et al. with additional dissociation steps using a gentleMACS automated dissociator (Miltenyi Biotec, Bergisch Gladbach, Germany) and some modifications. (85) The tumor tissue was cut into small (3-5 mm) pieces and collected in gentleMACS C-tubes (Miltenyi Biotec) containing PBS and Collagenase B 2 mg/mL (Roche, Mannheim, Germany). C-tubes were then connected to the gentleMACS dissociator and tumor dissociation was run with the program for human tumor number 1. The minced tumors were incubated in the C-tubes using a MACSmix Tube Rotator (Milteny Biotec) under continuous rotation for one hour at 37°C. Following incubation, a second dissociation step was performed on the gentleMACs using the human tumor program number 2. The resulting single cell suspension was then filtered through a 70 µm cell strainer and centrifuged at 300xg for 5 min. Red blood cells were lysed using an ammonium chloride solution (STEMCELL Technologies, Grenoble, France) and the cells were then transferred to ultra-low attachment flasks (Corning, Acton, MA, USA) containing DMEM/F12 media (Gibco by life technologies) supplemented with human recombinant EGF (20 ng/mL), bFGF (20 ng/mL; both Peprotech, Vienna, Austria), B27 (Gibco by life technologies) and 4 µg/mL Heparin (Gilvasan, Vienna, Austria). Media was changed twice a week. (84)

3.3.3. Culturing of spheroids from primary cells

Brown spots in the center of the spheroids were indicators that apoptosis was beginning due to insufficient access of nutrients. In that case spheroids were dissociated with TrypLE (Gibco by life technologies). In later passages of spheroids, cells were also grown in adherent conditions, and therefore, a proportion of the cells was further cultured, with DMEM/F12 media and 10% FBS (Biochrom) in standard flasks (Costar by Sigma Aldrich).

3.4. Characterization of established cell lines from primary tumors

3.4.1. Multicolor- Immunofluorescence

Our multicolor immunofluorescence protocol is based on the indirect immunofluorescence method. Through this, a specific first antibody targets the antigen of interest. Additionally, a secondary antibody that is linked with a fluorochrome targets the F_c part of the first antibody.

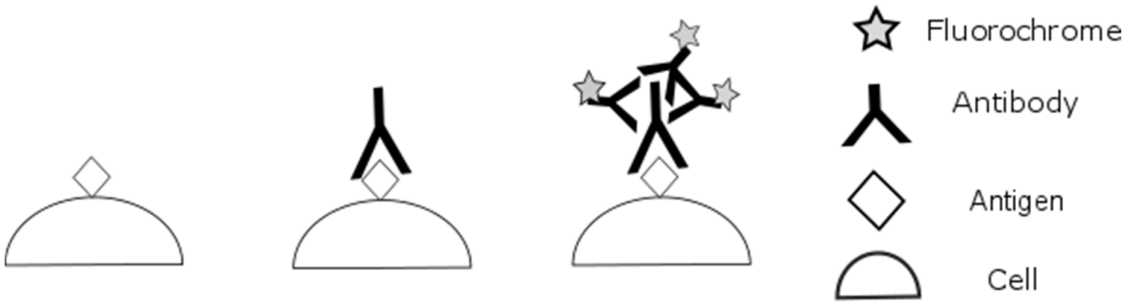

Figure 2. Principe of the indirect immunofluorescence: The first antibody detects and binds to the protein (antigen) of interest. The second antibody, which is fluorescently labeled, binds to the tail region (Fc region) of the first antibody. Multiple secondary antibodies can bind and amplify the signal.

The expression of selected cancer-related proteins was analyzed with multicolor immunofluorescence staining (proteins of interest were summarized in table 2). Cytospins from single cells or compact spheres, chamber slides with adherently grown cells (Lab-Tek by Sigma Aldrich) and adhesion slides (Marienfeld, Lauda-Königshofen, Germany) for spheroid cells were prepared and used. After fixation with 3.7% paraformaldehyde buffer and blocking with normal goat serum for 30 min, samples were incubated with a primary monoclonal antibody cocktail against certain antigens that were obtained from a mouse or rabbit for 1 hour at room temperature (see table 2 for antibodies in use). After washing with PBS, slides were incubated for 1 hour with a secondary fluorescent labeled antibody cocktail consisting of 488 nm goat anti rabbit and 550 nm goat anti mouse (Thermo Fischer, Waltham, MA, USA). Cells were washed again and slides were coverslipped with the SlowFade® gold antifade mounting media with DAPI (life technologies). Image analysis was performed with a confocal LSM (Zeiss).

Table 2. Summary of antibodies used for immunofluorescence and immunohistochemistry.

AB/Target	Clone	Company	Cat. No.	Dilution	Reactivity	Host
1st Antibodies						
ALDH1	44/ALDH	BD	611195	1:100	human	mouse
Ki67	MIB-1	Dako	M7240	1:100	human	mouse

CD133/1	AC133	Miltenyi Biotec	130-090-422	1:50	human	mouse
CD44	156-3C11	Thermo Scientific	MS-688-P1	1:150	human	mouse
CD45	2B11+PD7/26	Dako	IR751	RTU	human	mouse
CK	polyclonal	Dako	Z0622	1:300	cow	rabbit
CK5/6	D5/16 B4	Dako	M7237	1:50	human	mouse
CK7	OV-TL 12/30	Dako	M7018	1:500	human	mouse
E-Cad	HECD-1	Invitrogen	13-1700	1:200	human	mouse
FN	polyclonal	Thermo Scientific	PA5-29578	1:100	human	rabbit
HEA	Ber-Ep4	Dako	M0804	1:1000	human	mouse
MUC1	214D4	Stemcell Technologies	1423	1:1000	human	mouse
Vim	3B4	Dako	M7020	1:100	human	mouse
LCA		Vector Lab.	RL-1042	1:1000		
2nd Antibodies						
Alexa Fluor 488	-	Life Technologies	A-11034	1:300	rabbit	goat
Alexa Fluor 594	-	Life Technologies	A-11005	1:300	mouse	goat

3.4.2. Immunohistochemistry (IHC)

Primary FFPE tumor material was retrieved from the Institute of Pathology at the Medical University of Graz for samples LT8, LT22, LT39 and LT67. Tissue sections were stained with immunohistochemistry, which is preferable for better orientation within the sample.

On the HM355S Rotary Microtome (Thermo Fisher), FFPE blocks were cut into 4 µm sections, which were placed onto Surgipath® X-tra® glass slides (Leica Biosystems, Vienna, Austria) and dried on a plate at 37°C. After deparaffinization, sections were pretreated with a low-pH retrieval solution (Dako, Vienna, Austria) for 10 min in the microwave at 360 W. For the immunostaining, the Ultravision LP Detection System based on horse radish peroxidase (HRP) polymer and 3,3'-Diaminobenzidine (DAB) Plus Chromogen (Thermo Scientific, Waltham, MA USA) was used according to the manufacturer's protocol. In brief, after blocking with ultra V block for 5 min, sections were incubated with the antibody of interest for 1 hour. The signal was enhanced through the incubation of a primary antibody enhancer. For visualization, the sections were first incubated with HRP polymer and then with DAB plus solution. The sections were counterstained with an attenuated hematoxylin eosin (HE) staining and mounted with Aquatex (Merck, Darmstadt, Germany). Samples were evaluated and discussed together

with Prof. Helmut Popper or Dr. Luka Brcic from the Institute of Pathology at the Medical University of Graz. (84)

For all immune staining experiments control samples were used to ensure that the labelling is correct. Negative controls were used to detect unspecific binding of the secondary antibody by replacing the first antibody with PBS. Well-characterized cell lines were used as positive controls. Besides evaluating the activity of the first antibody, it ensures the correct performance of the whole staining protocol.

3.4.3. Flow cytometry and cell sorting

For enrichment of putative CSC population, different antibody panels with CSC-associated markers were used. For one panel, single cells were blocked with 0.5% bovine serum albumin/PBS for 10 min at room temperature (RT). $1*10^6$ isolated pleural cells were incubated with .5 µL of anti-CD44 Allophycocyanin (APC) and 5 µL anti-CD24 Fluorescein isothiocyanate, and cultured lung tumor cells were incubated with 2.5 µL of anti-CD44 APC and 5 µL of anti-EpCam Phycoerythrin (PE) (all BD Bioscience, Schwechat, Austria) for 30 min at 4°C.

The second approach was to measure the ALDH1 activity with an Aldefluor assay kit (Stem Cell Technologies) for both pleural breast and primary lung cancer samples. This assay is based on the enzyme activity of ALDH1. Thereby, a boron-dipyrromethene compound (bodipy) is bound to aminoacetaldehyde. This molecule can enter the cell via passive diffusion, where it is modified into a negatively charged bodipy-aminoacetate that is fluorescently active. One tube contained the ALDH1 inhibitor N,N-diethylaminobenzaldehyde (DEAB), the other one had $1*10^6$ single cells. 5 µL of the bodipy-molecule were added to the cell suspension and immediately half of it was transferred to the tube with the inhibitor and incubated at 37°C for 40 min. Subsequently, only lung cancer cells were incubated with 8 µL of anti-CD133 APC and 5 µL anti-EpCAM PE for 30 min at 4°C. After two washing steps, the stained cells were measured on the LSRII (BD Bioscience). Cells without staining, single stained cells and isotype controls (BD Bioscience) were used as controls in the experiments. Side scatter and forward scatter profiles were used to eliminate cell doublets and apoptotic cells were excluded by using 7-aminoactinomycin D (7-AAD; BD Bioscience). Data analysis was performed using Diva software 7.0 (BD Bioscience). All monoclonal antibodies were pretitered to determine their optimal dilutions before use. Since FITC and PE have a spectral overlap in their emission spectra, a compensation step was included using UltraComp eBeads (eBioscience Inc., San Diego, CA USA). (81, 84)

To generate flow cytometry results, flow cytometry sorting was performed on the fluorescence-activating cell sorter (FACS) Aria (BD Bioscience). These experiments were

supervised by the Core Facility for Flow Cytometry at the Medical University of Graz. Sorted cells were seeded into standard or ultra-low attachment flasks for *in vitro* assay performance. Additionally, DNA and RNA were extracted from sorted fractions for sequencing and gene expression analyses.

3.4.4. Quantitative real-time polymerase chain reaction (qRT-PCR)

qRT-PCR was performed and analyzed according to the MIQE guidelines. (86)

3.4.4.1. RNA isolation and reverse transcription

For RNA isolation, cells were split and counted. $5*10^5$-$1*10^6$ cells were resuspended in RNA lysis buffer (Qiagen, Hilden, Germany) and RNA was extracted with the RNeasy Mini Kit (Qiagen) according to the manufacturer's protocol. The isolated RNA was eluted in 30 µL RNase free water. Reverse transcription of 1 µg of RNA into cDNA was done with the QuantiTect reverse transcription kit (Qiagen) according to the manufacturer's instructions.

3.4.4.2. qRT-PCR on Light cycler 480

qRT-PCR was performed using the KAPA SYBR Green assay (KapaBio, Boston MA, USA) on a Light Cycler 480 (Roche) with 96-well plates. Reactions were performed in a total volume of 20 µL containing 1x mastermix SYBR green I, 25 µM of each primer and 20 ng cDNA. The PCR program was started with an initial denaturation step at 95°C for 3 min run for 45 cycles, starting with the denaturation step at 95°C for 10 sec, then an annealing step at 60°C for 20 sec, and an elongation step at 72°C for 1 sec. For quality control, it ended with a melting step of the PCR product. A non-amplification control and a no-template control were included in each plate as technical controls. qRT-PCR reactions were performed in duplicates and relative quantification was performed using the second derivative method algorithm. Cycle threshold values were averaged. The calculation of expression values was done using the qBase^{plus} software (Biogazelle) (87). Glycerinaldehyd-3-phosphat-Dehydrogenase (GAPDH) and TATA-Box Binding Protein (TBP) were determined as appropriate reference genes using the geNorm module in qBase^{plus} and were used to normalize gene expression levels. The gene expression levels in spheres were compared to expression in adherent cells. Primers are summarized in table 3. (84)

Table 3. Primer sequences for qRT-PCR.

Genes	Forward primer (5´-3´)	Reverse primer (5´-3´)	Amplicon (bp)
HKG			
GAPDH [a]	CCACTCCTCCACCTTTGAC	ACCCTGTTGCTGTAGCC	102
TBP [a]	CGGTTTGCTGCGGTAATC	TCTGGACTGTTCTTCACTCTTG	108
LDHA [a]	TGTAGCAGATTTGGCAGAGAG	CATCATCCTTTATTCCGTAAAGAC	95
Cancer stem cell markers			
CD44 [b]	TGCCGCTTTGCAGGTGTAT	GGCCTCCGTCCGAGAGA	66
ALDH1 [a]	AGAAGGAGATAAGGAGGAT	AATCAGCCAACTTGTATAATAG	125
CD133 (PROM 1) [b]	AGAGCTTGCACCAACAAAGTACAC	AAGCACAGAGGGTCATTGAGAGA	91
Stem cell markers			
OCT4 [c]	GACAACAATGAAAATCTTCAGGAG	CTGGCGCCGGTTACAGAACCA	216
SOX2 [c]	GCACATGAACGGCTGGAGCAACG	TGCTGCGAGTAGGACATGCTGTAGG	207
NANOG [c]	CAGCTGTGTGTACTCAATGATAGATTT	ACACCATTGCTATTCTTCGGCCAGTTG	179
EMT markers			
E-Cadherin (CDH1) [b]	TGAGTGTCCCCCGGTATCTTC	CAGTATCAGCCGCTTTCAGATTTT	87
Vimentin [c]	CAACCTGGCCGAGGACAT	ACGCATTGTCAACATCCTGTCT	113
Fibronectin [c]	CCGCCGAATGTAGGACAAGA	TGCCAACAGGATGACATGAAA	100
N-Cadherin [c]	GACGGTTCGCCATCCAGAC	TCGATTGGTTTGACCACGG	67
EMT transcription factors			
SNAIL [c]	GCTGCAGGACTCTAATCCAGAGTT	GACAGAGTCCCAGATGAGCATTG	130
SLUG [c]	GCGATGCCCAGTCTAGAAAA	GCAGTGAGGGCAAGAAAAAG	203
TWIST [c]	GGAGTCCGCAGTCTTACGAG	TCTGGAGGACCTGGTAGAGG	201
Zeb1 [c]	GCCAATAAGCAAACGATTCTG	TTTGGCTGGATCACTTTCAAG	101
Zeb2 [c]	CCCTTCTGCGACATAAATACG	TGTGATTCATGTGCTGCGAGT	192

3.5. Genotypic characterization and profiling

3.5.1. Copy number profiling

Cancer arises because of multiple abnormalities in the genomes of certain cells. These aberrations could be detected with next-generation sequencing methods. Using these methods, regions with deletions and amplifications could be detected and linked to a known or unknown tumor suppressor or oncogenes. This method was carried out at the Institute of Human Genetics under the supervision of Assoc. Prof. Dr. Ellen Heitzer.

Genome-wide copy number aberrations (CNA) were established using low-coverage whole genome sequencing. Shotgun libraries were prepared using the TruSeq DNA Nano LT Sample Preparation Kit (Illumina, San Diego, CA, USA) with slight modifications of the manufacturer's

[a] http://www.ncbi.nlm.nih.gov/tools/primer-blast/

[b] http://www.rtprimerdb.org/

[c] Palafox M. et al. Cancer Research 2012

protocol. Depending on the DNA concentrations, 50-100 ng of DNA from sorted cell fractions and 1-2 µg of DNA from tumor samples were fragmented in 130 µL using the Covaris System (Covaris, Woburn, MA, USA). After concentrating the volume to 50 µL, end repair, A-tailing and adapter ligation were performed following the manufacturer's instructions. For selective amplification of the library fragments which have adapter molecules on both ends, we used 8-15 PCR cycles. Libraries were quality checked on an Agilent Bioanalyzer using a DNA 7500 Chip (Agilent Technologies, Santa Clara, CA, USA) and quantified using qPCR with a commercially available PhiX library (Illumina, San Diego, CA, USA) as a standard. Six libraries were pooled equimolarily and sequenced on an Illumina MiSeq in a 150bp single read run. Following the completion of the run, data were base called, demultiplexed on the instrument (provided as Illumina FASTQ 1.8 files, Phred+33 encoding), and FASTQ format files in Illumina 1.8 format were used for downstream analysis. Copy number analysis was performed as previously described. (88) Briefly, low-coverage whole-genome sequencing reads were mapped to the pseudo-autosomal-region (PAR)-masked genome and reads in different windows were counted and normalized by the total number of reads. The read counts were further normalized according to the GC-content using LOWESS-statistics. In order to avoid position effects, the sequencing data was normalized with GC-normalized read counts of a set of 30 non-malignant control samples. (88) Subsequently, segments of similar copy-number values were generated by applying circular binary segmentation and gain and loss analysis of DNA. For each segment, a z-score, that compared GC-corrected read counts for samples and controls was calculated. (84, 88)

3.5.5. Authentication of origin of cells

In order to verify the common origin of different cell populations, passages and tumor samples, short tandem repeat (STR) profiling and analysis of mitochondrial DNA (mtDNA) was performed.

With STR analysis, the relation of the cells in culture compared to the patient leukocytes was investigated. (89) For STR analysis 0.7 ng of extracted DNA were amplified with the PowerPlex 16HS System (Promega, Mannheim, Germany) according to the manufacturer´s instruction on a thermocycler MyCycler (Biorad, Vienna, Austria). In this analysis, 16 STR loci such as Penta E, D18S51, D21S11, TH01, D3S1358, FGA, TPOX, D8S1179, vWA, Amelogenin, Penta D, CSF1PO, D16S539, D7S820, D13S317 and D5S818 were evaluated and used for the comparison. The amplified fragments were detected with a capillary electrophoresis on the 3730 Genetic Analyzer (Applied Biosystem, Vienna, Austria). (84)

The second method was based on the copy number profiling assay results. Therefore, mitochondrial genomic sequences were extracted from whole genome sequencing data and haplotypes were compared for each sample.

3.6. *In vitro* functional assays

Results from phenotypic and genotypic characterization suggested CSC enrichment under spheroid conditions. Therefore, the next step was to evaluate their malignancy with functional assays. Established assays were accomplished to evaluate the aggressiveness of cells with CSC marker expression, which can be reflected in their growth characteristics. Experiments were all performed with low cell density to ensure self-renewing conditions. (90)

3.6.1. Colony formation assay

200 cells were sorted into a 6-well plate with adherent media and incubated for 8 days. Culture media was added up to counteract evaporation. Cells were fixed with ice-cold methanol for 10 min, following the staining with 0.5% crystal violet solution for 10 min. Staining was rinsed off with ddH_2O. The well plates were scanned and colonies were counted with ImageJ software.

3.6.2. Sphere formation assay (SFA)

Tumor spheres evolve from the proliferation of a single progenitor cell. (91) Special media conditions, which were mentioned in chapter 3.3., facilitate spheroid formation. The formation of spheroid structures is a potential site for CSCs that allows us to evaluate their self-renewing capacity. First of all, initial primary cultures from pleural or isolated single cell suspension samples were cultured under spheroid conditions to enable CSC enrichment for further characterization. Secondly, subpopulations with expressions of putative CSC-markers were compared to non-CSC subpopulations regarding their sphere formation capacity. Therefore, 1000 cells were sorted in triplicates into ultra-low attachment 6-well plates. Spheres were evaluated under a light microscope and spheres with a minimum size of 50 µm were counted. (92)

3.6.3. Soft agar assay

Another carcinogenic behavior is studied with soft agar assay. Cells growing and proliferating in an anchorage-independent surrounding are considered to have a high tumorigenic potential. (93)

Agarose stock was prepared with 0.9 g of 2-hydroxyethyl agarose (Sigma Aldrich) solved in 30 mL of AD. The agarose solution was autoclaved before use. A bottom layer of 0.6% agar was prepared to prevent attachment. 0.3% soft agar in media was mixed with 800 sorted cells and plated onto the bottom layer. (94) After 3 weeks of sphere formation, the

plate was stained with 0.005% crystal violet and the total number of colonies were counted under a light microscope.

All assays, including colony formation, sphere formation and soft agar assay, were calculated according to the following equation.

$$Sphere\ or\ colony\ formation\ efficiency = \frac{\#spheres\ or\ colonies\ per\ well}{\#\ seeded\ cells\ per\ well} * 100$$

The sphere/colony formation efficiency is the quotient of the spheres/colonies that evolved per well, divided by the number of seeded cells, multiplied by 100. All assays were performed with 3 different culture passages of each cell line and each subpopulation was seeded as 3 technical replicates. The results were summarized in bar graphs with the relative sphere/colony forming efficiency using the GraphPad Prism 6 software.

3.6.4. Migration assay

The migratory potential of putative CSCs was evaluated with 2-well µ-dish (Ibidi, Martinsried, Germany). Cells were seeded in both wells and left to attach for 24 h. The dish was washed 2 times with HBSS to remove cells that were not attached and covered with DMEM/F12 media with 10% FBS. The dish was photographed hourly during a 24 h period to observe cell migration. The gap distance was determined with ImageJ and the migration velocity was calculated according to the linear equation of time-to-distance relation.

3.7. Chorio-allantoic membrane assay

The chorio-allantoic membrane (CAM) in chicks develops 7 days after the egg was fertilized and is a part of the extraembryonic compartment. It is attached to the shell membrane and consists of three layers called the chorionic epithelium, the intermediate mesodermal layer and the allantoic epithelium, which can be seen in figure 3. (95) During the maturation of the embryo, the CAM serves as a barrier for gas exchange and waste storage. Various advantages such as the nutrient-rich environment, the good vascularization and the immune deficiency make it an ideal model system for tumor cell behavior studies. We favored this assay, because comparison of different culture conditions with conventional *in vitro* functional assays would be difficult. This *ex ovo* system provides a complex microenvironment for the primary cells.

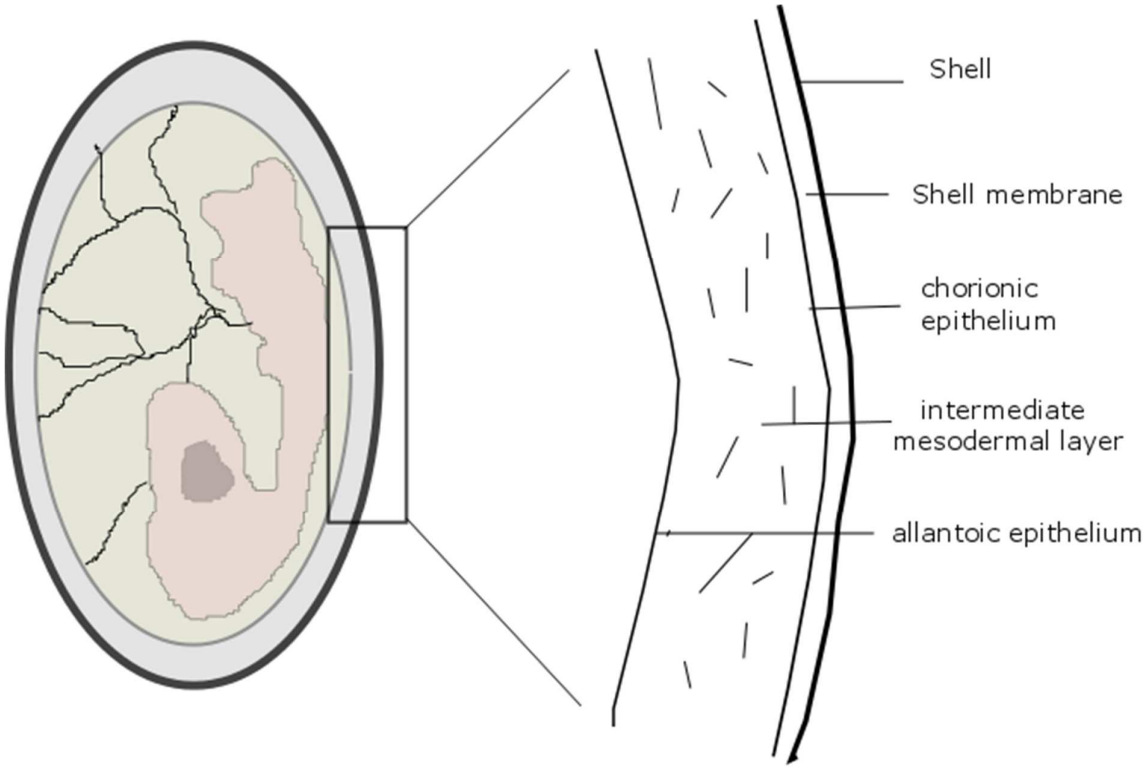

Figure 3. Structure of CAM within the chicken egg.

Fertilized white leghorn eggs (Schropper, Gloggnitz) were washed with 5% H_2O_2 and incubated at 37.6°C, 5% CO_2 and 70–75% humidity, under constant rotation. For better accessibility to the experimental site, we performed *ex ovo* method in our study. Therefore, on day 3, the eggs were dipped in Ethanol and cracked carefully. Intact eggs were put in a pre-sterilized covered dish and incubated under the same conditions as previously mentioned, for another 7 days. On day 10, silicon rings with a diameter of 5 mm were placed onto the CAM. $1*10^6$ single tumor cells resuspended in PBS were mixed 4:1 with matrigel (growth factor reduced, BD Bioscience) and grafted into the silicon rings. Xenografts were allowed to grow for 72 hours. Subsequently, tumors and surrounding tissue were removed with sterile tools. The xenograft was washed in PBS and fixed for 16 hours in PFA. After the xenograft passed an ascending alcohol series and toluene to dehydrate the tissue, it was dipped in Paraffin type 6 and embedded in Paraffin type 9 (both Thermo Fisher). Paraffin sections of 4 µm were cut with the Microtome MICROM HM335E and transferred onto glass slides. A work plan of CAM experiment is summarized in figure 4. (84)

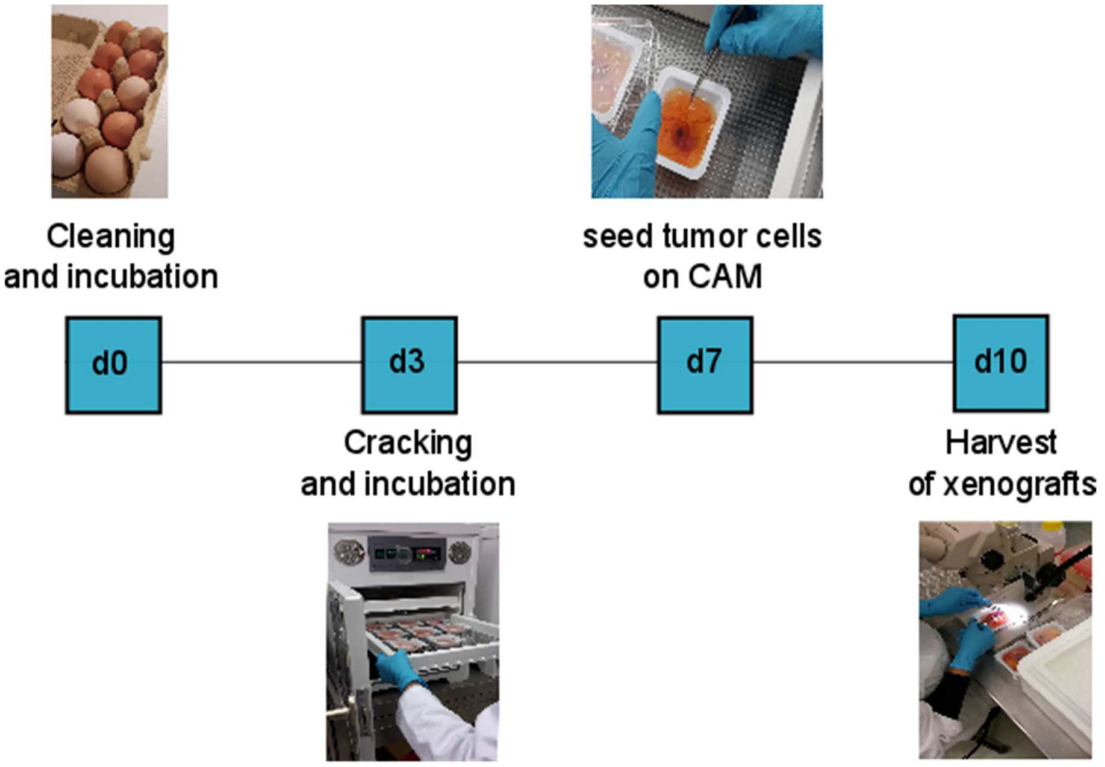

Figure 4. Workflow of CAM assay starting from receiving the fertilized eggs and ending with the xenograft harvest.

3.7.1. CAM neoangiogenesis assay according to Quingley

As tumor size increases, cells in the core of the tumor lack nutritional supply; causing the tumor´s need to organize the building of blood vessels. This angiogenesis process is driven by cytokines and growth factors, which are released from tumor cells. (96)

The eggs were prepared in the same way as for the *ex ovo* CAM assay. On day 10, a Nitex nylon mesh with a grid size of 180 µm was cut into 2x2 mm and 3x3 mm squares and irradiated with UV-light for 20 min. By keeping the grids constantly wet with 70% Ethanol, the smaller grids were put on top of the larger grids. 50 µL of the supernatant mix (table 4) were pipetted onto each grid and incubated for 30 min at 37°C.The grids were carefully placed onto the CAM. 6 eggs were taken for each condition and on every egg, we placed 6 grids. The angiogenic assay was incubated for 72 hours. The neoangiogenic potential was evaluated under a stereomicroscope (Olympus SZX 16). Therefore, the ratio of counted numbers of vascularized squares to the number of total squares of the grid was calculated. The results were statistically compared using an unpaired t-test with Welsh correction.

Table 4. Ingredients for supernatant mix

Substance	Volume [µL] for 25 grids
Supernatant	322.5
Collagen 2 mg/mL	390.0
HEPES 1 mM	7.5
NaOH 1 M	30.0
Total	750.0

3.8. Drug treatment assay

Reasons for failure of traditional therapy approaches have been attributed to CSCs. Multiple resistance mechanisms provide CSCs with a substantial survival advantage. Therefore, the viability of the patient-derived cells under chemotoxic condition were investigated. Common chemotherapeutics for lung adenocarcinoma such as Cisplatin (Accord Healthcare, Salzburg, Austria) and Pemetrexed (Lilly, Indianapolis IN, USA) were tested on the established cell lines. Additionally, Salinomycin (Sigma Aldrich), an anti-CSC agent was used. (97)

On day one, cells were seeded into 96-well plates. The cell number depended on the proliferation rate of the different tumors and culture conditions. The cell amounts varied between 1000 cells per well with LT22a cells and 2500 for all spheres. 24 hours later, the cells were treated with the chemotherapeutic in varying concentrations for determination of IC_{50} concentrations. Concentrations were determined as found in literature (98-102) and a pipetting scheme is listed in table 5. Untreated cells and cells treated with solvent of chemotherapeutic (vehicle control VC) served as controls. After 72 hours, the PrestoBlue reagent (Invitrogen, Vienna Austria) was added in a 1:10 ratio according to manufacturer´s instruction. Thereby a blue non-fluorescent reagent is converted to a red fluorescent dye by the reducing condition of present viable cells. Well plates were mixed on a rotation plate 500 rpm for one minute and centrifuged at 500 rpm for one minute. For the progress of the biochemical reaction the plates were incubated at 37°C for 30 min and the fluorescence emission was measured on the FLUOstar omega plate reader (BMG-Labtech, Ortenberg Germany). The fluorescent intensity was normalized to VC and the decrease in viability from both conditions LT#s and LT#a were summarized in bar graphs created with GraphPad Prism 6 Software. (84)

Table 5. Pipetting scheme for drug treatment viability assay.

Salinomycin			
Concentration in Eppendorf	**Concentration in well**	**Chemotherapeutic**	**Media**
Salinomycin stock solution 6,66 µM was diluted 1:100		4µL stock solution	396 µL
20 µM	10 µM	360 µL from 1:100 dilution	840 µL
10 µM	5 µM	600 µL from 20 µM	600 µL
5 µM	2.5 µM	600 µL from 10 µM	600µL
2 µM	1 µM	480 µL from 5 µM	720 µL
1 µM	0.5 µM	600 µL from 2µM	600 µL
0.2 µM	0.1 µM	240 µL from 1 µM	960 µL
0.02 µM	0.01 µM	70 µL from 0,2 µM	630 µL

Cisplatin			
Concentration in Eppendorf	**Concentration in well**	**Chemotherapeutic**	**Media**
Cisplatin stock solution 333,3 µM was diluted 1:10		80 µL Stock solution	720 µL
200 µM	100 µM	720 µL of 1:10 dilution	480 µL
100 µM	50 µM	600 µL from 200 µM	600 µL
50 µM	25 µM	600 µL from 100 µM	600 µL
20 µM	10 µM	480 µL from 50 µM	720 µL
10 µM	5 µM	600 µL from 20 µM	600 µL
1 µM	0.5 µM	90 µL from 10 µM	810 µL
0.5 µM	0.25 µM	300 µL from 1 µM	300 µL

Pemetrexed			
Concentration in Eppendorf	**Concentration in well**	**Chemotherapeutic**	**Media**
Pemetrexed stock solution 585 µM was diluted 1:100		3µL Stock solution	297 µL
100 µM	50 µM	205 µL of 1:100 dilution	1000 µL
50 µM	25 µM	600 µL from 100 µM	600 µL
20 µM	10 µM	480 µL from 50 µM	720 µL
10 µM	5 µM	600 µL from 20 µM	600 µL
2 µM	1 µM	240 µL from 10 µM	960 µL
0.2 µM	0.1 µM	70 µL from 2 µM	630 µL

3.9. *in vivo* mouse experiments

The following experiment was performed by EPO Berlin-Buch under the coordination of Dr. Reiner Zeisig. $3*10^7$ cells of LT22s and LT22a cells were gathered in DMEM/F12 media with 10% DMSO and frozen in liquid nitrogen. The cells were sent to Berlin and were cultured under the same conditions as mentioned in chapter 3.3. After two passaging periods, cells were used for mouse transplants.

Female NOD/SCID mice (Taconic), kept under conditions summarized in table 6, were stratified at day 0 into two groups, each with 3 mice. For subcutaneous injection, $1x10^7$ cells were re-suspended in 100 µL PBS/Matrigel (1:1) and transplanted subcutaneously to the left flank of each mouse. LT22s cells were transplanted to mice of group A, while LT22a cells were transplanted to mice of group B. (84)

Table 6 Summary of animal conditions. (84)

Subject	Conditions
Animals, gender and strain	Female NOD/SCID
Age	9-10 weeks
Body weight	21.4 to 24.1 g (mean 22.5 ± 1.1 g) at time of cell inoculation
Supplier	Taconic, Cologne, Germany
Environmental conditions	Strictly controlled and standardized barrier conditions, IVC System Tecniplast DCC (TECNIPLAST DEUTSCHLAND GMBH)
Drinking water	Autoclaved tap water in water bottles (acidified to pH 4 with HCl)
Feeding and drinking time	Ad libitum 24 hours per day
Room temperature	22±1°C
Health control	The health of the mice was examined at the start of the experiment and twice per day during the experiment

3.9.1. Evaluation of tumor xenograft

Tumor diameters were measured two times a week with a caliper. The tumor volumes were calculated according to V = (length x (width)2)/2. For calculation of the relative tumor volume (RTV), the tumor volumes were related to the day of the first treatment at each measurement day and the median and mean tumor volumes per group were calculated. (84)

Mice with generated tumors were sacrificed on day 42 by cervical dislocation and inspected for gross organ changes. The lung and liver tissues of each mouse were macroscopically inspected for metastatic nodules with the aim of quantifying the number of metastases as well as differentiating between different sizes. Furthermore, tissues from these selected organs were also evaluated for the presence of human cells (corresponding to formed metastases) by human PCR. After the isolation of genomic DNA from two samples of each tissue, a human-specific DNA was amplified by the fragment of the alphasatellite region of human chromosome 17. The ΔCt values, which were calculated by subtracting the experimental mean Ct value from that of the negative control (mouse tissue), are indicated.

Genomic DNA of the human mammary carcinoma xenograft 3366 was used as a positive control, and water as reagent (negative) control. (84)

3.10. CTC enumeration from whole blood

3.10.1. Composition of the filter device

The centerpiece of the entire filter device is a parylene membrane with a pore size of 8 µm. The diameter was adjusted to the size of the cells in circulation. Blood cells such as erythrocytes, granulocytes and leukocytes should pass the filter and CTCs should remain on the filter, due to their significantly larger size. Zabaglo et al. found a reduction from 50 million leukocytes to 7000 by using a pore size of 8 µm with a concomitant high recovery of CTCs. (103) A positive property of parylene is the transparency of the material under visible- and UV light exposure. Therefore, the microscopic evaluation after the staining of the captured cells can be done directly on the filter.

3.10.2. Filtering process

Peripheral blood was collected in CellSave Preservative tubes (Veridex LLC, Raritan, NJ). Samples were processed within 24 hours. The blood samples were immediately fixed with 1% paraformaldehyde (Sigma Aldrich, Vienna, Austria), for 10 minutes at room temperature under rotating conditions.

The characteristics of the microfilter and the assembly of the filter device were described in detail in previous publications. (104) In brief, a parylene membrane filter with a size of 0.6x0.6 cm and a pore diameter of 8 µm was placed on the polydimethylsiloxane (PDMS) surface that is further connected to an acrylic filter cassette. The filter was sandwiched with a second part of the acrylic cassette and clamped together. The assembly is shown in figure 5 A. The blood sample is loaded into a syringe which was attached via a Luer-Lock system to the housing cassette. With a constant flow rate of 75 mL/h, a syringe pump (Landgraf Laborsysteme, Langenhang, Austria) pressed the blood through the filter devices. The filtration process is pictured in figure 5 B. An additional rinse with 10 mL PBS was performed with the same settings. The filter was removed from the housing cassette and dried overnight on a Whatman® paper (GE Healthcare, Chalfont, UK). Tumor cells were distinguished from contaminating blood cells according to their morphology and different antigen expression. This visualization of the captured CTCs was done with multiple-color immunofluorescence as described in section 3.4.1. The amount of captured CTCs was manually counted under a laser scanning microscope (LSM 510 Zeiss, Jena, Germany). The whole filter was optically scanned and CTCs were identified and distinguished from blood cells through their positive CK (green) and negative CD45 (red) signal and an intact

nuclear Dapi staining. The patient characteristics correlated with the number of counted CTCs.

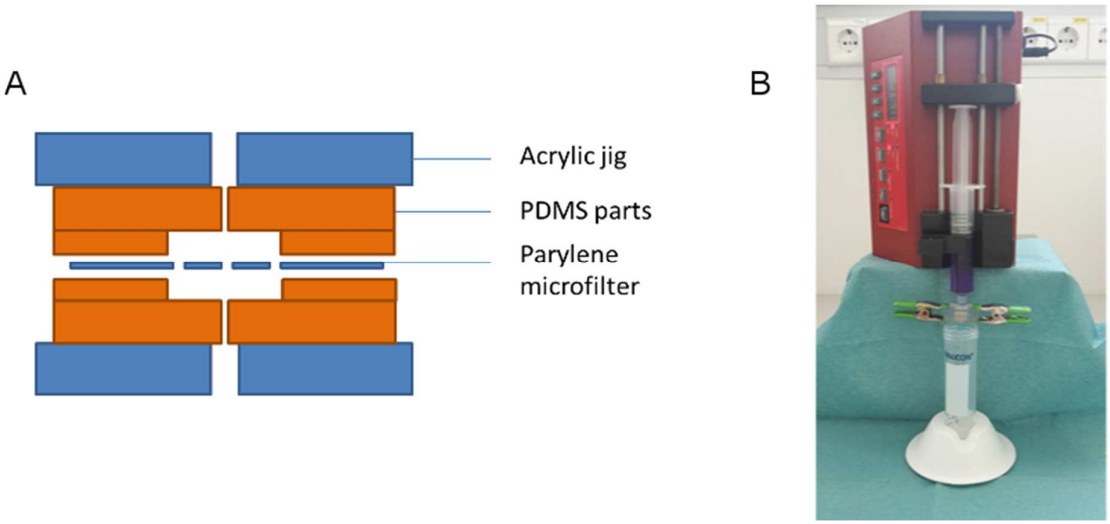

Figure 5. CTC enrichment with a parylene microfilter as size-exclusion method: CTCs would be captured on the filter, whereas blood cells would flow through. (A) assembly of filter cassette (B) syringe pump set up for filtering process.

3.11. Statistical analyses

Sphere/colony-forming efficiency data were tested for normal distribution with D´Agostino and Pearson tests and differences between the CSC-marker positive and negative population were statistically analyzed using a paired t-test. Comparison between the viability of adherent and spheroid-grown cultures during treatment was calculated with 2-way ANOVA and Sidak´s multiple comparison test. The statistics were calculated in GraphPad Prism 6 (La Jolla, CA, USA). For all analysis, a p-value of < 0.05 was considered statistically significant. Clinical and pathological patient data were associated with CTC positivity using the Chi square test. This analysis was conducted by using SPSS Statistics v.23 software (IBM SPSS Inc. Chicago, IL, USA).

4. Results

4.1. Method evaluation

4.1.1. Results from the study of pleural effusion aspirates from breast cancer patients, which share the methods used in the main study

The main work of this project was preceded by another study in which cells from pleural effusion aspirates of metastatic breast cancer patients were isolated and cultured *in vitro*. After isolation, cells were sorted for breast CSC markers including ALDH1 and $CD44^{+}/CD24^{-/low}$ within a week and seeded for sphere formation assay. A higher success rate of primary spheres was achieved with unsorted cells (14 out of 18; 77.8%) as opposed to sorted CSC subpopulations. Both putative breast CSC subpopulations expressing the ALDH1 and the $CD44^{+}/CD24^{-/low}$ phenotype, showed similar sphere formation efficiency. To add further details, we were able to generate primary spheres from four out of 13 (30.77%) subpopulations with the stem cell phenotype $CD44^{+}/CD24^{-/low}$ and five out of 16 (31.25%) subpopulations with high expression of ALDH1. (81)

After culturing and sorting, we could isolate enough DNA from nine sorted primary pleural samples, which could be genotypically characterized by low-coverage whole genome sequencing (six $ALDH1^{+}$ samples and three $CD44^{+}/CD24^{-/low}$ samples). Five out of these nine sorted samples had an aberrant profile compared to the respective primary tumor. A closer look at the sample Pleura 21 in figure 6 showed that most of the copy number alterations from the sorted $CD44^{+}$ and unsorted samples were also found in the primary tumor sample. Detected aberrations situated as gains at chromosomes 1q, 6, 7, 8, 10, 13q, 14q, 15q, 17, and 18p and losses at chromosomes 4q, 8p, 9p, 11q, or 13q were frequently observed in breast cancer. In contrast, the $ALDH1^{+}$ subpopulation showed only a few focal amplifications of chromosomes 6, 16 and 17 with lower amplitudes, which could indicate a smaller tumor fraction. (81)

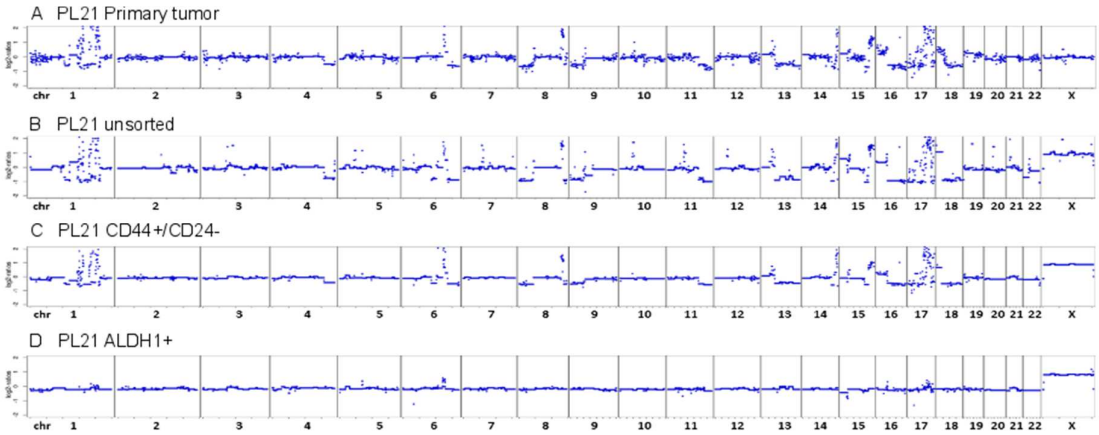

Figure 6. Copy number profiles from pleura 21: (A) FFPE primary tumor, (B) Pleura 21 unsorted cells. (C) Pleura 21 $CD44^{+}/CD24^{-}$ sorted cells and (D) Pleura 21 $ALDH1^{+}$ cells. X- axes list the chromosomes 1-22 and X, y-axes show log-2 ratios. Signals above 0 were amplifications and signals below 0 indicate losses. (81)

From one unsorted sample Pleura 24, we could establish a long-term cell line, which was characterized with IF (figure 7). CSC markers CD44 and ALDH1 were positively expressed and an epithelial phenotype could be observed through positive ECad and CK expression and negative Vimentin expression. Additionally, the Her2neu overexpression of the primary tumor could be confirmed with an intensive Her2neu positive staining of the spheres. (81)

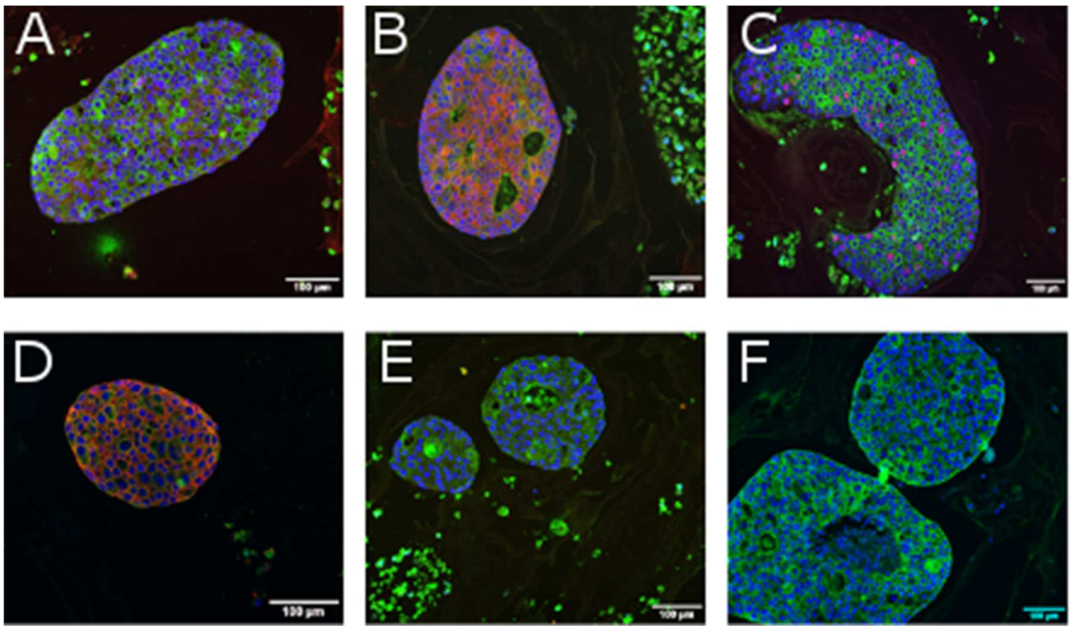

Figure 7. Representative picture of mammospheres from Pleura 24 embedded in paraformaldehyde and stained following the IF protocol: (A) ALDH1 (red) and CK (green), (B) CD44 (red) and CK (green), (C) Ki67 (red) and CK (green), (D) ECad (red) and CK (green), (E) Vim (red) and CK (green) and (F) Her2neu (green). All samples were counterstained with nuclear DAPI staining (blue).

Samples were investigated using an Olympus BX51 fluorescent microscope. Measuring bar indicates 100 µm. (81)

The established methods from the above-mentioned study such as primary tumor cell culturing, flow cytometry and cell sorting, copy number profiling, immunofluorescence and sphere formation were next tested on common lung cancer cell lines and then used for the primary lung tumor samples.

4.1.1. Method evaluation on lung cancer cell lines

Preliminary experiments were performed using commercially available cancer cell lines, which were originally isolated from patients with an adenocarcinoma of the lung. Initially, the cell lines were cultured under adherent conditions and subsequently sphere formation assay was performed (figure 8). Media composition was different from breast cancer cells. RPMI 1640 with 10% FBS was used for adherent cells and DMEM/F12 instead of MEBM media for sphere formation.

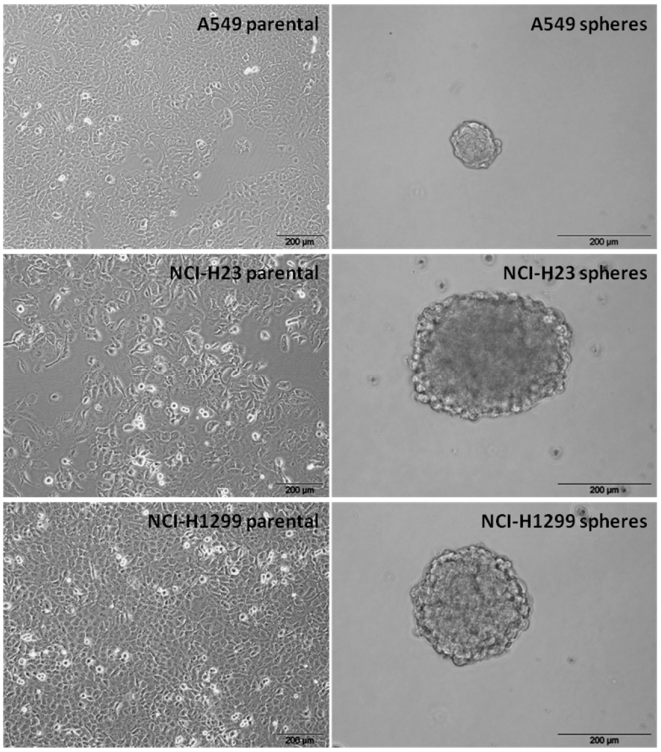

Figure 8. Culturing lung cancer cell lines: Representative pictures from lung cancer parental cell lines under adherent conditions (left column) and under spheroid conditions (right column). Measuring bar indicates 200 µm.

Next, the goal of the staining was to characterize the cells and to determine their origin and phenotype. Therefore, the methods and the antibodies were tested on lung cancer cell lines before protocols were applied on the primary lung cancer cells. The protocols from the

breast cancer project could successfully be applied without any modifications. As an example, figure 9 shows the immunofluorescent staining pictures of NCI-H441. The majority of the cells in figure 9 were positive for ECad in adherent cultures and as spheroids. This is in concordance with the NCI-H441 origin, since this cell line was isolated as epithelial cells from a pericardial fluid of a patient with lung AC. Only some single cells stained positive for Vimentin. CSC marker ALDH1 was not expressed in both culture conditions; however, CD44 could be enriched in the spheroid culture. The staining results from all NSCLC cell lines are summarized in table 7.

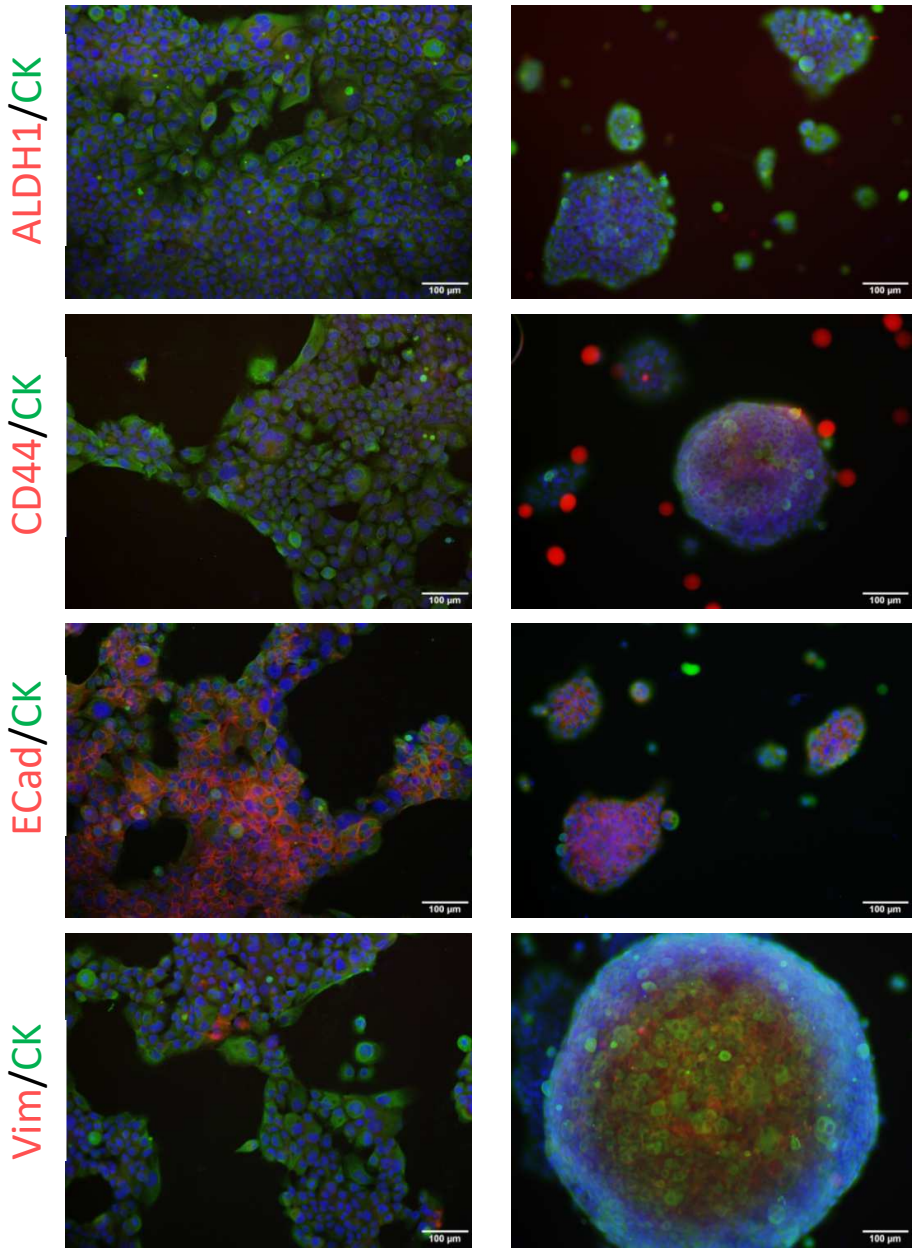

Figure 9. Representative picture of NSCLC cell line NCI-H441 IF staining with important CSC (CD44 and ALDH1) and EMT markers (ECad and Vim). Images were investigated under Zeiss confocal LSM. Measuring bar indicates 100 µm.

Table 7. Summary IF results from lung cancer cell lines.

Target	A549a	A549s	H441a	H441s	H1299a	H1299s	H23a	H23s
ALDH1	+	+	~	-	-	+	~	~
panCK	~	+	+	+	~	+	+	~
CD44	+	+	~	+	++	++	++	+
ECad	+	++	++	++	~	~	~	-
Vim	+	+	~	+	++	+	+	++

++ bright signal in all cells; high expression of target protein
+ signal was not in all cells; expression of target protein in the majority of cells
~ signal was only detected in some single cells; expression of target protein in the minority of cells
- no signal; no expression of target protein

Other analysis such as flow cytometry and qRT-PCR could be performed with the same protocols as established for breast cancer cell lines. Considering the high relation of CD133 expression with CSCs, this could unfortunately not be addressed in the lung cancer cell lines. Even after sphere formation no expression could be detected with any of the used methods. Therefore, to verify the validity of the antibodies, CD133 staining was tested on CaCo2 cells (data not shown).

4.2. Characteristics from lung tumor patients

In total, 95 (100%) patients with lung tumors could be recruited for this study at the division of thoracic and hyperbaric surgery. After tumor resection, we obtained fresh primary tumor tissue from the department of pathology in 87 (91.6 %) cases and could proceed to isolate and culture primary CSCs. The tumor tissue was examined thoroughly by a pathologist, but in 8 (8.4%) cases the tumor was too small to allow further analysis according to our protocols. The study cohort consisted of 46 (48.4%) female and 49 (51.6%) male patients, and the median age was 65.5 with a range of 46-82 years. After the histological evaluation of the primary tumor, the medical examination confirmed 78 (82.1%) adenocarcinoma tumors, 11 (11.6%) tumors of squamous cell carcinoma and 6 (6.3%) with other tumors. More than half of all patients (65.3%) were in an early stage at the time of surgery. Detailed information can be found in table 8 and a flow chart as figure 10 summarizes the workflow with the 95 lung tumor samples.

Table 8. Patient characteristics of all lung tumor patients.

Characteristics of all recruited patients N=95 (100%)		
Gender	Male	49 (51.6)
	Female	46 (48.4)
Age	<60	23 (24.2)
	≥60	72 (75.8)
Histology	AC	78 (82.1)
	SCC	11 (11.6)
	OC	6 (6.3)
Smoking status	Never	12 (12.6)
	Former	32 (33.7)
	Current	31 (32.6)
	No information	20 (21.1)
Staging	0-I	41 (43.2)
	II	21 (22.1)
	III	29 (30.5)
	IV	4 (4.2)

AC: adenocarcinoma
SCC: squamous cell carcinoma
OC: other cancer; large cell carcinoma, small cell carcinoma, carcinoid, in situ adenoma

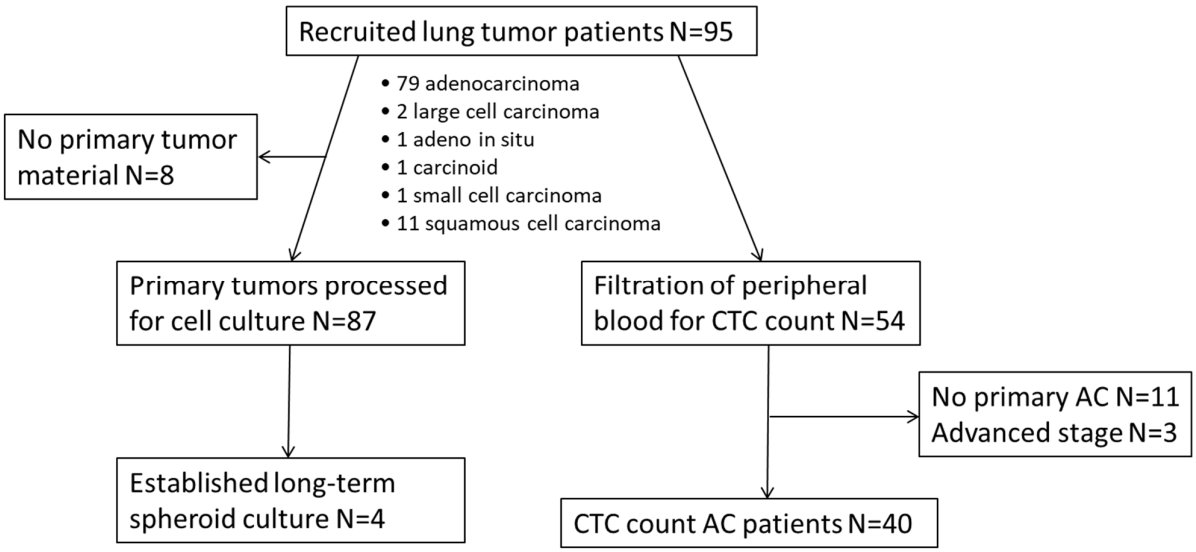

Figure 10. Flow chart of patient recruitment.

4.3. Primary cell culturing

Out of 87 received primary lung tumor samples (LT#), four primary spheroid cell lines could be established. These four cell lines could be further passaged. Overall, one third (33.3%) of all primary tumors started to form spheres or contained potentially viable cells for sphere formation in the first few passages, but could not be repeatedly passaged (figure 11). There may be several reasons for this low efficiency, including the possibility that only few CSCs were isolated, or that bacterial contamination of the primary tumor tissue occurred or cells were lost due to concomitant permanent media change in order to proceed against the bacteria. In the beginning, cells were exclusively cultured under non-adherent and serum free conditions (designated as LT#s). As a secondary goal cells were also cultured in adherent conditions (designated as LT#a) to observe the behavior of cells under differentiation conditions.

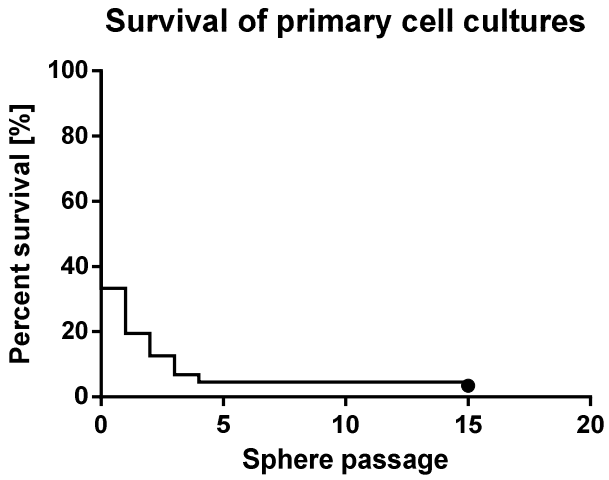

Figure 11. Primary cell culturing survival rate: After cell isolation, the condition of the culture was examined and recorded daily. The survival of all lung tumor samples was documented and summarized in this survival graph.

The *in vitro* behavior was different among the 4 patient samples, which are pictured in figure 12. In detail, LT8s cells were rarely able to proliferate, when they were cultured in adherent conditions with FBS, and passaging of the cells was not possible. No further experiments could be done with LT8a cells. The spheroid structure of LT8s cells was rather loose. Under the microscope, single cells that built up the spheroids could be observed. In contrast, LT22s spheres were compact with a well-rounded smooth border. These spheres were the most rapidly growing. In the first few passages, viable single cells also appeared next to the spheroids. Thus, we also initiated an adherent culture under FBS condition (LT22a). The LT22a culture was the first of all patient-derived tumors, to be successfully cultured under

adherent conditions as well. This adherent cell culture was fast growing and contained a large proportion of spindle-shaped cells which were not able to reach 100 % confluency. These cells showed various shapes and sizes and displayed loose contact with neighboring cells. In the LT39s culture, a lot of single cells which proliferated very fast, were present. Spheroids evolved only from a low percentage of cells within the culture flask and were loosely packed. After 9 passages in spheroid cultures, an adherent culture (LT39a) was also initiated. Cells had different shapes and sizes and grew fast.

The last spheroid culture was generated from LT67. The morphology of these spheres was comparable with LT22s cells, and these were also fast-growing and compact. The media of these cells quickly changed from orange to yellow when compared to other cell lines, indicating high nutrient consumption and fast metabolic activity of LT67s cells. Adherent cells were established at passage 3 and their media consumption was also fast. Morphological differences could already be perceived in the pictures and were further characterized with immuno-staining methods and gene expression analysis.

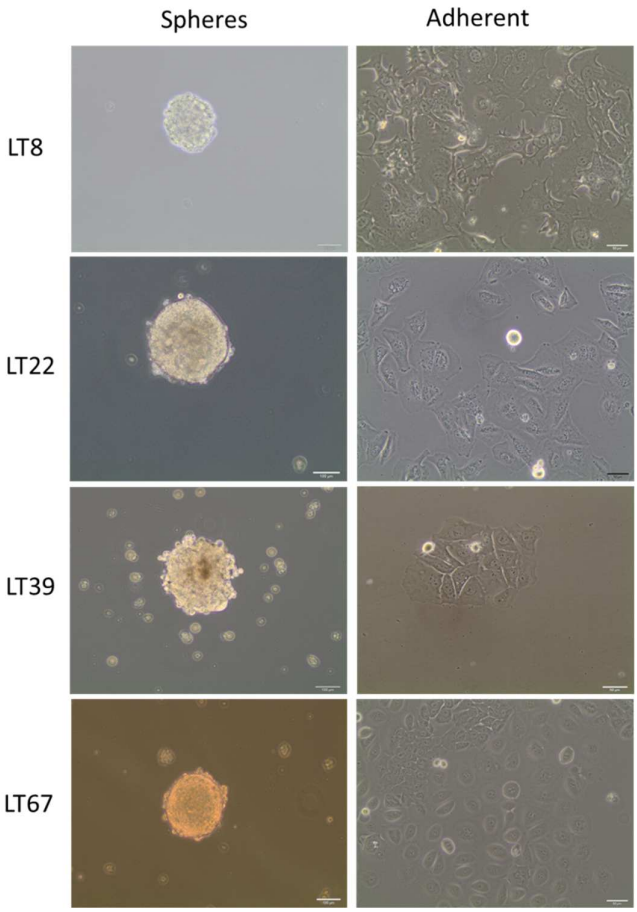

Figure 12. Morphology of long-term cell cultures from four primary lung adenocarcinomas: Representative pictures of the morphology from patient-derived cell cultures. (Left panel) Cells

under non adherent serum free conditions and (Right panel) cells under adherent condtions. Pictures were taken with a Zeiss light microscope. Measuring bar indicates 100 µm.

4.5. Characterization of patient-derived lung cancer cells

Gene expression and protein profiles of the primary cell cultures were evaluated. With immunofluorescent staining, we could categorize the cells into epithelial or mesenchymal phenotypes and determine the expression of CSC markers. The subsequent flow cytometry analysis was performed to evaluate CSC marker expression, as shown below. Additionally, qRT-PCR was performed to validate the results generated by immunostaining.

Immunofluorescent staining was performed on entire spheres on adhesion slides and adherent cells grown on chamber slides. With this technique, the morphology of the cells was preserved well. Spheroids and adherently grown cells were stained with the selected EMT and CSC markers as described. The expression of primary cells was evaluated and compared between different culture conditions and to the FFPE primary tumor tissue, which was stained with immunohistochemistry.

4.5.1. LT8 characterization

Characterization of LT8a cells was not possible, due to minimal proliferation under adherent conditions. The LT8 primary tumor was histopathologically classified as AC and this could be verified with a positive CK7 staining of LT8s cells. The epithelial origin of LT8s cells was confirmed by positive ECad staining and 95% positivity of EpCam with FACS analysis. In addition, these cells did not express Vim. ALDH1 expression was rather poor with only 1.8% detected with FACS. qRT-PCR could not be performed, because as mentioned earlier, we were not able to isolate enough RNA from LT8a cells due to the limited proliferation of these cells.

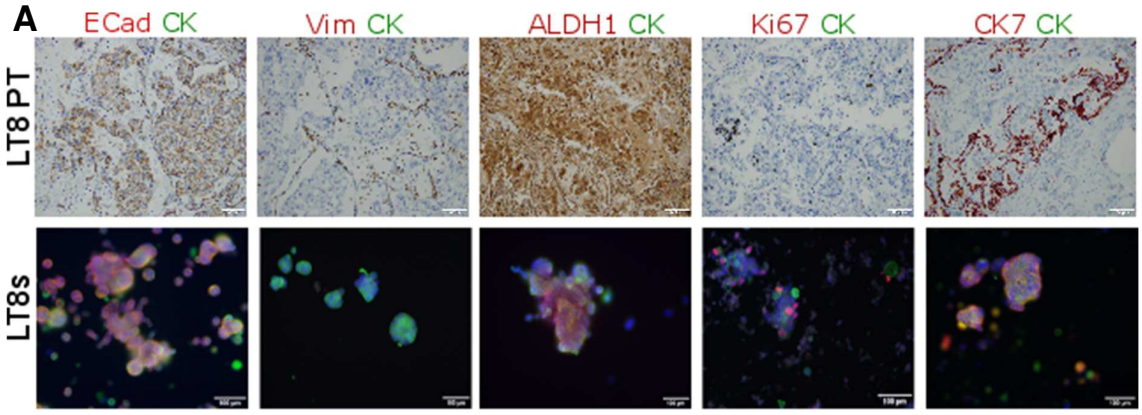

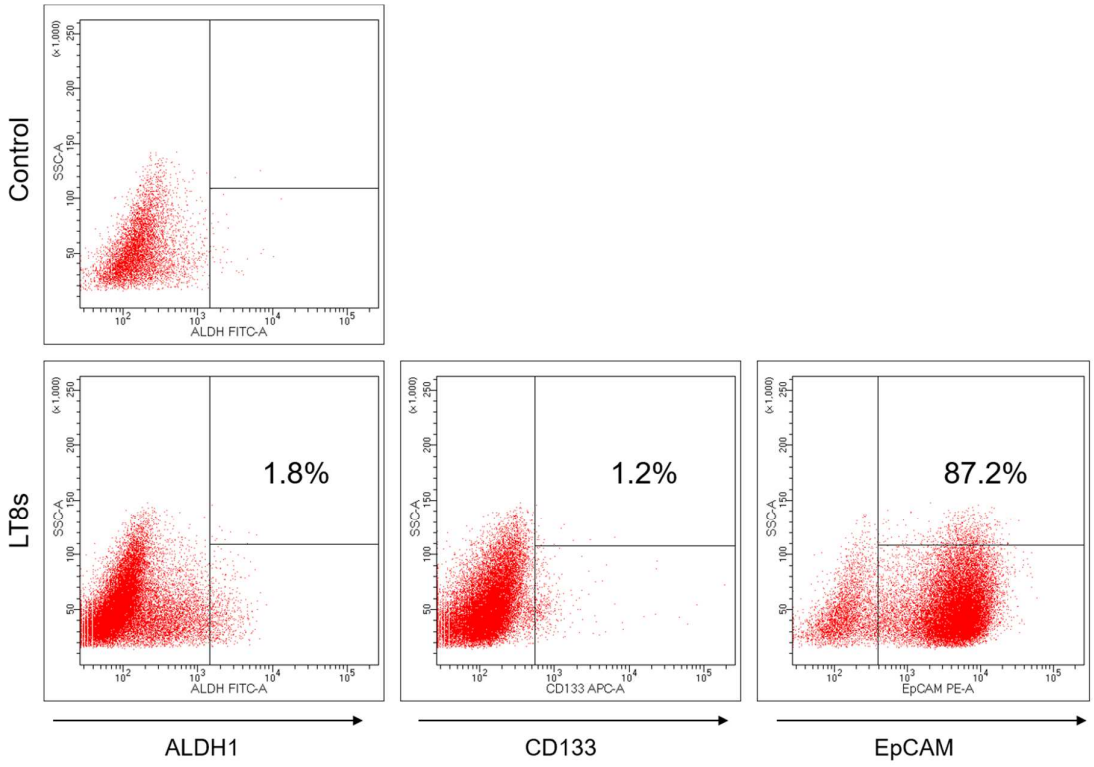

Figure 13. Characterization of LT8 cells and primary tumor: (A) Upper row shows representative pictures of LT8 primary tumor stained with IHC staining. Brown areas show expression of the corresponding protein. Lower row, LT8s cells stained with multi-color immunofluorescence for ECad, Vimentin, ALDH1, Ki67 and CK7 (all red) and CK (green), counterstained with Dapi (blue). All measuring bars depict 100 µm. (B) Dot plots from FACS analysis: upper row, DEAB control for Aldefluor assay; lower row, LT8s cells stained with ALDH1 CD133 and EpCam.

4.5.2. LT22 characterization

The expression of selected markers in the cell culture was compared to the FFPE of the corresponding primary tumor. For evaluation of primary tumors, only IHC was used, in order for better orientation within the tissue sample.

The IHC staining of the primary tumor LT22 revealed the following characteristics summarized in figure 14: the tumor was diagnosed as an adenocarcinoma with positive staining for CK7, but negative for TTF1. In the analysis of EMT markers E-Cad, staining was positive, whereas Vim and alpha smooth muscle actin (alpha-SMA) were negative. There were few single cells which stained positive for the EMT transcription factor Snail. With 60% of cells positive for Ki67, the primary tumor was highly proliferating. Furthermore, both CSC markers ALDH1 (40%) and CD133 (20%) were expressed in the primary tumor.

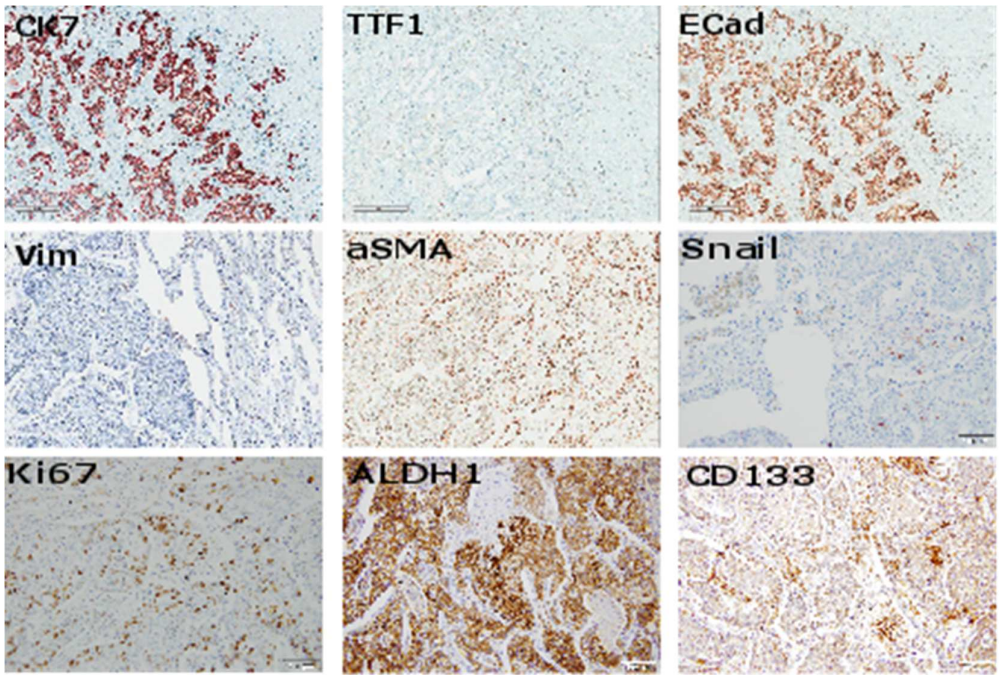

Figure 14. IHC staining of primary tumor LT22: Sections from FFPE blocks were stained for various CSC, EMT and AC markers. (84)

Similar comparative marker analyses were performed in LT22s and LT22a. In LT22s, 80% of cells expressed the cancer stem cell marker ALDH1 with IF and 10% of cells were CD133 positive with IF, and 87,6% could be detected with FACS in figure 16. Therefore, the CSC fraction in LT22s cells was more enriched with ALDH1 positive cells compared to the primary tumor (70% versus 40%). In LT22a cells, on the other hand, neither ALDH1 nor CD133 expression could be detected. Additional staining was performed to further characterize LT22s and LT22a. The expression of representative epithelial and mesenchymal markers was performed. Epithelial markers, including ECad, HEA, panCK, and in particular CK7 were clearly positive in LT22s. In contrast, in LT22a, a weak expression of epithelial markers could be detected, with only few cells positive for CK7 (10%) (figure 15). The mesenchymal marker Vimentin was expressed in 90% of LT22a cells. Therefore, the staining profile of LT22a cells revealed a mesenchymal phenotype which was not comparable with the primary tumor sample. The high proliferative rate (Ki67 staining) seen in the primary tumor was sustained under both culture conditions LT22s and LT22a, with up to 60% of cells positive for Ki67 respectively. These results were summarized in figure 15 and 16. (84)

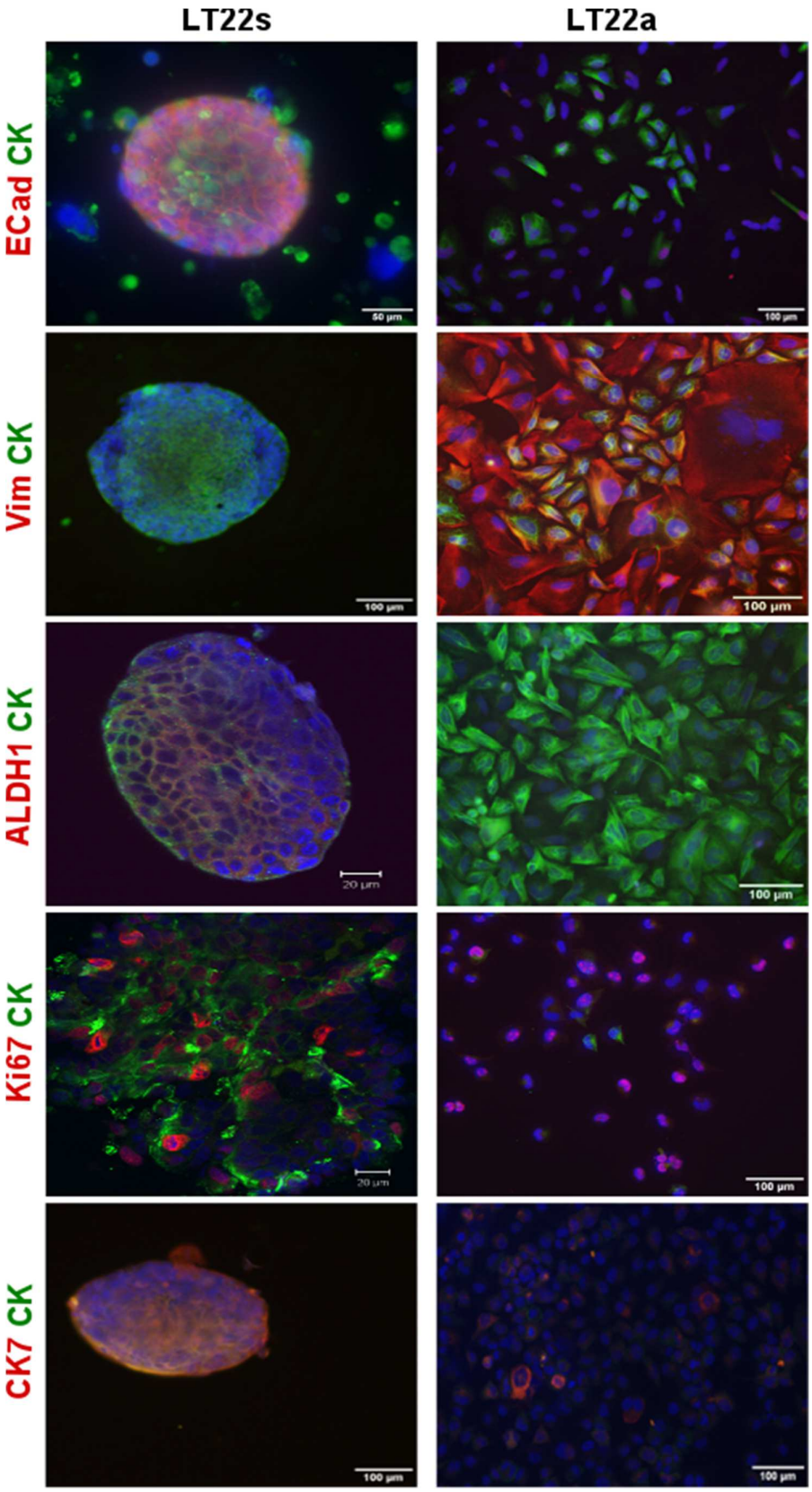

Figure 15.Characterization of LT22 cells with immunofluorescent staining: (Left panel) LT22s and (right panel) LT22a cells were stained for ECad, Vimentin, ALDH1, Ki67and CK7 (all red) and panCK

(green) protein expression and counterstained with Dapi (blue) for nuclear localization. Measuring bars 20-100 µm. (84)

Results from qRT-PCR supported the results of the immunostainings. An increase of CD133 expression in LT22s cells over passages could be observed, as shown in figure 17. Although ALDH1 gene expression decreased over passages, it was still prominent at the protein level. Concordantly; ECad mRNA levels were also upregulated. We did not detect any expression of mesenchymal markers or EMT transcription factors in LT22s.

In concordance with the immunostaining results, no mRNA expression of the cancer stem cell markers ALDH1 and CD133 could be detected in LT22a cells. While there was no detectable ECad expression, mesenchymal markers such as Vimentin, NCad and Fibronectin were increased. EMT transcription factors, including Slug, Snail, Twist, Zeb1 and Zeb2, were upregulated at the mRNA level (figure 17). These findings once more underline the LT22a cells´ mesenchymal phenotype which could not be found within the primary tumor. (84)

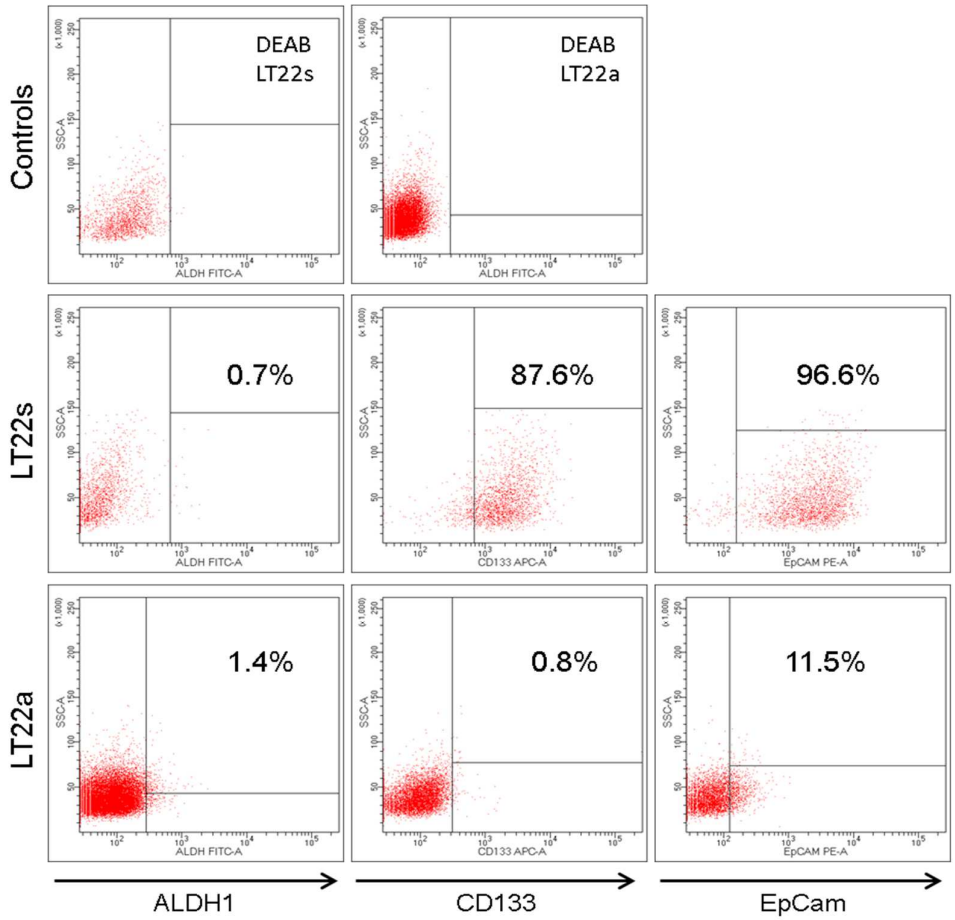

Figure 16. Characterization of LT22 cells with flow cytometry: Representative dot plots (upper row) DEAB controls from aldefluore assay, (middle row) LT22s cells and (lower row) LT22a cells stained for ALDH1, CD133 and EpCam. (84)

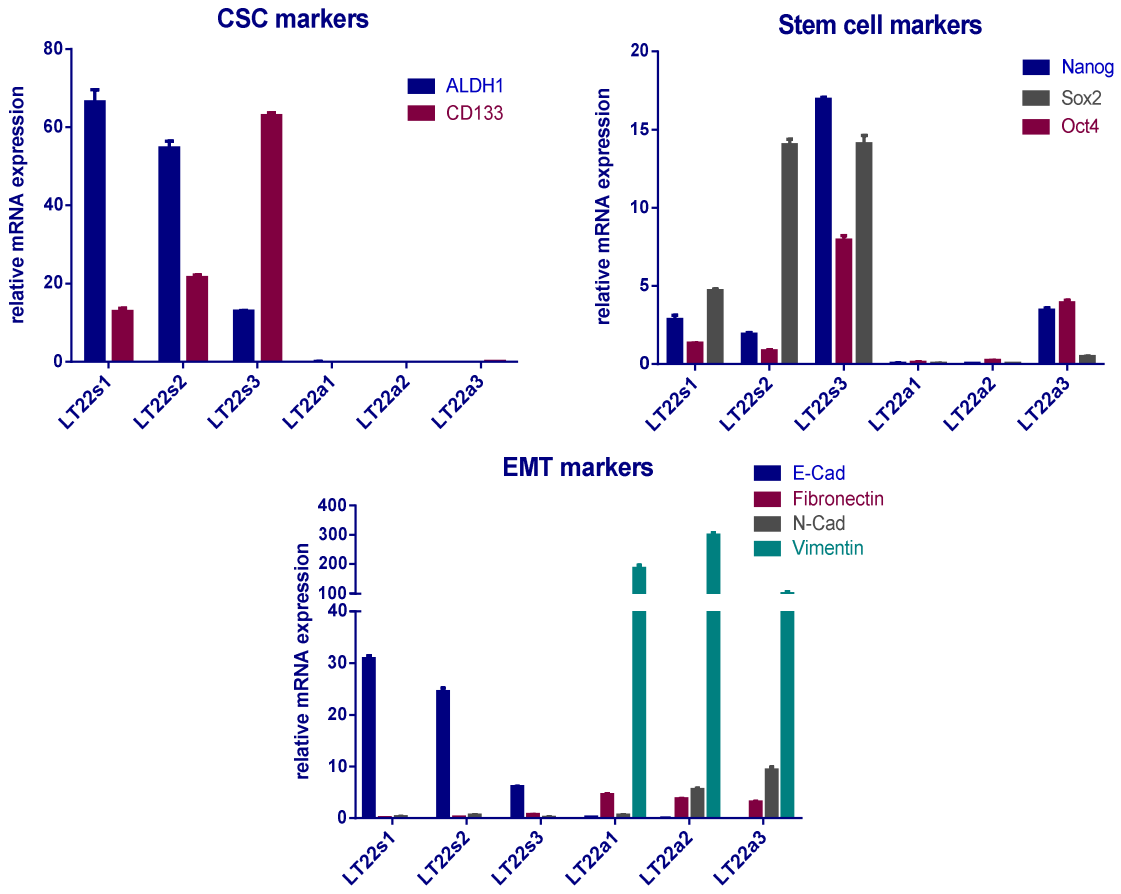

Figure 17. Gene expressions analysis of LT22 cells: Expression of genes related to CSCs and EMT were evaluated in three different passages of LT22s (LT22s1-s3) and LT22a (LT22a1-a3) cells. mRNA expression was calculated with the ΔCt-method normalized to the house-keeping genes GAPDH and TBP und summarized in bar graphs (mean+/-S.D.). (84)

Finally, stem cell associated markers Oct4, Sox2 and Nanog were analyzed by qRT-PCR (figure 17). These markers were upregulated in LT22s, with a subsequent increase over passages. There was little to no expression of these stem cell markers in LT22a.

Taken together, these results confirm the epithelial and stem cell associated phenotype of LT22s cells and the mesenchymal phenotype of LT22a cells at the mRNA and at the protein levels. These results are also consistent with the morphologic characteristics of the two cell populations. (84)

4. 5. 3. LT39 characterization

LT39s cells are very interesting because, as shown in the middle column of the figure 18, many cells under spheroid culture conditions remain single cells rather than spheres. LT39 cells appear with intensive Ki67 staining in all culture conditions and in the primary tumor. This is reflected in the high proliferation rate of these cells in suspension. Some of these

cells were enormous in adherent culture compared to other cells, which can be seen in the Ki67 and CK7 staining in figure 18. A follow-up examination revealed that the AC, characterized by positive CK7 staining was associated with a pleomorphic carcinoma, with giant cells as their specific histological characteristic. Both LT39s and LT39a cells show a strong epithelial phenotype characterized by a bright ECad and CK staining and the lack of Vimentin staining. The CSC marker ALDH1 is scarcely expressed among LT39 samples. Tumor cells in the primary tumor sample showed weak expression of ALDH1 because the tumor cells appeared to be darker as the surrounding cells, but LT39 cells in culture did not show positive staining of ALDH1.

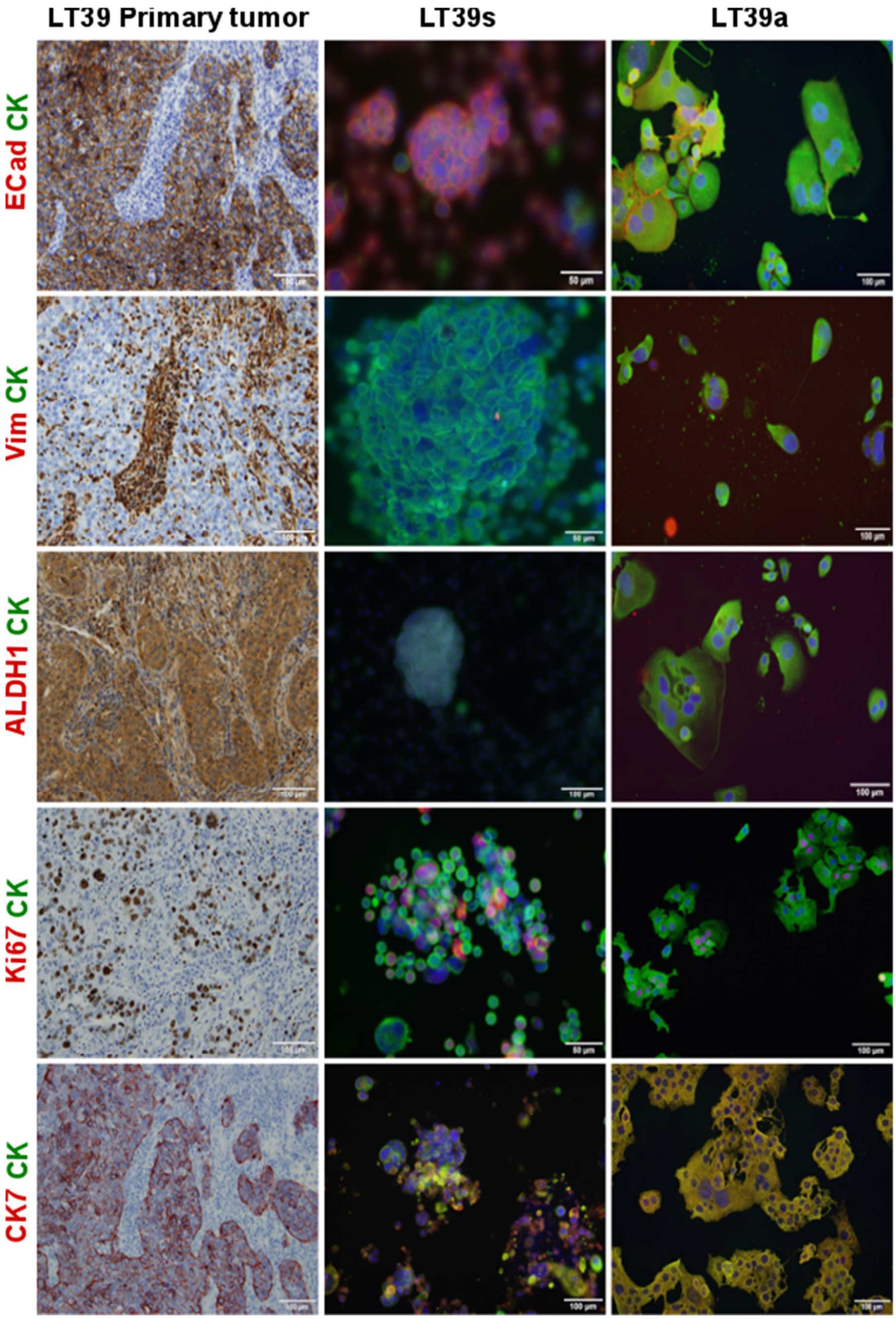

Figure 18. Characterization of LT39 sample with immunostaining: (left column) LT39 primary tumor stained with IHC method, (middle column) LT39s cells and (right column) LT39a cells with immunofluorescence staining. Cells were stained for ECad, Vimentin, ALDH1, Ki67 and CK7 (red),

panCK (green) and counterstained with Dapi for nuclear localization. Measuring bar depicts 50-100 µm.

The immunofluorescence results could be confirmed with qRT-PCR. ECad was increased in all passages of both conditions, whereas Vim and EMT transcription factors Slug and Snail were scarcely expressed. Additionally, stem cell markers were also rarely expressed. Oct4 is the only marker that was increased in LT39a cells. These results suggest an epithelial phenotype of LT39 cells with CD44 expression as a potential CSC marker.

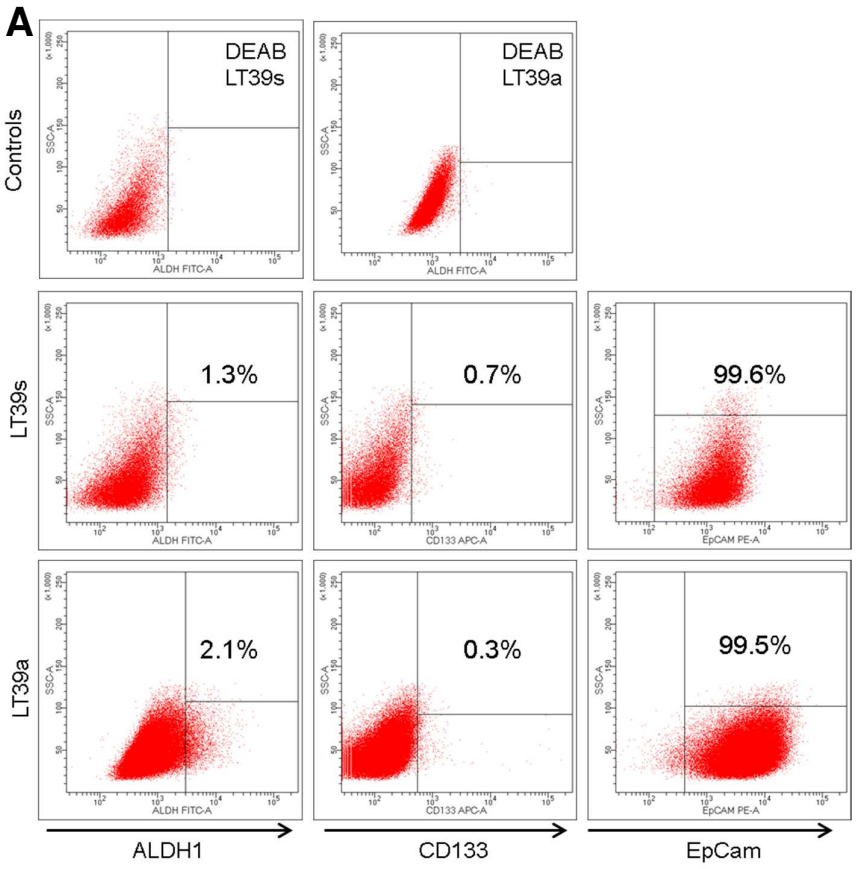

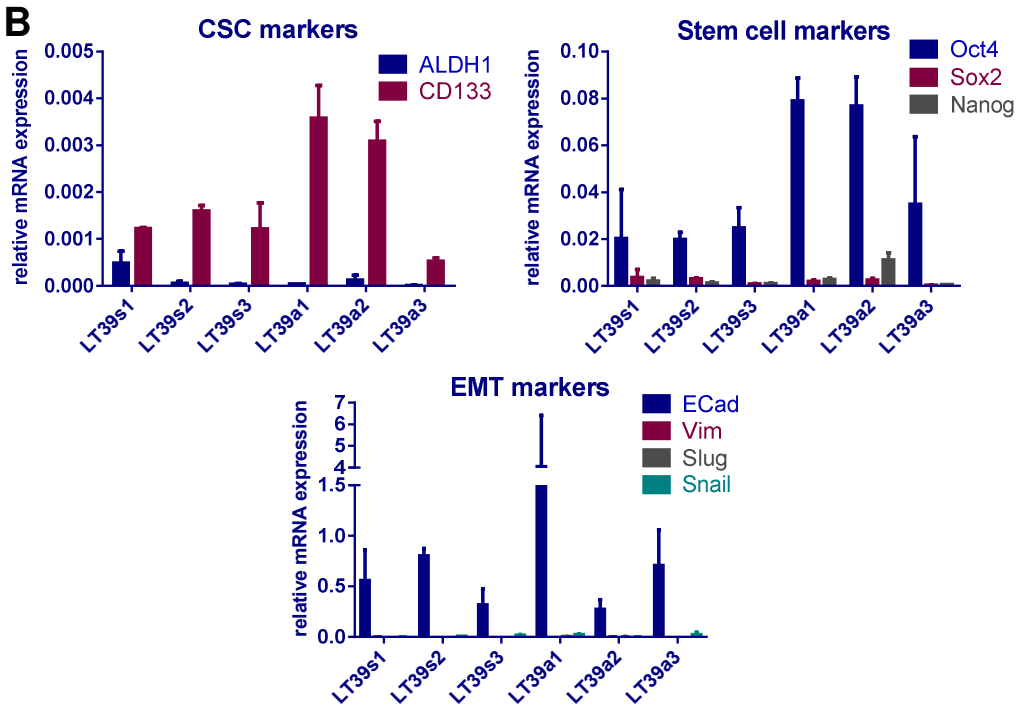

Figure 19. Characterization of LT39cells: (A) Representative dot plots of flow cytometry results. (Upper row) DEAB controls from Aldefluor assay, (middle row) LT39s cells and (lower row) LT39a cells stained for ALDH1, CD133 and EpCam. (B) Gene expression analysis of CSC and EMT markers in three passages of LT39s (LT39s1-s3) and LT39a (LT39a1-a3) cells. mRNA expression was calculated using the ΔCt-method relative to house-keeping genes GAPDH and TBP.

4.5.4. LT67 characterization

The primary diagnosis of LT67 at the time of surgery was AC, but after re-evaluation of the resected primary tumor by the pathologist, it was diagnosed as a squamous cell carcinoma (SCC). The negative CK7 staining in figure 20 also excluded the classification as an AC. An additional staining of p40, a common SCC marker, in suppl. figure 3 confirmed the SCC subtype. Although LT67 was isolated from an SCC, it shared some features with an AC tumor sample. The epithelial origin of this cancer type is also reflected in the positive ECad and CK staining. In contrast to the other tumor cell lines, cultured LT67 cells also have some single Vimentin positive cells, a finding which was also confirmed with qRT-PCR data (figure 21 B). Some single cells within the primary tumor areas also showed positive Vimentin staining. The CSC marker ALDH1 was not prominent in the primary tumor sample, but it could be enriched, especially under spheroid conditions, which is seen in the immunofluorescent staining and in the FACS analysis, with 11.2% of LT67s cells positive for ALDH1, as shown in figure 21 A. Similarly, to the other tumor samples, LT67 had a high Ki67 expression of 30%. A difference in CD133 expression in 53.1% of LT67s cells compared to 0.9% of LT67a cells could not be confirmed with qRT-PCR results.

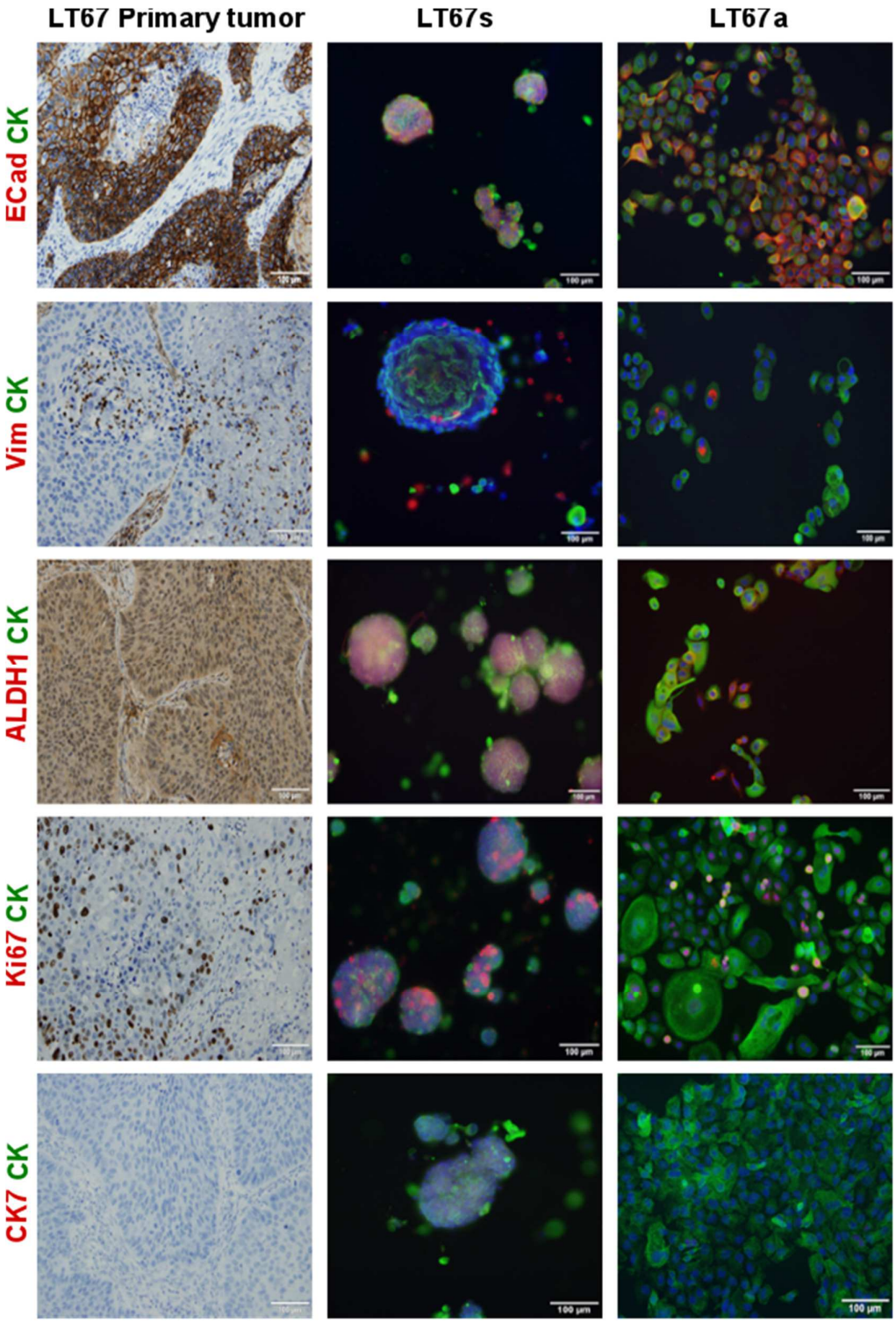

Figure 20. Characterization of LT67 tumor samples with immuno staining: Representative pictures of an LT67 primary tumor stained with IHC (left column), LT67s cells (middle column) and LT67a cells stained with multicolor immunofluorescence (right column). Cells were stained for ECad, Vimentin, ALDH1, Ki67 and CK7 (red), panCK (green) and counterstained with Dapi for nuclear localization. Measuring bar depicts 100 µm.

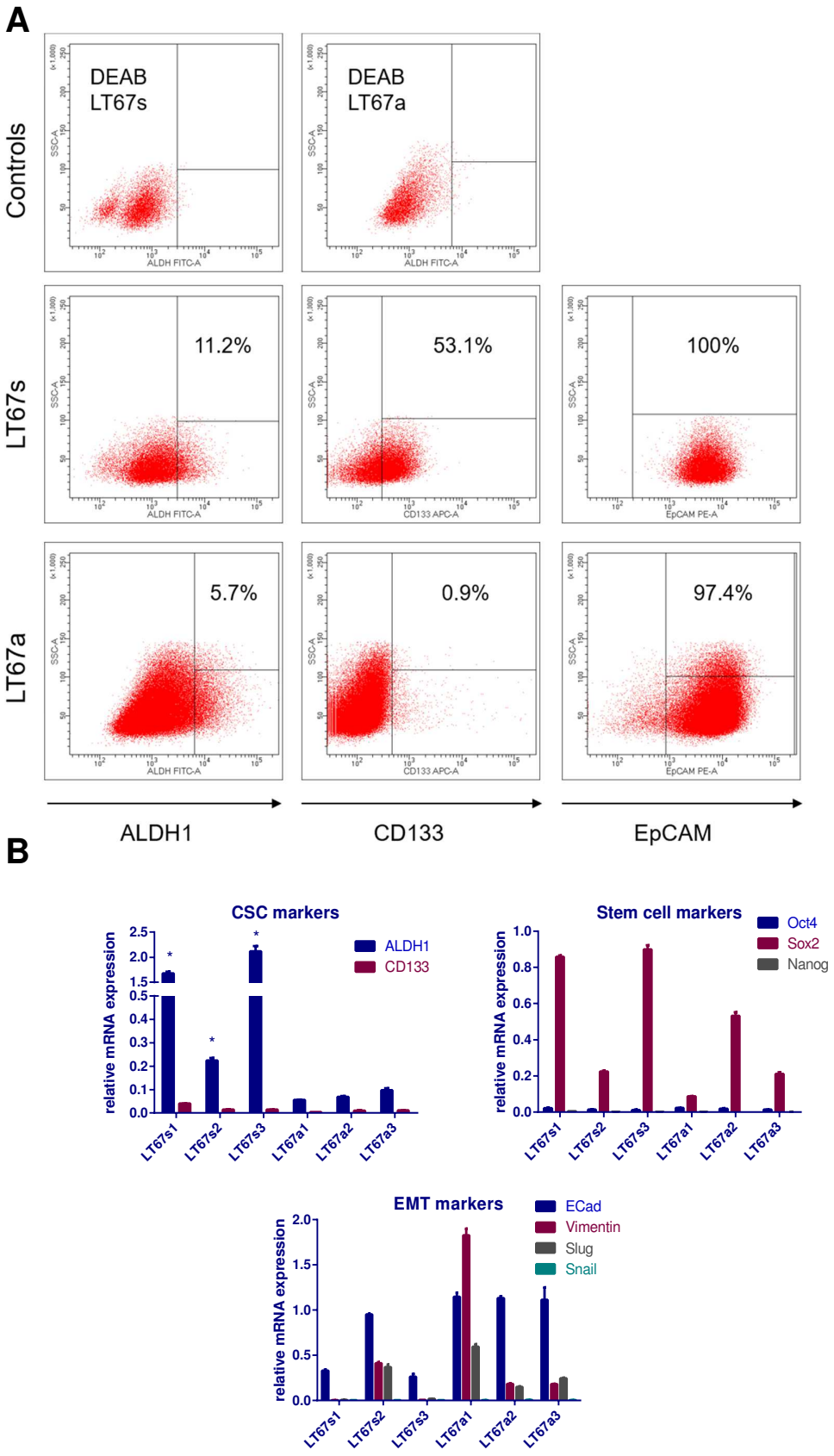

Figure 21. Characterization of LT67 cells: (A) Representative dot plots of flow cytometry results. (Upper row) DEAB controls from Aldefluor assay, (middle row) LT67s cells and (lower row) LT67a

cells stained for ALDH1, CD133 and EpCam. (B) Gene expression analysis of CSC and EMT markers in three passages of LT67s (LT67s1-s3) and LT67a (LT67a1-a3) cells. mRNA expression was calculated using ΔCt-method relative to house-keeping genes GAPDH and TBP.

4.6. CNV- sequencing for genomic characterization

After phenotypic characterization of the 4 long-term cultures was completed, we investigated their copy number profile using low-coverage whole genome sequencing. Copy number profiling of cultured cells should verify their tumorigenic origin and identify possible driver gene mutations. Additionally, the leukocyte fraction and the FFPE of the primary tumors were analyzed and compared. In all adenocarcinoma samples, including LT8, LT22 and LT39, several recurrent somatic copy number aberrations (SCNA) were detected in the primary tumors (figure 22 A, B and C) and in the corresponding primary cell cultures, such as the amplifications on chromosomes 1q, 7, and 8, and deletions on 3p, 4p, 8p and 13 that are frequently observed among lung adenocarcinoma (105, 106). These multiple aberrations suggest dysregulations of biological functions and confirm tumorigenic potential. It is of note that aberrant regions were less prominent in the primary tumors than in the cultured cells. First of all, sequencing of FFPE material is challenging, due to poor DNA quality after isolation, which results in a lower signal to noise ratio. Minor amplifications and deletions are difficult to identify from these archival specimens. Additionally, FFPE material contains a heterogeneous cell pool, whereas under cell culture conditions, we enriched a certain subpopulation, leading to a more prominent signal. Some medium-represented signals may remain undetected.

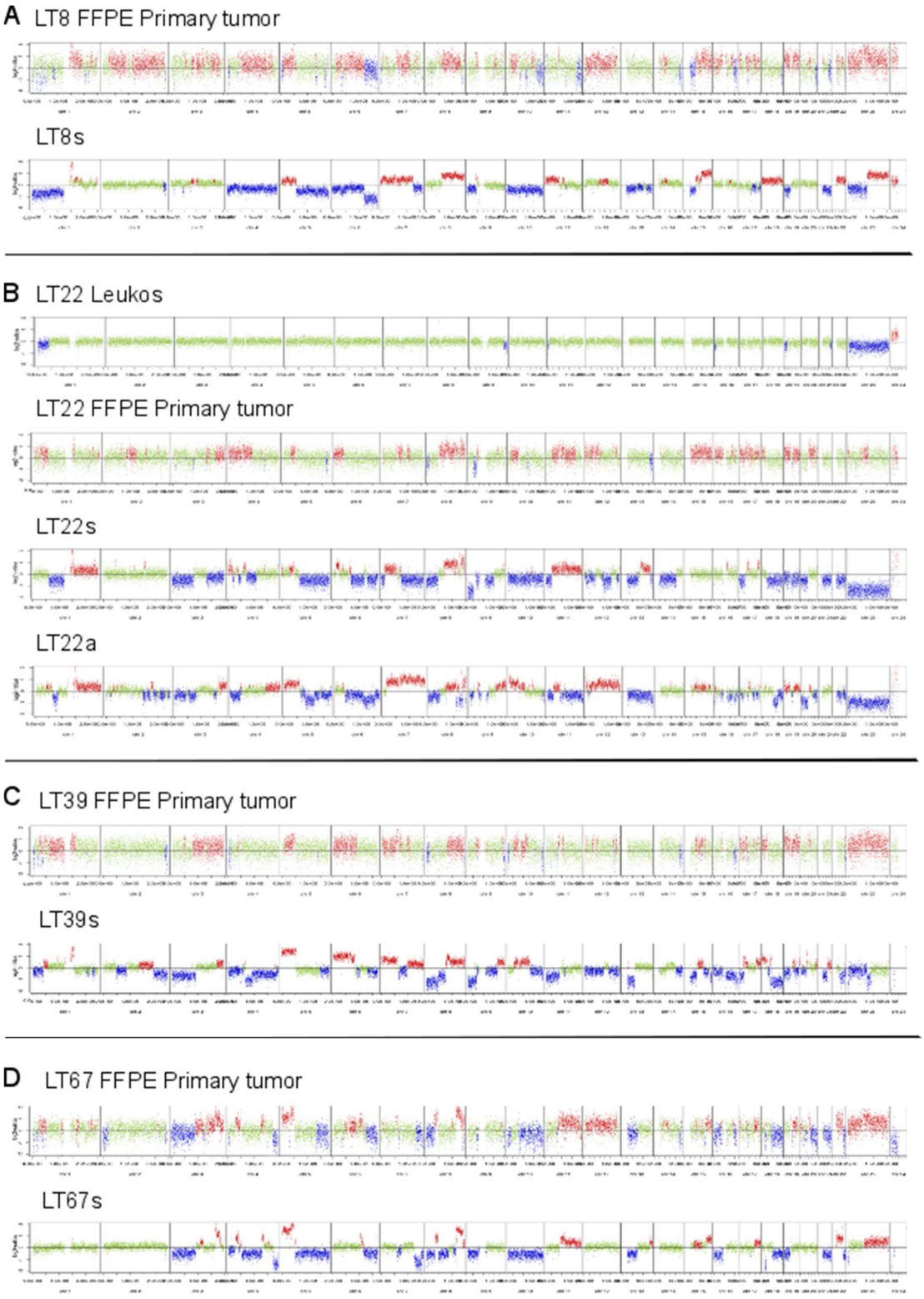

Figure 22. CNV-profiles from low coverage whole genome sequencing on Illumina MySeq: Depicted are segmented log2-ratio plots. The X- and Y-axes indicate the chromosome and the log2-ratios, respectively. Red areas show amplifications of a gene region, lost regions are blue, and green indicates balanced segments.

The initial idea was to find distinct abnormalities in the genome profile of CSC subpopulations, as defined by phenotypic CSC markers. However, when we analyzed the two LT22 cell populations after cell sorting based on CD133 expression for LT22s and EpCam expression for LT22a, we did not observe any difference between the two cell fractions. This finding may indicate that the expression of these markers is driven by mechanisms other than SCNAs, such as point mutations and regulatory mechanisms at the transcriptional level. Therefore, we did not continue to sort for CSC markers and perform further genomic profiling with this approach. Interestingly, the SCNA patterns of LT22s compared to LT22a were also dissimilar, indicating that substantial chromosomal alterations contribute to the different phenotypes. The most prevalent differences included 2q, 4p, 6p, 7q, 8q, 9p, 10p, 11, 13q and 20q. (84)

Correspondingly, LT67 genetic profiles also exhibited common SCNAs for SCC, found at chromosome 3q and 8q, as seen in figure 22 D. In more detail, significant aberrations of oncogenes, including Sox2 on position 3q 26, MYC on position 8q24 and CCND1 on position 11q13 could be detected in LT67 sample. (107)

4.6.1. Authentication of established cell line origins

4. 6. 1. 1. STR- analysis

The comparison of the number of repetitions from different microsatellites for LT8, LT22, LT39 and LT67 are listed in their respective tables (table 9 and 10). The repetitions of STR Loci in LT8s cells were in concordance with the primary tumor FFPE sample. Leukocytes and DNA from the primary FFPE tumor were identical to those from LT22 samples. Additionally, LT22s and LT22a shared most of the repetitions, but under culture conditions, some of these were lost. The loss of the Y chromosome was already known because it occurs rather frequently. (108) In 9 further STR loci of LT22s and LT22a DNA, one repetition of the microsatellite is missing when compared to LT22 leukocytes. Detailed evaluation of the CNV profiles (figure 22) revealed that the area of 8 STR loci was found to be underrepresented in the genome of the cells in culture and might have been lost.

Also, LT39s cells were comparable with LT39 leukocytes. 5 repetition numbers were not present, which also might have been lost during the cell culture. The results from LT8, LT22 and LT39 showed a clear concordance with the corresponding leukocytes and therefore, contaminations with other cell lines or other patient material could be excluded. However, the number of repetition of 3 loci was different in LT67s cells compared to the reference material. According to the CNV profile, all three loci were located in a deleted region of LT67s genome. Based on this nonconformity, profiles were also compared with mtDNA method.

Table 9. STR analysis results from LT22.

STR Locus	LT22 Leukos	LT22 FFPE	LT22s	LT22a
D3S1358	16, 17	16, 17	16	16
TH01	6, 7	6, 7	7	7
D21S11	32.2	32.2	32.2	32.2
D18S51	15, 17	15, 17	15, 17	15, 17
Penta E	13, 14	13, 14	13, 14	13, 14
D5S818	11	11	11	11
D13S317	12	12	12	12
D7S820	8	8	8	8
D16S539	12, 14	12, 14	12, 14	12, 13, 14
CSF1PO	12, 13	12, 13	13	13
Penta D	9, 11	9, 11	11	11
Amelogenin	X, Y	X, Y	X	X
vWA	16, 17	16, 17	16, 17	16, 17
D8S1179	11, 13	11, 13	13	13
TPOX	8, 9	8, 9	8	9
FGA	19, 22	19, 22	19, 22	19, 22

Table 10. STR analysis results from LT8, LT39 and LT67 samples.

STR Locus	LT8 FFPE	LT8s	LT39 Leukos	LT39s	LT67 FFPE	LT67s
D3S1358	15,19	15	14, 17	14,17	15,17	15
TH01	7,8	7,8	7, 9	7, 9	9.3	9.3
D21S11	30.2, 31.2	30.2, 31.2	29, 30	29, 30	28,29	31.2
D18S51	15,16	15,16	12, 14	12	14,18	18,19
Penta E	7,10	-	10, 17	10	17	12,17
D5S818	12	12	10, 12	10, 12	11,13	11
D13S317	11,13	11,13	10, 14	14	8,11,12	8,11,12
D7S820	10,12	10,12	8, 12	8, 12	10,11	12
D16S539	10,12	10,12	12	12	13	12,13
CSF1PO	10	-	10, 12	10, 12	11	11
Penta D	12,13	-	13	13	9,13	13
Amelogenin	X, Y	X, Y	X, Y	X	X, Y	X
vWA	15,17	15,17	17, 18	18	16,18	16,18
D8S1179	12,15	12,15	10, 13	10, 13	10,15	13
TPOX	8	8	8, 11	8, 11	8,9	8,9
FGA	24	22,24	21, 25	25	20,24	24

4. 6. 1. 2. mtDNA analysis

With the CNV profile results, we were also able to extract mtDNA data and compare each data set from samples in the culture with the corresponding primary tumor. mtDNA analysis is based on the same principle as STR analysis, but it focuses on regions of the circular mtDNA strand. We performed this analysis as a second method for authentication of the established cell lines, because STR profiles in LT67 gave equivocal results. Suppl. Figure 2 shows the mtDNA profile of LT22s and LT22a. The colored lines show different mutants, which should match within the same individual. This was true for all LT22-derived cells. LT8, LT39 and LT67 samples were summarized in a circular graph as seen in figure 23. In this case, the red lines indicate the mutants and the pattern matches in LT8 and LT67 culture

cells and primary tumors, respectively. However, LT39 variants did not match between FFPE and cell culture DNA material. A lot of grey areas in the mtDNA profile of the FFPE sample could be evidence of poor DNA quality.

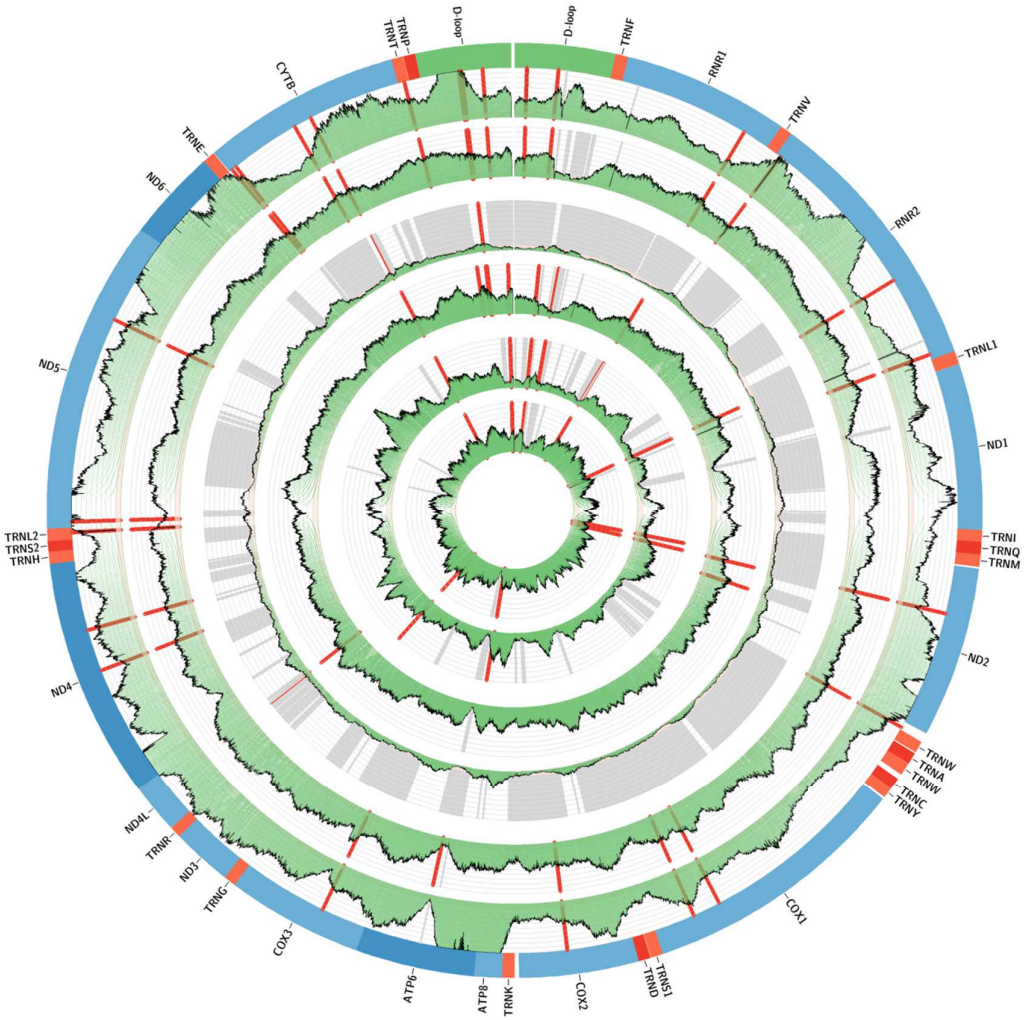

Figure 23. Circular presentation of mtDNA analysis: (From outer ring to inner ring) LT8 FFPE, LT8s; LT39FFPE, LT39s; LT67FFPE, LT67s. Red bars indicate mutants, green areas show the coverage of the mtDNA sequence, grey areas are regions were no prediction is possible.

4.7. *In vitro* assays

All assays were performed with sorted and unsorted cells from all primary cell cultures. Surprisingly, unsorted cells were more likely to form spheres/colonies, suggesting that cell sorting is a potential stressor for cells (data not shown). All primary cell lines were initially tested for their marker expression, which were depicted in the dot plots of the respective

cell lines. According to these results we chose the marker of interest and sorted the cells for subsequent *in vitro* assays. The percentages of the individual subpopulations which were seeded again for *in vitro* assays are summarized in table 11. Since some marker expressions changed with advancing passages, some experiments could not be repeated.

Table 11. CSC marker expression [%] taken as sorting proportion for *in vitro* assays.

	CSC marker	
	EpCam +	**EpCam -**
LT22a	13.3%	75.7%
	22.9%	70.6%
	13.9%	70.0%
	CD133 +	**CD133 -**
LT22s	10.3%	85.9%
	21.4%	70.9%
	18.9%	58.8%
LT67s	30.6%	36.7%
	ALDH1 +	**ALDH1 -**
LT39s	4.4%	86.4%
LT39a	2.2%	87.8%

4.7.1. Colony formation assay

Only LT22a cells could be used for colony formation assay. After sorting, cells from other samples neither attached nor proliferated. LT22a colony formation efficiency was comparable in $EpCam^+$ and in $EpCam^-$ subpopulation (figure 24) suggesting that EpCam is a cancer cell marker, but not a CSC specific biomarker.

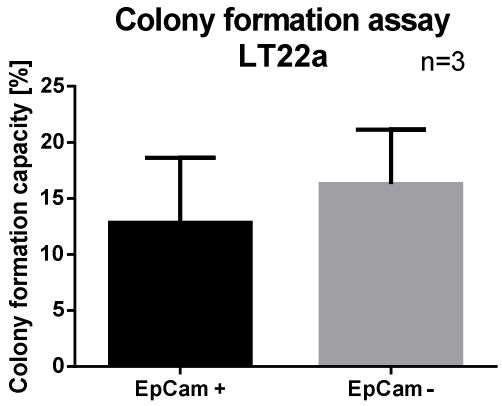

Figure 24. Colony formation assay: LT22a EpCam sorted subpopulations were seeded into 6-well plates. Formed colonies were counted and relative amount compared to seeded cells were summarized in this bar graph. (84)

4.7.2. Sphere formation assay

A sphere formation assay was used to evaluate the ability of self-renewal in enriched cancer stem cells. A low number of cancer cells was seeded into 6-well plates. Additionally, where possible, sorted cells were also evaluated for the sphere formation assay. Cells were sorted according to table 10. LT22s and LT67s cells were sorted for the cancer stem cell marker CD133. Both showed a significantly higher sphere formation capacity of cells expressing $CD133^+$ (figure 25 A and D) compared to $CD133^-$ cells (p-value < 0.05). LT39s and LT39a cells were sorted for ALDH1, but no significant differences in their sphere forming capacity could be observed between ALDH1 positive and negative populations (figure 25 B and C), only a slight trend towards a higher sphere-forming efficiency of ALDH1 positive, as shown in figure 25 B. Repetition of the experiments would have made these results more relevant, but due to the change in CSC marker expression, we could not confirm the data.

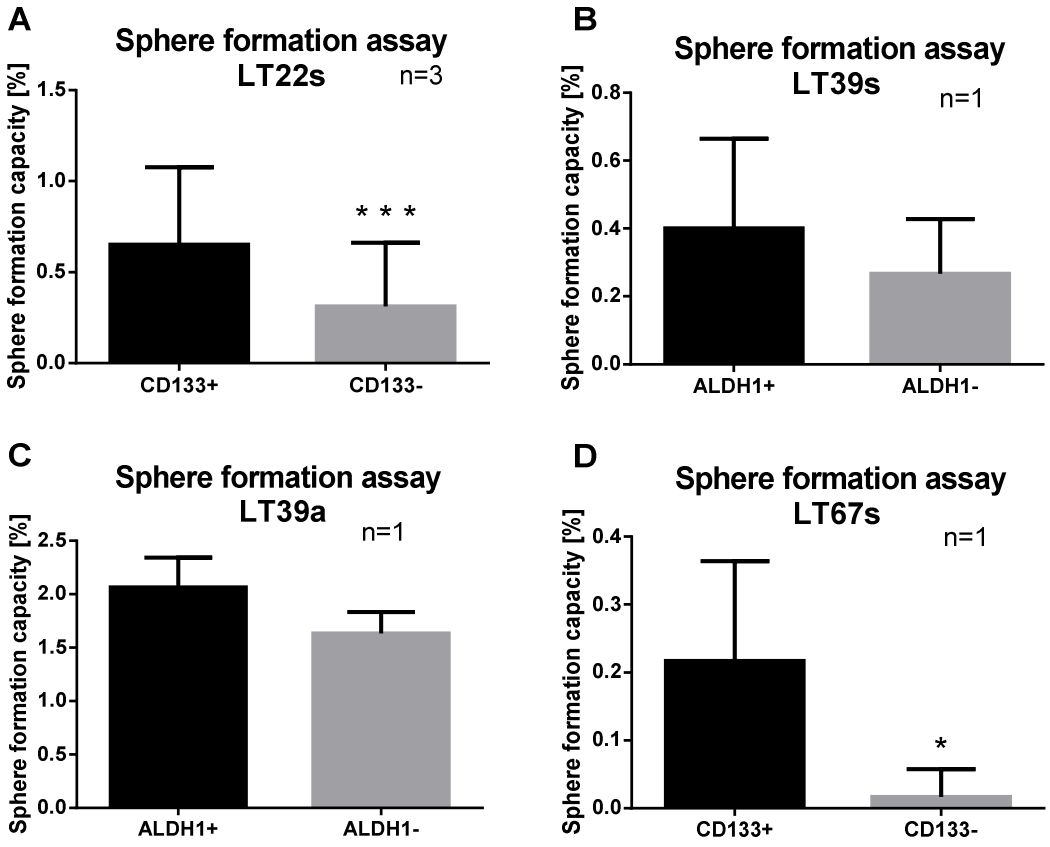

Figure 25. Sphere formation assay: Cells from primary cell culture were sorted according to their CSC marker expression. (A) LT22s cells (84) and (D) LT67s cells were sorted for CD133 expression, and (B) LT39s cells and (C) LT39a were sorted for ALDH1 subpopulations. Generated spheres ≥50 µm were counted and sphere formation capacity was calculated relative to the seeded cell number.

4.7.3. Soft agar assay

In LT22a cells we investigated whether the expression of EpCam had an influence on their ability to form colonies in soft agar conditions. However, both $EpCam^+$ and $EpCam^-$ subpopulations formed colonies to a similar extent (figure 26 A). LT22s cells sorted for CD133, on the other hand, formed significantly more colonies in soft agar, in their CD133 positive subpopulation (p-value 0.0001) compared to the CD133 negative cells, as shown in figure 26 B. These results indicate that $CD133^+$ cells have enhanced abilities for anchorage-independent growth.

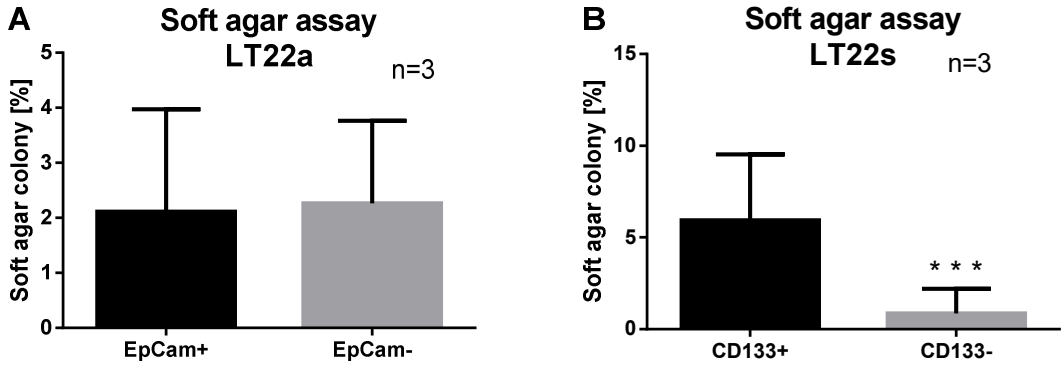

Figure 26. Soft agar assay: (A) LT22a cells sorted according to EpCam expression and (B) LT22s cells sorted according to CD133 expression were seeded into 12-well plates for soft agar assay. Formed colonies were counted and displayed as relative value to the amount seeded. (84)

4.7.4. Migration assay

The migration of cancer cells to distant sites is the initial step for tumor metastasis, which is still the major reason for cancer-related death. CSCs are involved in the migration process. Besides their maintaining functions within the primary tumor, at least some CSC populations have migratory capabilities. (109) Therefore, we evaluated established primary cell cultures for their migration potential using Ibidi chamber dishes with removable chambers. For this assay, we could only use and evaluate the migration potential of the adherently grown cells, which are able to provide a well-defined cell-free gap between two opposite cell fronts. The potential of covering the cell-free area was measured by image interpretation with ImageJ software. Therefore, cells were periodically photographed for 26 hours. Termination of the assay was set according to growing influence of cell division. Examples can be found in figure 27 A and the obtained data was summarized for every cell line in XY-Graphs.

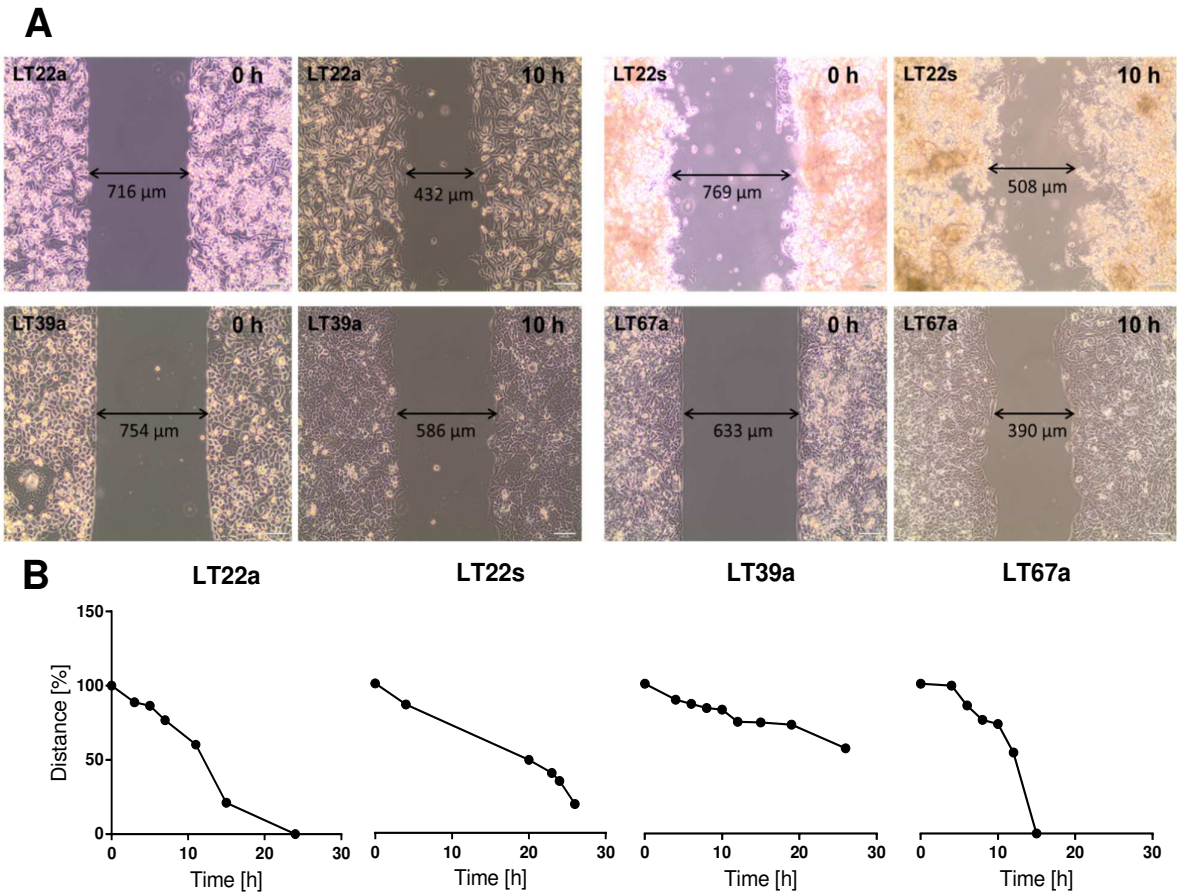

Figure 27. Migration assay: Migration potential was evaluated over time. (A) The pictures show the cells at 0 h and after 10 h. The arrow indicated the gap length and measuring bar is 100 µm. (B) The decreasing gap lengths were plotted against the time to calculate the velocity for each cell line.

First of all, we compared the LT22 cells according to their different culture conditions. LT22a cells were faster-moving than LT22s cells. However, this assay required the LT22s cells to attach and, therefore, the cells were cultured in adherent media. Secondly, we compared all adherent cell cultures to each other and the calculated velocities are summarized in table 12. LT67a cells were the fastest-migrating cells with 16.3 µm/h, whereas LT39a cells had the slowest migratory velocity of 3.95 µm/h.

Table 12. Summary of calculation for migration velocity.

	Linear equation	k	velocity [µm/h]
LT22a	y = -32,263x + 743,3	32.2	16.10
LT22s	y = -21,26x + 765,87	21.3	10.65
LT67a	y = -32,584x + 627,3	32.6	16.30
LT39a	y = -7,902x + 509,91	7.9	3.95

4.8. Chorio-allantoic membrane assay

4.8.1. Invasion assay on CAM

The tumorigenicity and the cultured cells´ ability to migrate and invade were tested in the CAM model, a well-established *in vivo* tumor system. One advantage of this model is its independence from culture conditions, because the cells grow directly in the CAM microenvironment. Cells were applied with $1*10^6$ single cells per on-plant onto the CAM of the chicken embryo to form xenografts. This experiment was performed with LT22s and LT22a cells to compare both cell lines in terms of invasion and migration potential. Based on the interesting results from LT22 cells, we also evaluated LT8s and LT67s cells for their growth behavior within an *in vivo* microenvironment. HE staining of LT8s and LT22s cells showed invasion through the membrane in both cases, indicating invasive potential in both cell types. For the LT22a cells, the tumor consisted of spindle-shaped cells, which infiltrated the membrane. A structural formation could not be observed; the cells arranged randomly around the chicken membrane. The LT8s and LT22s cells also invaded the membrane but formed glandular structures (figure 28), recapitulating the primary lung AC. Additionally, LT67s cells could reinitiate the tumor and form nodular structures, as common in SCC.

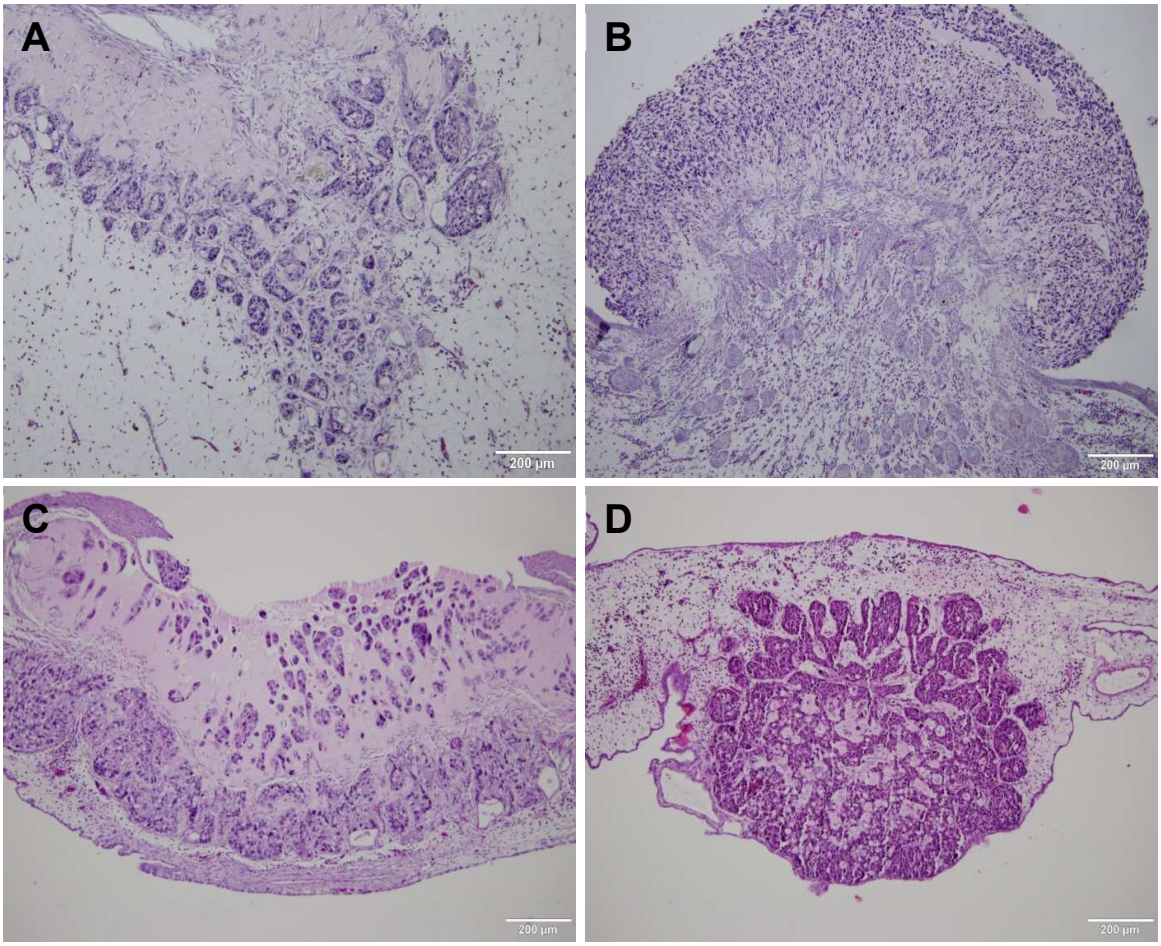

Figure 28. HE staining of CAM xenografts: (A) LT22s, (B) LT22a, (C) LT8s and (D) LT67s cells were seeded in CAM model to form xenografts. After 72h xenografts were removed from the chicken egg and embedded into paraffin. 4 µm sections were HE stained. Pictures were taken with an Olympus BX51 microscope. Measuring bar 200 µm.

Immunostaining revealed that LT22s cell clusters were positive for ECad, ALDH1, panCK, CK7 and Ki67. Vimentin was negative in tumor cells, but stained the mesenchymal cells of the chicken egg. Additionally, LT22a cells stained negative for ECad, panCK and ALDH1. Only few cells stained positive for CK7. Vimentin was positive in all cells. Ki67 was expressed in 60% of the tumor cells (figure 29). These results remained in concordance with the cell culture analysis. (84)

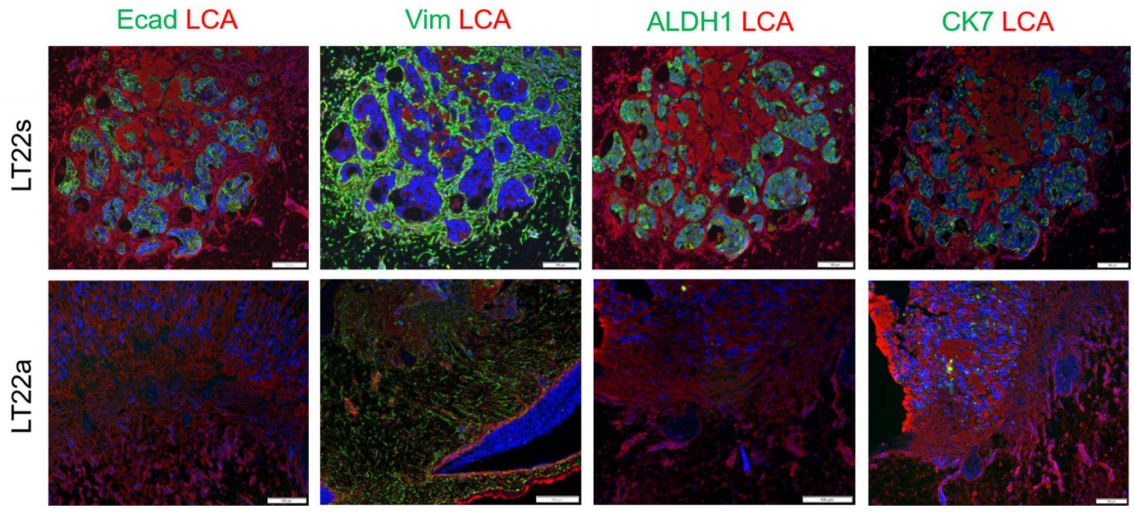

Figure 29. Immunofluorescent staining of CAM xenografts: Sections were stained according to immunofluorescent protocol. Upper row shows sections from LT22s cells and lower row sections from LT22a cells in CAM stained for ECad, Vimentin, ALDH1 and CK7 (green) and were counterstained with LCA (red). Measuring bar 100-200 µm. (84)

Similar to the observations in LT22s cells, LT8s also kept the initial phenotype during invasion of the CAM microenvironment, reflected in positive ECad, ALDH1 and CK7 staining and negative Vimentin staining of cancer cells, as shown in figure 30. Accordingly, LT67s cells, which were isolated from an SCC, were CK7 negative. Positive ECad and negative Vimentin staining were the same as in the cell culture, whereas the ALDH1 signal seemed more intense here.

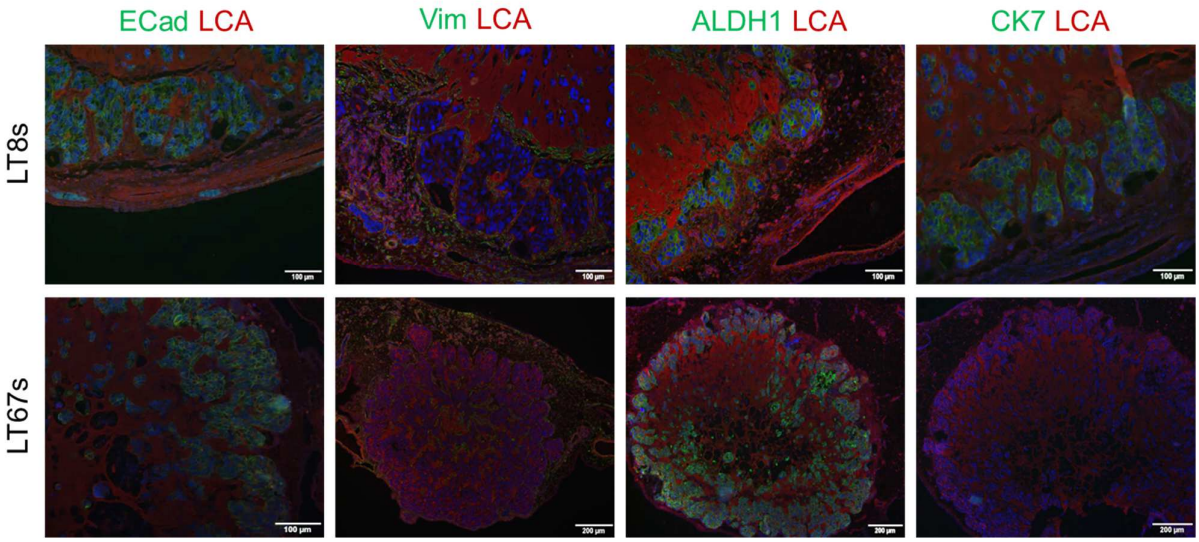

Figure 30. IF staining of CAM assay: Upper row shows LT8s cells and in the lower row LT67s cells in CAM stained for ECad, Vimentin, ALDH1 and CK7 (green), Dapi (blue) and LCA (red). Measuring bar 100-200 µm.

Taken together, these results correspond to the immunostaining results of the primary cells *in vitro*. No phenotypic changes could be observed under the influence of the microenvironment of the chicken egg. Cells that migrated and recapitulated the primary tumor kept their positive ECad expression.

4.8.2. Neoangiogenic assay

Supernatants of LT22a and LT22s cells were assessed for the neoangiogenic potential induced by tumor factors. Vessels that evolved and grew around the nylon grid were counted as positive, and the relation from the total number of squares from one grid to the number of infiltrated squares was determined.

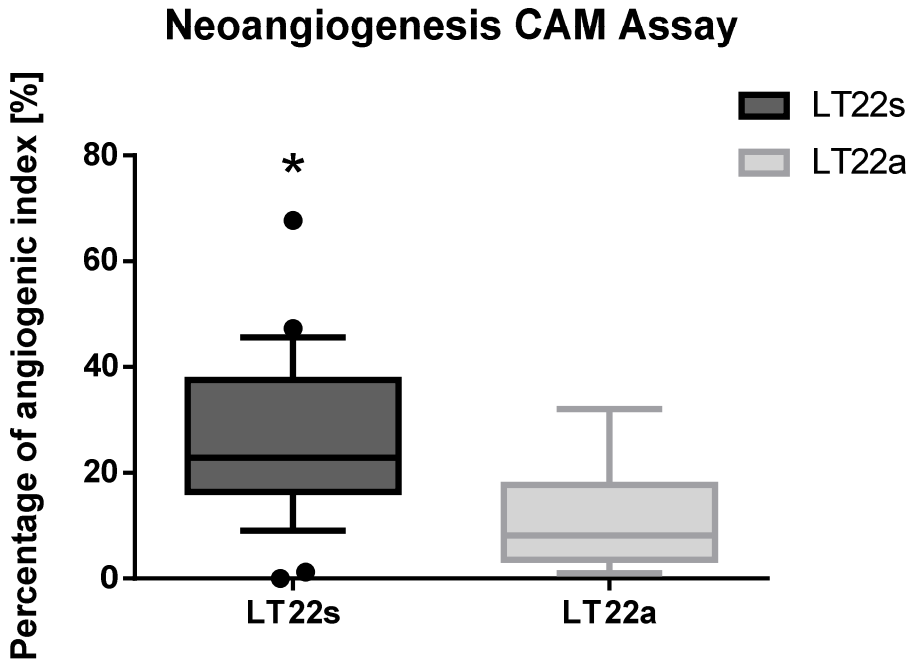

Figure 31. Supernatant of LT22a and LT22s cells were gelled around a nylon grid. Positive infiltrated grids were counted and normalized to total grids. The results of the supernatants from LT22s and LT22a were figured as box-plots. A significantly higher neoangiogenesis potential was achieved with LT22s supernatant. (p-value 0.0001).

Grids with LT22s cell supernatant were infiltrated by newly evolved blood vessels significantly more often than grids with LT22a supernatant with an average of 22.9% (± 15%) induced vascularization compared to 11.0% (± 9%) (figure 31). Therefore, the supernatant of LT22s cells contained more proangiogenic factors, which promoted vascularization in this region.

4.9. Drug treatment

CSCs have been associated with resistance to therapy. (110) However, Salinomycin has been shown to be specifically toxic to stem-like cancer cells (111). Additionally, two common anticancer drugs (Pemetrexed and Cisplatin) for lung adenocarcinoma were used for viability assays. Patient-derived cells were treated with chemotherapeutic compounds at various concentrations for 72 hours. Viability was measured by the reduction of PrestoBlue reagent in living cells.

Conventional Cisplatin could decrease viability with increasing concentrations in all cell lines, which is shown in figure 32. Higher doses of Cisplatin were needed in spheroid cells than in adherent cells. In LT22 cells, calculated IC_{50} values of 18.91 µM in LT22s were over 3 times higher compared to 5.97 µM in LT22a cells, and the difference was statistically significant (p-value < 0.05). In LT8s the highest concentration of Cisplatin was needed to eliminate LT8s cells with an IC_{50} value of 33.95 µM. LT8s cells responded to chemotherapeutic compounds as expected from CSCs.

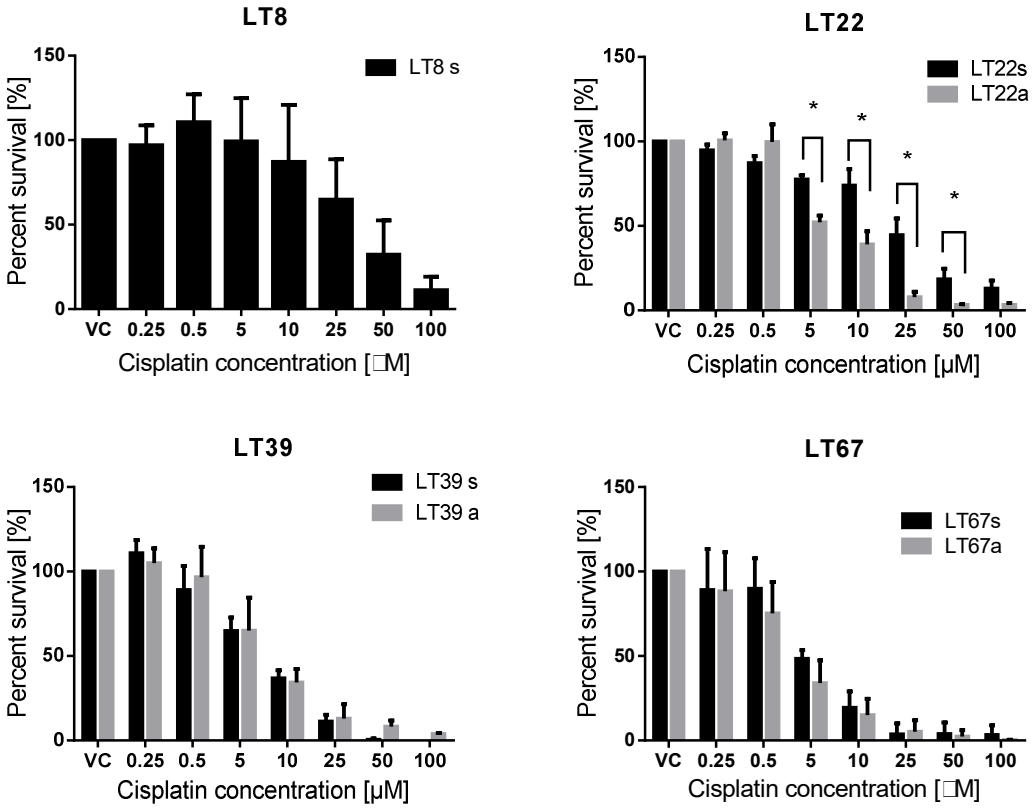

Figure 32. Cisplatin treatment: Relative metabolic activity in percent (y-axes) of LT8, LT22, LT39 and LT67 cells treated with increasing concentrations of Cisplatin (x-axes). Viability was measured

using PrestoBlue assay after 72 h. Fluorescence emission was read out with Fluostar Omega. Survival was calculated relative to cells treated with vehicle solution and summarized in bar graphs.

Salinomycin was more effective in AC cell lines than in the SCC cell line, which is reflected in lower IC_{50} values, as summarized in table 10. Furthermore, in AC cell lines, spheroid cells had slightly lower IC_{50} values compared to their corresponding adherent cell cultures, which can be seen in figure 33. LT39s cells had the lowest IC_{50} value of 0.11 µM. One reason for the lower IC_{50} value may be that LT39s cells did not form compact spheres and Salinomycin reagents had better sensitivity due to better access to all cells.

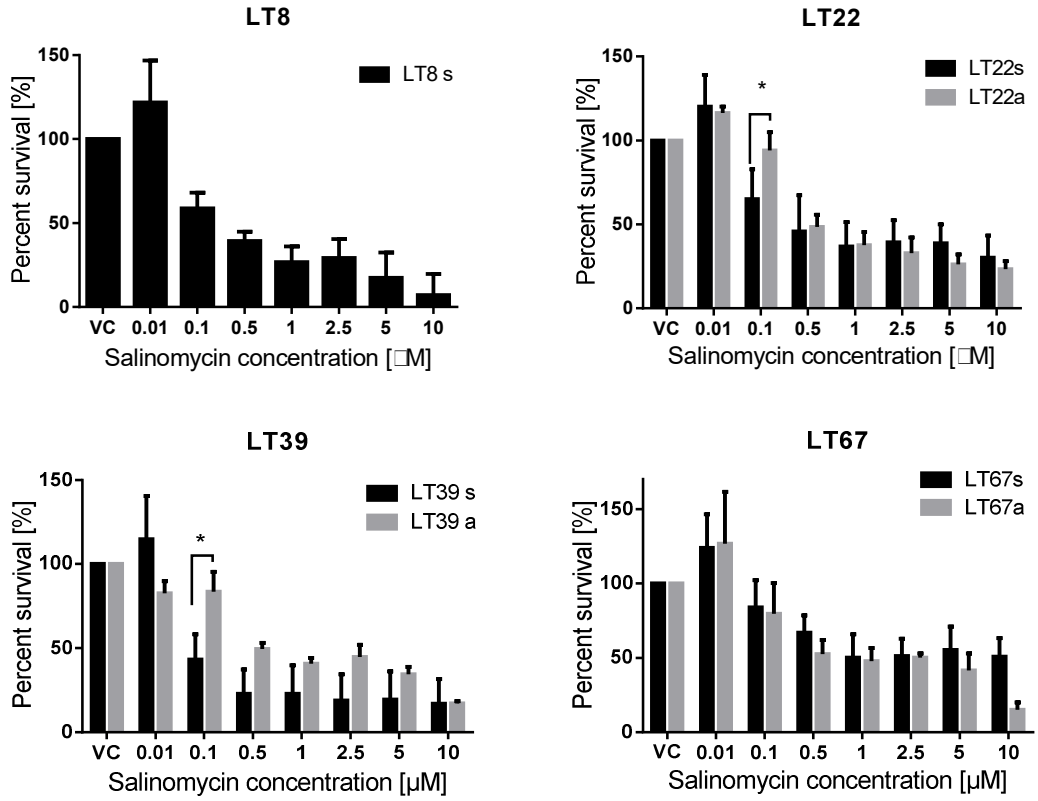

Figure 33. Salinomycin treatment: Relative metabolic activity in percent (y-axes) of LT8, LT22, LT39 and LT67 cells treated with increasing concentrations of Salinomycin (x-axes). Viability was measured using PrestoBlue assay after 72 h. Fluorescence emission was read out with Fluostar Omega.

The viability of all cell cultures could not be decreased with increasing Pemetrexed concentration and therefore no IC_{50} values could be calculated (figure 34, table 13). Cells were also treated with 10 times higher concentrations and even then, no decrease in viability could be observed (data not shown).

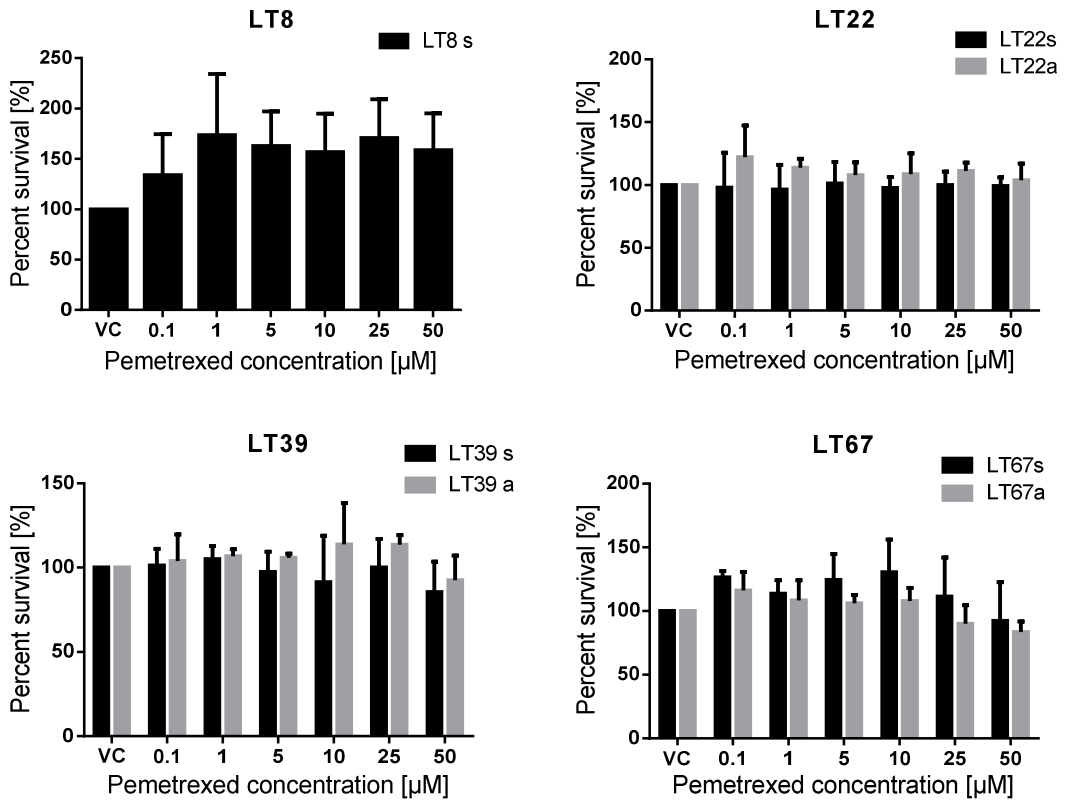

Figure 34. Pemetrexed treatment: Relative metabolic activity in LT8, LT22, LT39 and LT67 cells treated with various concentrations of Pemetrexed (Alimta). Viability was measured using PrestoBlue assay after 72 h. Fluorescence emission was read out with Fluostar Omega.

Table 13. Summary of IC_{50} values [µM] calculated with GraphPad Prism.

	Cisplatin	Salinomycin	Pemetrexed
LT8s	33.95 µM	0.27 µM	-
LT22s	18.91 µM	0.68 µM	-
LT22a	5.97 µM	0.80 µM	-
LT39s	7.16 µM	0.11 µM	-
LT39a	7.07 µM	0.80 µM	-
LT67s	3.83 µM	4.37 µM	-
LT67a	1.93 µM	1.22 µM	-

4.10. *in vivo* mouse experiments

The results of the mouse experiments were generated at EPO Berlin and the following chapter is a summary of the results presented in their report. After subcutaneous inoculation, both cell lines started to develop a tumor until day 6, when tumor growth stopped (LT22s) or the volume of the tumor was reduced again (LT22a). After day 10, LT22s

tumor began to re-grow again and reached a volume of 1.5 cm^3 on day 32 after transplantation (figure 35 A). Mouse A3 had to be sacrificed for ethical reasons on day 27 because of tumor ulceration; both other mice of this group were sacrificed on day 32, when the mean tumor volume was 1.5 cm^3, for the same reason. Tumor development of LT22a (figure 35 A) was delayed until day 39. At this time, the tumors of mouse B1 and B2 seemed to reinitiate the tumor growth again, but at a low level. Mice were sacrificed at day 42 and evaluated by gross autopsy. (84)

No metastases could be found by macroscopic evaluation. PCR was used to detect and quantify human cells in liver and lung (micro-metastases). The results revealed the presence of human cells in the livers and lungs of both groups of mice, but to a different degree. Two (A1 and A2) of the three mice of group A, transplanted with LT22s cells had micro-metastases in liver and lung, while mouse A3 had only micro-metastases in the lung, but to a relatively strong extent (figure 35 B). LT22a derived tumor-bearing mice also had detectable micro-metastases despite relatively slow tumor growth. However, metastasis occurred at a lower degree (figure 35 B) than in group A. In both groups, metastasis into lung was more pronounced than into liver. (84)

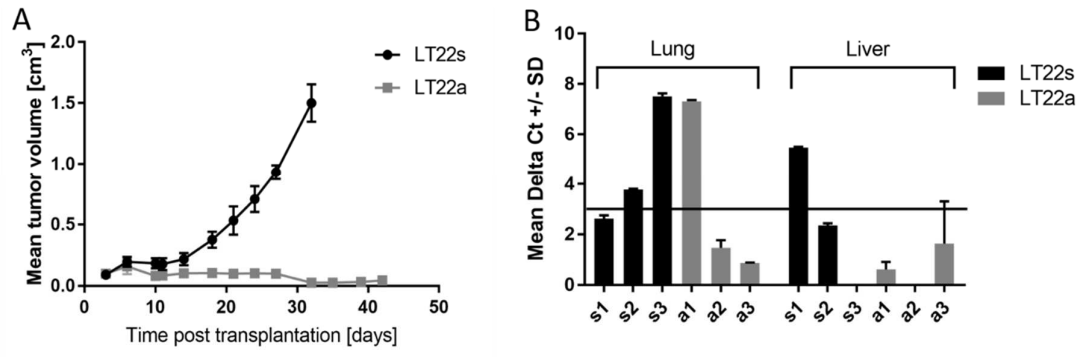

Figure 35 *in vivo* mouse xenografts. (A) Average tumor volumes of mouse cohort A transplanted with LT22s cells compared to mouse cohort B transplanted with LT22a cells. The graph shows the mean tumor volume +/- S.D. for three mice/cell lines over time. (B) Mice were sacrificed and lung and tumor tissues were investigated for micro-metastasis by using qRT-PCR. Shown is the ΔCt-value +/- S.D. for liver and lung tissue (n=2) as indicator for micro metastases. The horizontal line indicates the cut-off value (ΔCt = 3.0) for metastasis. Values >3,0 indicate metastasis. (84)

4.11. Circulating tumor cells (CTCs)

At a later stage of the study, we started blood collection; therefore, 52/95 (54.7%) blood samples were obtained, and from 45/95 (47.4%) patients, both peripheral blood and primary tumor samples were available. Peripheral blood was drawn just prior to surgery and all samples were filtered on the same day of receival. The filters were immunofluorescently

stained for cytokeratin (CK), CD45 and Dapi. The whole area of the microfilter was scanned with the confocal LSM and the CTC were counted as positive when they showed intact nucleated DAPI staining, positive CK (green) and negative CD45 (red) signals. Figure 36 shows examples from captured CTCs counted as positive. According to our initial idea of evaluating early stage AC patients, we restricted the samples to patients with primary AC for statistical analysis. (43) Therefore, 3 AC patients with late-stage disease and peripheral metastasis were excluded, to analyze a homogeneous patient cohort, which is shown in an overview as figure 37. For further statistical analysis, data from 40 patients were used.

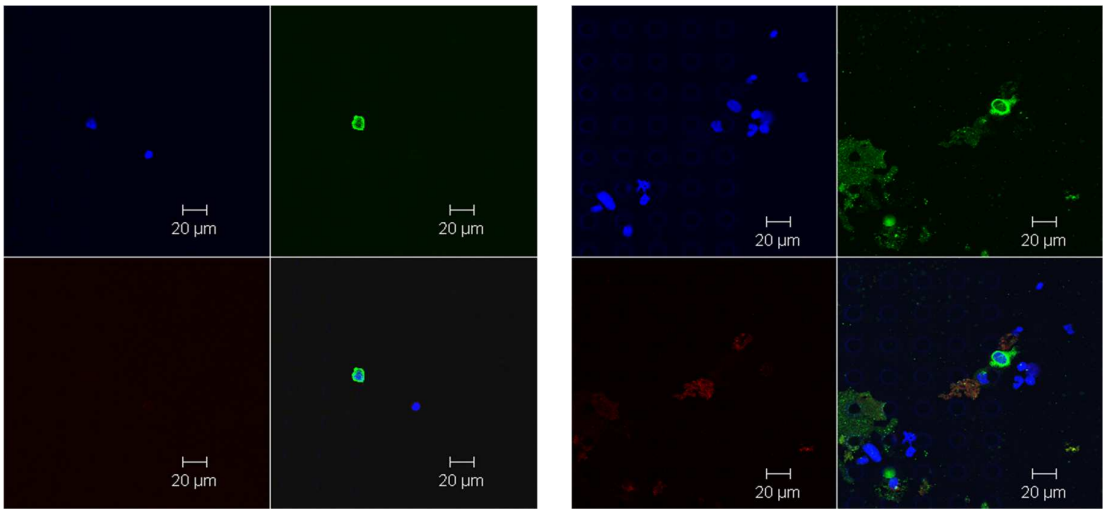

Figure 36. CTC count on parylene microfilter: Images from CTC microfilters from two different patients, which were IF stained against CK (green), CD45 (red) and Dapi (blue) and scanned under confocal LSM. Cells with intact Dapi, CK^+ and $CD45^-$ staining were counted as positive CTC. Scale bar indicates 20 µm.

In 15/40 (37.5%) patients, one or more positive CTCs were found per 7.5 mL blood on the microfilter. Within the positive CTC cohort, a median of 3 CTCs (range 1-44) were found. The correlation analysis had no significant influence between CTC counts and age, tumor size or recurrence. However, female AC patients had higher CTC counts than male AC patients. The patient´s smoking status had a tremendous effect on CTC levels. Only in one patient of the non-smokers we could detect CTCs, but the amount was <5, whereas in more than half of the smokers or former smokers CTCs could be detected (p-value =0.007 for ≥1 and p- value = 0.065 for ≥ 5). Furthermore, the influence of the TNM status and the correlation with the presence of CTC was evaluated. We found a positive correlation of CTC count and the stage of the disease. No stage IAP patient was found to have ≥5 CTCs and in advanced stages, more CTC-positive samples were discovered. Lymph node metastasis

were found to have a trend in impact on CTC count (p=0.089) when a threshold of <5 CTCs was predefined.

Table 14. Univariate analysis between CTC count and clinical-pathological data.

Characteristics		<1 CTC	≥1 CTC	<5 CTCs	≥5 CTCs
Gender	Male	9	7	16	0
	Female	16	8	18	6
	p-value	*0.505*		*0.030*	
Age	<60	4	4	7	1
	≥60	21	11	27	5
	p-value	*0.414*		*0.825*	
Smoking status	Never	12	1	13	0
	Current/Former	13	14	21	6
	p-value	0.007		0.065	
Staging	IA	9	3	12	0
	IB	5	2	6	1
	IIA	3	4	4	3
	IIB	0	1	0	1
	IIIA	8	5	12	1
	p-value	*0.425*		*0.013*	
T	T1a	5	3	8	0
	T1b	6	2	8	0
	T2a	8	6	11	3
	T2b	3	2	4	1
	T3	3	2	3	2
	p-value	*0.947*		*0.212*	
N	N0	15	8	20	3
	N1	5	3	5	3
	N2	5	4	9	0
	p-value	*0.879*		*0.089*	
Recurrence	No	18	7	23	2
	Yes	7	8	11	4
	p-value	*0.109*		*0.109*	

T: Tumor size
N: Lymph node metastasis

5. Discussion

5.1. Cell lines versus primary cells

Established cancer cell lines have provided fundamental knowledge in the battle against cancer. Their robustness, ease of handling and high proliferation rate allows for a wide range of applications. We and others have used cell lines for feasibility studies and the establishment of new methods. (112) Nowadays, almost 200 cell lines which mimic different subtypes and genomic profiles are commercially available. From these, we selected four different adenocarcinoma cell lines to perform sphere formation and test primers and antibodies for CSC and EMT markers. Sphere formation was possible in all four cell lines, but common CSC markers such as CD133 and ALDH1 could not be detected with IF or qRT-PCR methods and could not be enriched under spheroid conditions. This was in contrast to our established primary cell cultures, which expressed higher levels of common CSC markers. Therefore, cell lines can be suitable for research, depending on the objectives of the study, but they have limitations which are becoming increasingly known. Gazdar et al. describe the benefits of using conventional cell lines and, more importantly, the issues to be encountered if they are taken advantage of. (113) Summarizing future approaches these should include an accurate authentication of cell lines, worldwide availability of all cell lines, public databases for genomic sequences of cell lines and new approaches for co-culturing and stem cell culturing. (113)

Besides the diverse areas of application for established cancer cell lines, primary cells that better reflect the complexity and diversity of primary tumors are needed. Although primary cells are more sensitive than established cancer cells, their heterogeneous cell composition distinguishes them as a beneficial model strongly associated with *in vivo* conditions. Based on our experiences in established-robust and reliable data for CSC biology, the first phase included method and feasibility studies using cell lines (112) and subsequently, the concept was proven on primary CSC models under *in vitro* and *in vivo* conditions. (81, 84)

5.2. Sphere formation and CSC enrichment

We tried to establish spheroid cultures promoting CSC enrichment from 87 lung cancer patients. Based on limitations of conventional cancer cell lines, we wanted to characterize cells that better reflect the physiological conditions. (114) Not only have cell lines been in 2D-culture for decades and accumulated genetic changes to facilitate growth under these conditions, but they have also been highly differentiated under FBS conditions. Therefore, it is difficult to establish a link with CSC-undifferentiated characteristics. (115) In our study, we were able to establish 4 (4,6%) long-term cell cultures from primary lung tumor material.

Comparable studies processing lung tumor tissue had a success rate of 4.7% for culturing CSCs. (116) There were also studies with considerably higher success rates of 75%, but these studies did not count long-term cultures. (117) The rather low success rate of our study may be due to the unsterile conditions during sample collection at the Institute of Pathology. Bacterial contaminations and the efforts to eliminate them were particularly unsupportive for the cells. According to our primary CSC isolation protocol, cells should be kept in the same media for the first week to enrich growth factors and other signals from isolated cells. Due to bacteria, we had to change media at least every second day to prevent bacterial outgrowth. Figure 11 reflects that at least 33.3% of all patient samples could be cultivated until passage 2, which indicates that the success rate could have been higher without intensive media change due to bacterial contaminations. Furthermore, most of our primary tumor samples originated from patients with early stage lung cancer without metastatic spread, whereas cell cultures from patients with advanced and aggressive disease have been observed to be easier to establish. (118)

5.3. Phenotypic and genotypic characterization of patient derived cell cultures

Characterization of the cell cultures with immunofluorescent FACS method and qRT-PCR was performed to verify the subtype category, the presence of EMT and the CSC marker expression. In general, the results were verified and supported with each method. However, in some cases data were only predominantly found with one method. The method of measuring ALDH1 expression with FACS is based on enzyme activity, which is rather sensitive to external influences. Factors such as stress can shut down unnecessary pathways and downregulate enzymatic activity of ALDH1. Results from flow cytometry of ALDH1 detected low enzymatic activity (0.7-11.2%) compared to IF results, which showed bright positive ALDH1 staining in figure 13, 15 and 20. Furthermore, a CD133 expression of 53.1% was detected in LT67s cells with the flow cytometry method, whereas qRT-PCR did not detect any CD133 mRNA expression. Cells were taken from different passages for each experiment, as RNA for qRT-PCR was isolated from spheroid cell passages between sp3 and sp9 and flow cytometry passages were >sp10. This example illustrates a possible disadvantage of primary patient-derived cells and the challenge of reproducing results. As the cells were not familiar with the culture conditions, changes and adaptations were part of a steady dynamic process and, the expression profile could change drastically in the span of one sphere passage. Results from cultured cells were comparable with the primary tumor material, which highlights the epithelial phenotype with positive ECad and EpCAM expression. Additionally, we were able to enrich putative CSC fractions under spheroid conditions such as ALDH1 increases in LT8 cells and CD133 increases in LT22 and LT67

cells. In general, no universal biomarker which was expressed in all patient samples could be found by phenotypic characterization. Interestingly, and confirming other studies, primary cell cultures reflected the characteristic features of their primary tumors and were an essential tool for the approaches of personalized medicine. (118, 119) Furthermore, the phenotypic characterization revealed that in LT22s and LT22a, cells are completely different in their marker expression. CNV profiles verify the observed differences with prevalent genomic differences including 2q, 4p, 6p, 7q, 8q, 9p, 10p, 11, 13q and 20q, on the one hand and the same aberrations in 1q, 7, and 8, and deletions on 3p, 4p, 8p and 13 on the other hand to confirm the same origin. In the case of LT22, we assumed that we could isolate two different subclones of the tumor, whereas in LT8, LT39 and LT67, the adherent and the spheroid culture did not show these extreme differences, suggesting that the LT39s and LT39a and LT67s and LT67a contained the same cell types, only cultured in different culture conditions.

5.4. Challenging the CSC and EMT association

A closer look at the different subclonal cells from sample LT22 revealed some interesting biological features that contradict scientific assumptions. In sharp contrast to the expected correlation between CSCs and EMT, LT22s cells enriched for CSC markers CD133 and ALDH1 were positive for epithelial markers including EpCam, CK and ECad, but lacked mesenchymal traits. The epithelial CSC phenotype was also consistent during the invasion process of the CAM assay. We could demonstrate that LT22s cells invaded the membrane and formed glandular structures, which was comparable to primary tumor cell formation. Thereby, the expression of epithelial and CSC markers persisted, and it seemed that these cells were able to invade without undergoing EMT.

In addition to the epithelial CSC-enriched spheroid culture (LT22s), we also isolated mesenchymal-like cells of the same tumor, with a high Vimentin expression and a prominent mesenchymal phenotype. These LT22a cells did not express any CSC markers, but revealed a spindle-shaped morphology together with a strong expression of mesenchymal markers at protein and mRNA levels. We also found that LT22a cells were not able to proliferate and form spheres under spheroid culture conditions. The origin of LT22a cells was rather unclear because no Vimentin positive cell population could be detected in the primary tumor. However, we did find single cells positive for the EMT transcription factor Snail. We therefore hypothesize that these Snail-positive cells may be the origin of the LT22a culture.

In contrast to our expectations, the epithelial subpopulation of cells was associated with CSC features, higher expression of stem cell marker genes, an aggressive phenotype,

enhanced invasion, and therapy resistance. Less aggressive cells, which were only capable of growth in adherent conditions, lacked stem cell and epithelial markers, and were more responsive to treatment, were largely of mesenchymal origin. Recently published papers share our observations. (120) Fischer et al. generated a triple transgenic mouse model where the EMT initiator fibroblast specific protein 1 (FSP-1) served as a switch for a Cre fluorescent alternation, which was not reversible. Cells with epithelial phenotypes emitted a red fluorescence, but when EMT occurred, they emitted a green fluorescence. Surprisingly, cells that traveled to the lung showed a red fluorescence staining and therefore kept their epithelial phenotype during the formation of metastasis. (121) These two seminal papers seriously challenge the role of EMT as a key element involved in cancer metastasis. Together with our observation, these studies question the association of EMT, CSCs and formation of metastasis. Nevertheless, it is important to mention that EMT is a dynamic and transient process and, consequently, experiments to capture this complicated process are challenging.

5.5. Functional assays: difficulties and new approaches

Subsequent *in vitro* assays for functional evaluation were rather difficult, due to different culture conditions. Functional assays where adaptations in one condition were necessary, e. g. colony forming assays, where spheroid cells were cultured with FBS and vice versa in sphere formation assays, were performed. Unfamiliar media conditions were accompanied with a decrease in proliferation and therefore, results of spheroids versus adherent cells were not comparable anymore. An obvious example can be observed in figure 27 A, where the LT22s cells were cultured in adherent media with FBS to attach in Ibidi chambers. First of all, for ideal migration assay conditions, cells needed to form a layer, which was impossible for these cells. Secondly, the morphology of the cells did not look very healthy as fragments from apoptotic cells were floating in the supernatant. These cells had a lower migration velocity compared to LT22a cells. An interpretation of these results was difficult and media-independent assays were needed.

As a consequence, we used the *ex ovo* CAM model to compare migration and invasion potential of each individual cell line. The egg and the CAM membrane serve as an ideal microenvironment for growing xenografts. All evaluated cells, including LT22s, LT22a, LT8s and LT67s, infiltrated chorionic epithelium and migrated within the intermediate mesodermal layer. LT22s, LT8s and LT67s could reestablish the tumor and arrange the cellular structure as seen in the primary tumor. This observation is in concordance with Xiao et al., who used the CAM model for *in vivo* studies of nasopharyngeal carcinoma by culturing small biopsies onto CAM, because they can simulate the clinical features of this type of tumor. (122) In contrast to this, LT22a cells were randomly distributed and invasion was not as advanced

as in LT22s cells because cells grew above the chorionic epithelium. The high proliferation rate and the minor invasive potential resulted in the appearance of a mop top shown in figure 28 B.

Subsequently, we tested the supernatants of LT22s and LT22a cells for pro-apoptotic factors. The levels of stimuli in the LT22s cell supernatant were significantly higher compared to the supernatant of LT22a cells. Besides the aggressive migratory potential, LT22s cells also indicated a high angiogenic potential which is not observed in the subclonal cells of LT22a cells.

These results were further confirmed with *in vivo* mouse experiments. The aggressiveness of LT22s cells was indicated in a high proliferation rate and a significant higher metastatic potential within the mouse, compared to LT22a cells.

Within the tumor heterogeneity there are cells which are resistant to conventional chemotherapy. By isolating and culturing cells in spheroid conditions, we wanted to enrich these populations that are also attributed as CSCs, especially with patient LT22, who was already treated with two cycles of neoadjuvant chemotherapy with Cisplatin (75 mg/m^2) and docetaxel (75 mg/m^2) and with concomitant radiochemotherapy with Cisplatin (75 mg/m^2) on day 1 and Navelbine (12.5 mg/m^2) on days 1, 7 and 15 of the cycle. Surgery was performed in a palliative setting to relief the tumor burden. The isolated cells came from a cancer cell population that was already resistant to chemotherapeutics. The IC_{50} of these cells (18.9 µM) was similar to other CSC populations from other studies, which had an IC_{50} of 16.6 µM. (123) LT8s had a much higher IC_{50} value of 34.0 µM indicating a Cisplatin resistant cell population. The second cytotoxic agent we assayed was Salinomycin, a promising anti-CSC drug which had a stronger effect on CSCs compared to Paclitaxel. (111) Treatment with Salinomycin strongly decreased viability in CSCs and resulted in low IC_{50} values of 0.11-4.37 µM, which showed even better response rates than earlier studies. (124) With Salinomycin the cytotoxic effect is said to be significantly stronger in CSC subpopulation; (125) considering the LT22s cells a CSC population and LT22a a non-CSC subpopulation, only a slightly lower IC_{50} value was observed in LT22s cells compared to LT22a cells. The mechanism responsible for eliminating CSCs has not been fully understood. Influence on the induction of apoptosis, the inhibition of ABC-transporters and the activation of Wnt-pathway have been described. (126-128) For future therapy with Salinomycin, it is important to focus on the molecular target in order to manage the adaptation of the chemical structure to a more efficient response linked with decreasing side effects. The third anti-cancer agent Pemetrexed is specific for non-squamous NSCLC patients. Therefore, the poor effect on LT67 cells isolated from a lung squamous cell carcinoma was expected. However, the scarce response in other cells was surprising, as

Pemetrexed is recommended as 1st, 2nd and/or 3rd line treatment. Pemetrexed, which can be used as a monotherapeutic agent, is also often combined with chemotherapeutics. (129) Perhaps combination with Cisplatin or Carboplatin would have triggered a reduction in viability.

5.6. Attributing putative CSCs

According to CSC attributes, not all LT samples fulfilled the requirements for CSCs. The most important feature of CSCs is their self-renewal capability. Sphere formation started with the isolation of tumor cells; therefore, all four LT#s cells were able to form spheres, even under low dilution. LT#a cells were also capable of forming spheres in respective media as LT8a, LT39a and LT67a were of the same cell type as their spheroid counterparts, except for LT22a cells. These cells were not able to form spheres in any condition and consequently could not be attributed as a CSC population. Another feature is CSC marker expression, such as CD133 and ALDH1. According to flow cytometry analysis, LT22s and LT67s could enrich CD133-expressing cell with increasing passage numbers. Furthermore, ALDH1 could be detected in IF staining of LT8s, LT22s and LT67s and LT67a cells. In LT39 cells, only a population of 2% ALDH1 positive cells could be detected with FACS analysis; however, results could not be confirmed with IF or qRT-PCR. In this sample, the similar sphere forming efficiency of ALDH1+ and ALDH- population was also detected, indicating that the sorting did not significantly separate cells according to CSC features.

CSCs were also made responsible for therapy resistance, which we tested with a viability assay. Treatment with conventional chemotherapeutics such as Cisplatin indicated that LT8s cells with an IC_{50} of 33.95 µM and LT22s cells with an IC_{50} of 18.91 µM could even tolerate higher doses of Cisplatin than described in literature for CSCs. After breaking it all down, we have two cell cultures left, LT8s and LT22s, that fulfill the requirements to be called putative CSCs.

5.7. CTCs and the correlation with physiological conditions

Besides the isolation of cancer cells from the primary tumor material, we also collected blood and enriched CTCs with a microfilter device. In recent years, CTC analysis as a surrogate of liquid biopsy has become more important as research within the field increased. Besides their function of enlightening the mechanism behind the metastatic process, CTCs serve as a biomarker for disease monitoring and therapy response. As CTCs are still rare in late stage NSCLC, the enrichment method is of tremendous value. As of now, only the CellSearch system, an EpCam-dependent isolation method, is FDA approved. (130) Nevertheless, during metastasis according to EMT, cells can downregulate

their epithelial characteristics such as EpCam expression to be able to escape from the primary tumor site and travel via the vascular system to peripheral sites.

In this study, we used a novel parylene microfilter which excludes cells according to their size and thus enriches CTCs. In 37.1% we detected 1 or more CTCs. This detection rate is lower compared to results from other studies using size-based enrichment methods which detected positive CTCs in 65-80% of all NSCLC patients. (131, 132) However, this analysis is the first analysis to show that their presence has a prognostic impact on early stage NSCLC. (133) Our filtration method is highly dependent on the user because manual skills are required in several steps, such as cutting the microfilter and filter cassette assembly. To avoid these potential influences, a prototype for a fully automated filter process was developed and is already in use at the Division of Oncology. With this prototype, the advantages of the microfilter become more prominent and may help to further increase the recovery rate by minimizing the amount of hands-on steps. However, even with manual microfiltration, the CTC detection rate was certainly in the range of CellSave and other antigen-dependent enrichment methods. (134) Filters with enriched CTCs were stained for CK/CD45 gene expression, whereas CK is characteristic for epithelial cells. Therefore, CTCs with other phenotypes with regards to EMT would not have been detected. As seen in figure 36, some cells were not positively stained for either CK or CD45. These cells can have a different marker expression which cannot be detected with our staining method. Therefore, putative CTCs with other marker expressions than CK were not counted and remained undetected.

Another reason for the low detection rate could be the early and non-metastatic stage of our patient cohort. Early stage lung cancer patients did show CTCs, but a slight correlation with advancing stage could be observed within our patient cohort. The early dissemination of CTCs in stage IA patients is already documented, along with a positive correlation of CTC number with increasing stage. (135)

In our study, we could find a highly significant correlation of CTC number with smoking status. This correlation could not be confirmed in other studies, but smoking is clearly a risk factor for all histological types of lung cancer. (136) Although AC is the most common type among non-smokers, the diverse carcinogenic compounds in tobacco smoke can irreversibly damage structures and functions within lung tissue. The DNA damage caused by tobacco smoke is the reason why a normal cell can turn into a cancer cell, with uncontrolled proliferation. (137)

CTC as a biomarker for disease monitoring and therapy response has already been proven in various studies for different tumor entities, but has yet to be implemented into daily clinical practice. To become an attractive tool for cancer management, CTC enumeration requires

comprehensive standardization and a uniform definition of CTC marker expression. (138) In a second step, biomarkers associated with CTCs may be evaluated and become clinically important.

6. Conclusion

In this study, we addressed the importance in considering whether cell lines are appropriate for answering the research question, or whether primary cells need to be isolated. Cell lines are more homogeneous and do not change with increasing passages under normal culture conditions. However, cancer tissue is very heterogenic and conclusions drawn from cell lines cannot be applied to the complex coherences of cancer biology. (115) Cell lines were cultured under adherent conditions for decades, which is against physiological conditions. Although primary cells have a closer relation to the *in vivo* conditions and this study confirms the observation in literature, the primary spheroid cultures retain the primary tumor characteristics and were able to reinitiate the tumor as xenografts. Concordantly, each of our patient samples was individual reflecting the primary tumor with its specific characteristics. Few similarities were found, which emphasizes the need for personalized medicine.

A major point in this study was also the difficult approach to verifying CSC features due to the lacking congruency in assumptions and perceptions. After all the methods were applied, it can be suspected that LT22s cells were most likely CSCs, LT8s cells shared CSC features and the rest demonstrated some CSC features. In literature, mouse xenografts, (90) which are time and money consuming, still remain the gold standard to characterize CSCs

. If cells from patients are available, mice as hosts are questionable, because not all their cellular mechanisms can be applied to humans. (139)

Overall, for the first time, we could show the independence of CSC markers and EMT features in primary cells derived from a lung cancer patient resistant to conventional treatment. We believe that our data provide important clinical evidence challenging the current model of EMT in cancer progression, resistance and metastasis. Our data suggest that epithelial tumor cells play a crucial role in progression, therapy resistance, and metastasis, and this study also addresses the focus on epithelial cancer cells in further studies.

7. References

1. Siegel RL, Miller K, Jemal A. Cancer statistics. CA Cancer J Clin. 2015;65(1):5–29.
2. Baldaszti E. Jahrbuch der Gesundheitsstatistik. Wien: Statistik Austria; 2017.
3. STATISTIK AUSTRIA. Luftröhre, Bronchien, Lunge 2016 [Available from: http://www.statistik.at/web_de/statistiken/menschen_und_gesellschaft/gesundheit/krebserkrankungen/luftroehre_bronchien_lunge/index.html.
4. De Flora S, Ganchev G, Iltcheva M, La Maestra S, Micale R, Steele V, et al. Pharmacological Modulation of Lung Carcinogenesis in Smokers: Preclinical and Clinical Evidence. Trends Pharmacol Sci. 2016;37(2):120–42.
5. Hecht S, Szabo E. Fifty Years of Tobacco Carcinogenesis Research: From Mechanisms to Early Detection and Prevention of Lung Cancer. Cancer Prev Res. 2014;7(1):1-8.
6. Jackman DM, Johnson BE. Small-cell lung cancer. The Lancet. 2005;366(9494):15-21.
7. Crinò L, Weder W, van Meerbeeck J, Felip E, ESMO GWG. Early stage and locally advanced (non-metastatic) non-small-cell lung cancer: ESMO Clinical Practice Guidelines for diagnosis, treatment and follow-up. Ann Oncol 2010;21.
8. Travis WD, Brambilla E, Nicholson AG, Yatabe Y, Austin JH, Beasley MB, et al. The 2015 World Health Organization Classification of Lung Tumors: Impact of Genetic, Clinical and Radiologic Advances Since the 2004 Classification. J Thorac Oncol. 2015;10(9).
9. Kenfield S, Wei E, Stampfer M, Rosner B, Colditz G. Comparison of Aspects of Smoking Among Four Histologic Types of Lung Cancer. Tob Control. 2008;17(3):198-204.
10. Travis WD, Asamura H, Bankier AA, Beasley MB, Detterbeck F, Flieder DB, et al. The IASLC Lung Cancer Staging Project: Proposals for Coding T Categories for Subsolid Nodules and Assessment of Tumor Size in Part-Solid Tumors in the Forthcoming Eighth Edition of the TNM Classification of Lung Cancer. J Thorac Oncol. 2016;11(8):1204-23.
11. Vansteenkiste J, Crino L, Dooms C, Douillard JY, Faivre-Finn C, Lim E, et al. ESMO Consensus Guidelines: Early stage non-small cell lung cancer consensus on diagnosis, treatment and follow-up. Ann Oncol. 2014.
12. Novello S, Barlesi F, Califano R, Cufer T, Ekman S, Giaj Levra M, et al. Metastatic non-small-cell lung cancer: ESMO Clinical Practice Guidelines for diagnosis, treatment and follow-up. Ann Oncol 2016;27.
13. Herbst RS, Soria JC, Kowanetz M, Fine G, Hamid O, Gordon M, et al. Predictive correlates of response to the anti-PD-L1 antibody MPDL3280A in cancer patients. Nature. 2014;515(7528):563-7.
14. Marrone KA, Brahmer JR. Using Immune Checkpoint Inhibitors in Lung Cancer. Oncology. 2016;30(8):713-21.
15. Gupta R, Dastane AM, Forozan F, Riley-Portuguez A, Chung F, Lopategui J, et al. Evaluation of EGFR abnormalities in patients with pulmonary adenocarcinoma: the need to test neoplasms with more than one method. Mod Pathol. 2009;22(1):128-33.
16. Hirsch FR, Varella-Garcia M, Bunn PA, Jr., Di Maria MV, Veve R, Bremmes RM, et al. Epidermal growth factor receptor in non-small-cell lung carcinomas: correlation between gene copy number and protein expression and impact on prognosis. Journal of clinical oncology : official journal of the American Society of Clinical Oncology. 2003;21(20):3798-807.
17. Dearden S, Stevens J, Wu YL, Blowers D. Mutation incidence and coincidence in non small-cell lung cancer: meta-analyses by ethnicity and histology (mutMap). Ann Oncol. 2013;24(9):2371-6.
18. Scagliotti GV, Selvaggi G, Novello S, Hirsch FR. The Biology of Epidermal Growth Factor Receptor in Lung Cancer. Clin Cancer Res. 2004;10(12).
19. Siegelin MD, Borczuk AC. Epidermal growth factor receptor mutations in lung adenocarcinoma. Laboratory Investigation 2014;94:129–37.

20. Massarelli E, Varella-Garcia M, Tang X, Xavier AC, Ozburn NC, Liu DD, et al. KRAS mutation is an important predictor of resistance to therapy with epidermal growth factor receptor tyrosine kinase inhibitors in non-small-cell lung cancer. Clin Cancer Res. 2007;13(10):2890-6.
21. Davies KD, Le AT, Theodoro M, Skokan M, Aisner D, Berge E, et al. Identifying and Targeting ROS1 Gene Fusions in Non–Small Cell Lung Cancer. Clinical cancer research : an official journal of the American Association for Cancer Research. 2012.
22. Burrell RA, McGranahan N, Bartek J, Swanton C. The causes and consequences of genetic heterogeneity in cancer evolution. Nature 2013;501:338-45.
23. Perez CA, Velez M, Raez LE, Santos ES. Overcoming the resistance to Crizotinib in patients with Non-Small Cell Lung Cancer harboring EML4/ALK translocation. Lung Cancer. 2014;84(2):110-5.
24. Doebele RC, Pilling AB, Aisner DL, Kutateladze TG, Le AT, Weickhardt AJ, et al. Mechanisms of resistance to crizotinib in patients with ALK gene rearranged non-small cell lung cancer. Clin Cancer Res. 2012;18(5):1472-82.
25. Stanta G, Jahn SW, Bonin S, G. H. Tumour heterogeneity: principles and practical consequences. Virchows Arch 2016.
26. Greaves M, Maley CC. Clonal evolution in cancer. Nature. 2012;481:306–13.
27. Farber E, Rubin H. Cellular Adaptation in the Origin and Development of Cancer. Cancer Res. 1991;51:2751-61.
28. Huang LE, Bindra RS, Glazer PM, Harris AL. Hypoxia-induced genetic instability--a calculated mechanism underlying tumor progression. J Mol Med. 2007;85(2):139-48.
29. Nowell PC. The clonal evolution of tumor cell populations. Science. 1976;194(4260):23-8.
30. Shackleton M, Quintana E, Fearon E, Morrison S. Heterogeneity in Cancer: Cancer Stem Cells versus Clonal Evolution. Cell. 2009;138(5):822–9.
31. Reya T, Morrison SJ, Clarke MF, Weissman IL. Stem cells, cancer, and cancer stem cells. Nature. 2001;414.
32. Eramo A, Lotti F, Sette G, Pilozzi E, Biffoni M, Di Virgilio A, et al. Identification and expansion of the tumorigenic lung cancer stem cell population. Cell death and differentiation. 2008;15(3):504-14.
33. Al-Hajj M, Wicha MS, Benito-Hernandez A, Morrison SJ, Clarke MF. Prospective identification of tumorigenic breast cancer cells. Proc Natl Acad Sci U S A. 2003;100(7):3983-8.
34. Visvader JE. Cells of origin in cancer. Nature. 2011;469:314-22.
35. Jamieson C, Ailles L, Dylla S, Manja Muijtjens M, Jones C, Zehnder J, et al. Granulocyte–Macrophage Progenitors as Candidate Leukemic Stem Cells in Blast-Crisis CML. N Engl J Med. 2005;351:657-67.
36. Kreso A, Dick JE. Evolution of the cancer stem cell model. Cell stem cell. 2014;3:275–91.
37. Brooks MD, Burness ML, Wicha MS. Therapeutic Implications of Cellular Heterogeneity and Plasticity in Breast Cancer. Cell Stem Cell. 2015;17(3):260–71.
38. Lottaz C, Beier D, Meyer K, Kumar P, Hermann A, Schwarz J, et al. Transcriptional profiles of CD133+ and CD133- glioblastoma-derived cancer stem cell lines suggest different cells of origin. Cancer Res. 2010;70(5):2030-40.
39. Quintana E, Shackleton M, Sabel MS, Fullen DR, Johnson TM, Morrison SJ. Efficient tumor formation by single human melanoma cells. Nature. 2008;459(7222):593-8.
40. Chen W, Dong J, Haiech J, Kilhoffer MC, Zeniou M. Cancer Stem Cell Quiescence and Plasticity as Major Challenges in Cancer Therapy. Stem Cells Int. 2016.
41. Rycaj K, Tang DG. Cell-of-Origin of Cancer versus Cancer Stem Cells: Assays and Interpretations. Cancer Res. 2015;75(19):4003-11.
42. Keysar S, Jimeno A. More than markers: biological significance of cancer stem cell defining-molecules. Mol Cancer Ther. 2010;9(9):2450-7.
43. Marcato P, Dean CA, Giacomantonio CA, Lee PWK. Aldehyde dehydrogenase: Its role as a cancer stem cell marker comes down to the specific isoform. Cell Cycle. 2011;10:1378-84.

44. Bertolini G, Roz L, Perego P, Tortoreto M, Fontanella E, Gatti L, et al. Highly tumorigenic lung cancer CD133+ cells display stem-like features and are spared by cisplatin treatment. Proceedings of the National Academy of Sciences of the United States of America. 2009;106(38):16281-6.
45. Okudela K, Woo T, Mitsui H, Tajiri M, Masuda M, Ohashi K. Expression of the potential cancer stem cell markers, CD133, CD44, ALDH1, and beta-catenin, in primary lung adenocarcinoma-their prognostic significance. Pathol Int 2012;62:792–801.
46. Wang J, Li ZH, White J, Zhang LB. Lung Cancer Stem Cells and Implications for Future Therapeutics. Cell Biochem Biophys. 2014;69(3):389-98.
47. Chen K, Huang Y, J. C. Understanding and targeting cancer stem cells: therapeutic implications and challenges. Acta Pharmacologica Sinica 2013;34:732–40.
48. Zavadil J, Bitzer M, Liang D, Yang Y, Massimi A, Kneitz S, et al. Genetic programs of epithelial cell plasticity directed by transforming growth factor-β. PNAS. 2001;98(12).
49. Grünert S, Jechlinger M, Beug H. Diverse cellular and molecular mechanisms contribute to epithelial plasticity and metastasis. Nat Rev Mol Cell Biol. 2003;4:657-65.
50. Lamouille S, Xu J, Derynck R. Molecular mechanisms of epithelial–mesenchymal transition. Nat Rev Mol Cell Biol. 2014;15(3):178–96.
51. Hay ED. An overview of epithelio-mesenchymal transformation. . Acta Anat (Basel). 1995;154(1):8-20.
52. Hay ED. The mesenchymal cell, its role in the embryo, and the remarkable signaling mechanisms that create it. Dev Dyn. 2005;233(3):706-20.
53. Yan C, Grimm WA, Garner WL, Qin L, Travis T, Tan N, et al. Epithelial to Mesenchymal Transition in Human Skin Wound Healing Is Induced by Tumor Necrosis Factor-α through Bone Morphogenic Protein-2. Am J Pathol. 2010;176(5):2247-58.
54. Kalluri R, Weinberg RA. The basics of epithelial-mesenchymal transition. J Clin Invest. 2009;119(6):1420-8.
55. Comijn J, Berx G, Vermassen P, Verschueren K, van Grunsven L, Bruyneel E, et al. The two-handed E box binding zinc finger protein SIP1 downregulates E-cadherin and induces invasion. Mol Cell. 2001;7:1267-78.
56. Peinado H, Portillo F, Cano A. Transcriptional regulation of cadherins during development and carcinogenesis. . Int J Dev Biol. 2004;48(5-6):365-75.
57. Yang J, Mani SA, Donaher JL, Ramaswamy S, Itzykson RA, Come C, et al. Twist, a master regulator of morphogenesis, plays an essential role in tumor metastasis. . Cell. 2004;117:927–39.
58. Valcourt U, Kowanetz M, Niimi H, Heldin CH, Moustakas A. TGF-beta and the Smad signaling pathway support transcriptomic reprogramming during epithelial-mesenchymal cell transition. Mol Biol Cell. 2005;16:1987-2002.
59. Yook JI, Li XY, Ota I, Fearon ER, Weiss SJ. Wnt-dependent regulation of the E-cadherin repressor Snail. . J Biol Chem. 2005;28:11740-8.
60. Timmerman LA, Grego-Bessa J, Raya A, Bertrán E, Pérez-Pomares JM, Díez J, et al. Notch promotes epithelial-mesenchymal transition during cardiac development and oncogenic transformation. Genes Dev. 2004;18:99-115.
61. Mani SA, Guo W, Liao MJ, Eaton EN, Ayyanan A, Zhou AY, et al. The epithelial-mesenchymal transition generates cells with properties of stem cells. Cell. 2008;133(4):704-15.
62. Nieto MA, Huang RY, Jackson RA, Thiery JP. EMT 2016 Cell. 2016;166(1):21–45.
63. Ilie M, Hofman V, Long-Mira E, Selva E, Vignaud J, Padovani B, et al. “Sentinel” Circulating Tumor Cells Allow Early Diagnosis of Lung Cancer in Patients with Chronic Obstructive Pulmonary Disease. PLoS ONE. 2014;9(10).
64. Coumans F, Dalum G, Beck M, Terstappen L. Filtration Parameters Influencing Circulating Tumor Cell Enrichment from Whole Blood. PLoS ONE 2013;8(4).
65. Riethdorf S, Fritsche H, Müller V, Rau T, Schindlbeck C, Rack B, et al. Detection of circulating tumor cells in peripheral blood of patients with metastatic breast cancer: a validation study of the CellSearch system. Clin Cancer Res. 2007;13(3):920-8.

66. Coumans F, Terstappen L. Detection and Characterization of Circulating Tumor Cells by the CellSearch Approach. Methods Mol Biol. 2015;1347:263-78.
67. Gorges TM, Tinhofer I, Drosch M, Röse L, Zollner TM, Krahn T, et al. Circulating tumour cells escape from EpCAM-based detection due to epithelial-to-mesenchymal transition. BMC Cancer. 2012;12.
68. Rao CG, Chianese D, Doyle GV, Miller MC, Russell T, Sanders RA, Jr., et al. Expression of epithelial cell adhesion molecule in carcinoma cells present in blood and primary and metastatic tumors. International journal of oncology. 2005;27(1):49-57.
69. Gabriel MT, Calleja LR, Chalopin A, Ory B, D. H. Circulating Tumor Cells: A Review of Non–EpCAM-Based Approaches for Cell Enrichment and Isolation. Clinical Chemistry. 2016;62(4):571-81.
70. Joosse SA, T.M.; G, Pantel K. Biology, detection, and clinical implications of circulating tumor cells. EMBO Mol Med. 2015;7(1): 1–11.
71. Lin HK, Zheng S, Williams AJ, Balic M, Groshen S, Scher HI, et al. Portable filter-based microdevice for detection and characterization of circulating tumor cells. Clinical cancer research : an official journal of the American Association for Cancer Research. 2010;16(20):5011-8.
72. Hou JM, Greystoke A, Lancashire L, Cummings J, Ward T, Board R, et al. Evaluation of circulating tumor cells and serological cell death biomarkers in small cell lung cancer patients undergoing chemotherapy. Am J Pathol. 2009;175(2): 808–16.
73. Cristofanilli M, Budd GT, Ellis MJ, Stopeck A, Matera J, Miller MC, et al. Circulating tumor cells, disease progression, and survival in metastatic breast cancer. The New England journal of medicine. 2004;351(8):781-91.
74. De Luca F, Rotunno G, Salvianti F, Galardi1 F, Pestrin M, Gabellini S, et al. Mutational analysis of single circulating tumor cells by next generation sequencing in metastatic breast cancer. Oncotarget. 2015;7(18).
75. Shaffer DR, Leversha MA, Danila DC, Lin O, Gonzalez-Espinoza R, Gu B, et al. Circulating tumor cell analysis in patients with progressive castration-resistant prostate cancer. Clinical cancer research : an official journal of the American Association for Cancer Research. 2007;13(7):2023-9.
76. Rosell R, Dafni U, Felip E, Curioni-Fontecedro A, Gautschi O, Peters S, et al. Erlotinib and bevacizumab in patients with advanced non-small-cell lung cancer and activating EGFR mutations (BELIEF): an international, multicentre, single-arm, phase 2 trial. Lancet Respir Med. 2017;5(5):435–44.
77. Tan CS, Chob BC, Soo RA. Next-generation epidermal growth factor receptor tyrosine kinase inhibitors in epidermal growth factor receptor -mutant non-small cell lung cancer. Lung Cancer. 2016;93:59–68.
78. Deng J, Wang L, Chen H, Hao J, Ni J, Chang L, et al. Targeting epithelial-mesenchymal transition and cancer stem cells for chemoresistant ovarian cancer. Oncotarget. 2016;7(34):55771-88.
79. Shien K, Toyooka S, Ichimura K, Soh J, Furukawa M, Maki Y, et al. Prognostic impact of cancer stem cell-related markers in non-small cell lung cancer patients treated with induction chemoradiotherapy. Lung Cancer. 2012;77(1):162-7.
80. Mancini R, Giarnieri E, De Vitis C, Malanga D, Roscilli G, Noto A, et al. Spheres derived from lung adenocarcinoma pleural effusions: molecular characterization and tumor engraftment. PLoS ONE. 2011;6(7).
81. Tiran V, Stanzer S, Heitzer E, Meilinger M, Rossmann C, Lax S, et al. Genetic profiling of putative breast cancer stem cells from malignant pleural effusions. PLoS ONE. 2017;12(4).
82. Fabisiewicz A, Grzybowska E. CTC clusters in cancer progression and metastasis. Med Oncol. 2017;34(1).
83. Martin OA, Anderson RL, Narayan K, MacManus MP. Does the mobilization of circulating tumour cells during cancer therapy cause metastasis? Nat Rev Clin Oncol. 2017;14(1):32-44.

84. Tiran V, Lindenmann J, Brcic L, Heitzer E, Stanzer S, Ghaffari Tabrizi-Wizsy N, et al. Primary patient-derived lung adenocarcinoma cell culture challenges the association of cancer stem cells with epithelial-to-mesenchymal transition. Sci Rep. 2017.
85. Singh S, K.;, Hawkins C, Clarke I, D.;, Squire JA, Bayani J, Hide T, et al. Identification of human brain tumour initiating cells. Nature. 2004;432:396-401.
86. Bustin SA, Benes V, Garson JA, Hellemans J, Huggett J, Kubista M, et al. The MIQE guidelines: minimum information for publication of quantitative real-time PCR experiments. Clin Chem. 2009;55(4):611-22.
87. Hellemans J, Mortier G, Paepe AD, Speleman F, Vandesompele J. qBase relative quantification framework and software for management and automated analysis of real-time quantitative PCR data. Genome Biol. 2007;8(2).
88. Heitzer E, Ulz P, Belic J, Gutschi S, Quehenberger F, Fischereder K, et al. Tumor-associated copy number changes in the circulation of patients with prostate cancer identified through whole-genome sequencing. Genome Med. 2013;5(4).
89. Nims RW, Sykes G, Cottrill K, Ikonomi P, E. E. Short tandem repeat profiling: part of an overall strategy for reducing the frequency of cell misidentification. In Vitro Cell Dev Biol Anim. 2010;46(10):811–9.
90. Pastrana E, Silva-Vargas V, Doetsch F. Eyes Wide Open: A Critical Review of Sphere-Formation as an Assay For Stem Cells. Cell Stem Cell. 2011;8(5):486–98.
91. Morata-Tarifa C, Jiménez G, García MA, Entrena JM, Griñán-Lisón C, Aguilera M, et al. Low adherent cancer cell subpopulations are enriched in tumorigenic and metastatic epithelial-to-mesenchymal transition-induced cancer stem-like cells. 2016;6:18772.
92. Lombardo Y, de Giorgio A, Coombes CR, Stebbing J, L. C. Mammosphere Formation Assay from Human Breast Cancer Tissues and Cell Lines. J Vis Exp. 2015;97.
93. Horibata S, Vo TV, Subramanian V, Thompson PR, Coonrod SA. Utilization of the Soft Agar Colony Formation Assay to Identify Inhibitors of Tumorigenicity in Breast Cancer Cells. J Vis Exp. 2015;22(90).
94. Borowicz S, Van Scoyk M, Avasarala S, Karuppusamy Rathinam MK, Tauler J, Bikkavilli RK. The Soft Agar Colony Formation Assay. J Vis Exp. 2014(92).
95. von Sochaczewski C, Wenke K, Metzger R, Loveland J, Westgarth-Taylor C, Kluth D. Reversible small bowel obstruction in the chicken foetus. Afr J Paediatr Surg. 2015;12(1):12-7.
96. Watnick RS. The Role of the Tumor Microenvironment in Regulating Angiogenesis. Cold Spring Harb Perspect Med. 2012;2.
97. Shi AM, Tao ZQ, Li H, Wang YQ, Zhao J. Cancer stem cells targeting agents – a review. Eur Rev Med Pharmacol Sci. 2015;19(21):4064-7.
98. Liu M, Ma S, Liu M, Hou Y, Liang B, Su X, et al. Synergistic killing of lung cancer cells by cisplatin and radiation via autophagy and apoptosis. Oncol Lett. 2014;7(6):1903-10.
99. Phi JH, Choi S, Kim S, Wang K, Lee JY, Kim DG. Overcoming Chemoresistance of Pediatric Ependymoma by Inhibition of STAT3 Signaling. Transl Oncol. 2015;8(5):376–86.
100. Del Bufalo D, Desideri M, De Luca T, Di Martile M, Gabellini C, Monica V, et al. Histone deacetylase inhibition synergistically enhances pemetrexed cytotoxicity through induction of apoptosis and autophagy in non-small cell lung cancer. Mol Cancer. 2014;13.
101. Zhu X, Du X, Deng X, Yi H, Cui S, Liu W, et al. C6 ceramide sensitizes pemetrexed-induced apoptosis and cytotoxicity in osteosarcoma cells. Biochem Biophys Res Commun. 2014;452(1):72-8.
102. Resham K, Patel P, Thummuri D, Guntuku L, Shah V, Bambal R, et al. Preclinical drug metabolism and pharmacokinetics of salinomycin, a potential candidate for targeting human cancer stem cells. Chem Biol Interact. 2015;240: 146–52.
103. Zabaglo L, Ormerod MG, Parton M, Ring A, Smith IE, Dowsett M. Cell filtration-laser scanning cytometry for the characterisation of circulating breast cancer cells. Cytom A 2003;55(2):102-8.

104. Zheng S, Lin H, Liu JQ, Balic M, Datar R, Cote RJ, et al. Membrane microfilter device for selective capture, electrolysis and genomic analysis of human circulating tumor cells. J Chromatogr A. 2007;1162(2):154-61.
105. Lu TP, Lai LC, Tsai MH, Chen PC, Hsu CP, Lee JM, et al. Integrated Analyses of Copy Number Variations and Gene Expression in Lung Adenocarcinoma. PLoS ONE. 2011;6(9).
106. Varella-Garcia M. Chromosomal and genomic changes in lung cancer. Cell Adh Migr. 2010;4(1):100–6.
107. Research Network TCGA. Comprehensive genomic characterization of squamous cell lung cancers. Nature. 2012;489(7417):519-25.
108. Parson W, Kirchebner R, Mühlmann R, Renner K, Kofler A, Schmidt S, et al. Cancer cell line identification by short tandem repeat profiling: power and limitations FASEB J. 2005;19(3):434-6.
109. Hermann PC, Huber SL, Herrler T, Aicher A, Ellwart JW, Guba M, et al. Distinct populations of cancer stem cells determine tumor growth and metastatic activity in human pancreatic cancer. Cell stem cell. 2007;1(3):313-23.
110. Leon G, MacDonagh L, Finn SP, Cuffe S, Barr MP. Cancer stem cells in drug resistant lung cancer: Targeting cell surface markers and signaling pathways. Pharmacology & Therapeutics. 2016;158:71–90.
111. Gupta PB, Onder TT, Jiang G, Tao K, Kuperwasser C, Weinberg RA, et al. Identification of selective inhibitors of cancer stem cells by high-throughput screening. Cell. 2009;138(4):645-59.
112. Balic M, Schwarzenbacher D, Stanzer S, Heitzer E, Auer M, Geigl JB, et al. Genetic and epigenetic analysis of putative breast cancer stem cell models. BMC Cancer. 2013;13(358).
113. Gazdar AF, Girard L, Lockwood WW, Lam WL, Minna JD. Lung Cancer Cell Lines as Tools for Biomedical Discovery and Research. J Natl Cancer Inst. 2010;102(17):1310–21.
114. Lee J, Kotliarova S, Kotliarov Y, Li A, Su Q, Donin NM, et al. Tumor stem cells derived from glioblastomas cultured in bFGF and EGF more closely mirror the phenotype and genotype of primary tumors than do serum-cultured cell lines. Cancer Cell. 2006;9:391-403.
115. Gillet JP, Varma S, Gottesman MM. The Clinical Relevance of Cancer Cell Lines J Natl Cancer Inst. 2013;105(7):452-8.
116. Zheng C, Sun Y, Ye X, Chen H, Ji H. Establishment and characterization of primary lung cancer cell lines from Chinese population. Acta Pharmacol Sin. 2011;32(3).
117. Wang P, Gao Q, Suo Z, Munthe E, Solberg S, Ma L, et al. Identification and Characterization of Cells with Cancer Stem Cell Properties in Human Primary Lung Cancer Cell Lines. PLoS ONE. 2013;8(3).
118. Qureshi-Baig K, Ullmann P, Rodriguez F, Frasquilho S, Nazarov PV, Haan S, et al. What Do We Learn from Spheroid Culture Systems? Insights from Tumorspheres Derived from Primary Colon Cancer Tissue. PLoS ONE. 2016.
119. Lee SH, Hong JH, Park HK, Park JS, Kim BK, Lee JY, et al. Colorectal cancer-derived tumor spheroids retain the characteristics of original tumors. Cancer Lett. 2015;367(1):34-42.
120. Ombrato L, Malanchi I. The EMT Universe: Space Between Cancer Cell Dissemination and Metastasis Initiation. Crit Rev Oncog. 2014;19(5):349-61.
121. Fischer KR, Durrans A, Lee S, Sheng J, Li F, Wong STC, et al. Epithelial-to-mesenchymal transition is not required for lung metastasis but contributes to chemoresistance. Nature. 2015;527:472–6.
122. Xiao X, Zhou X, Ming H, Zhang J, Huang G, Zhang Z, et al. Chick Chorioallantoic Membrane Assay: A 3D Animal Model for Study of Human Nasopharyngeal Carcinoma. PLoS ONE. 2015;10(6).
123. Lopez-Ayllon BD, Moncho-Amor V, Abarrategi A, Ibañez de Cáceres i, Castro-Carpeño J, Belda-Iniesta C, et al. Cancer stem cells and cisplatin-resistant cells isolated from non-small-lung cancer cell lines constitute related cell populations. Cancer Med. 2014;3(5):1099-111.
124. Arafat K, Iratni R, Takahashi T, Parekh K, Al Dhaheri Y, Adrian TE, et al. Inhibitory Effects of Salinomycin on Cell Survival, Colony Growth, Migration, and Invasion of Human Non-Small Cell Lung Cancer A549 and LNM35: Involvement of NAG-1. PLoS ONE. 2013;8(6).

125. Larzabal L, El-Nikhely N, Redrado M, Seeger W, Savai R, Calvo A. Differential Effects of Drugs Targeting Cancer Stem Cell (CSC) and Non-CSC Populations on Lung Primary Tumors and Metastasis. PLoS ONE. 2013;8(11).
126. Kim KY, Yu SN, Lee SY, Chun SS, Choi YL, Park YM, et al. Salinomycin-induced apoptosis of human prostate cancer cells due to accumulated reactive oxygen species and mitochondrial membrane depolarization. Biochem Biophys Res Commun. 2011;413(1):80-6.
127. Kim WK, Kim JH, Yoon K, Kim S, Ro J, Kang HS, et al. Salinomycin, a p-glycoprotein inhibitor, sensitizes radiation-treated cancer cells by increasing DNA damage and inducing G2 arrest. Invest New Drugs 2012;30(4):1311-8.
128. Naujokat C, Steinhart R. Salinomycin as a Drug for Targeting Human Cancer Stem Cells. J Biomed Biotechnol 2012.
129. Tomasini T, Barlesi F, Mascaux C, Greillier L. Pemetrexed for advanced stage nonsquamous non-small cell lung cancer: latest evidence about its extended use and outcomes. Ther Adv Med Oncol. 2016;8(3):198-208.
130. Miller MC, Doyle GV, Terstappen LW. Significance of Circulating Tumor Cells Detected by the CellSearch System in Patients with Metastatic Breast Colorectal and Prostate Cancer. J Oncol. 2010.
131. Krebs MG, Hou JM, Sloane R, Lancashire L, Priest L, Nonaka D, et al. Analysis of circulating tumor cells in patients with non-small cell lung cancer using epithelial marker-dependent and -independent approaches. J Thorac Oncol. 2012;7(2).
132. Mascalchi M, Falchini M, Maddau C, Salvianti F, Nistri M, Bertelli E, et al. Prevalence and number of circulating tumour cells and microemboli at diagnosis of advanced NSCLC. J Cancer Res Clin Oncol 2016;142(1):195-200.
133. Dandachi N, Tiran V, Lindenmann J, Brcic L, Fink-Neuboeck N, Kashofer K, et al. Frequency and clinical impact of preoperative circulating tumor cells in resectable non-metastatic lung adenocarcinomas. Submitted for publication. 2017.
134. Chen X, Wang X, He H, Liu Z, Hu J, Li W. Combination of Circulating Tumor Cells with Serum Carcinoembryonic Antigen Enhances Clinical Prediction of Non-Small Cell Lung Cancer. PLoS ONE. 2015;10(5).
135. Wan JW, Gao MZ, Hu RJ, Huang HY, Wei YY, Han ZJ, et al. A preliminary study on the relationship between circulating tumor cells count and clinical features in patients with non-small cell lung cancer. Ann Transl Med. 2015;3(22).
136. Pesch B, Kendzia B, Gustavsson P, Jöckel K, Johnen G, Pohlabeln H, et al. Cigarette smoking and lung cancer--relative risk estimates for the major histological types from a pooled analysis of case-control studies. Int J Cancer. 2012;131(5):1210-9.
137. Peacock CD, Watkins DN. Cancer Stem Cells and the Ontogeny of Lung Cancer. J Clin Oncol. 2008;26(17):2883-9.
138. Hanssen A, Loges S, Pantel K, Wikman H. Detection of circulating tumor cells in non-small cell lung cancer. Front Oncol. 2015;5.
139. Voskoglou-Nomikos T, Pater JL, Seymour L. Clinical Predictive Value of the in Vitro Cell Line, Human Xenograft, and Mouse Allograft Preclinical Cancer Models. Clinical cancer research : an official journal of the American Association for Cancer Research. 2003;9:4227-39.

8. Supplements

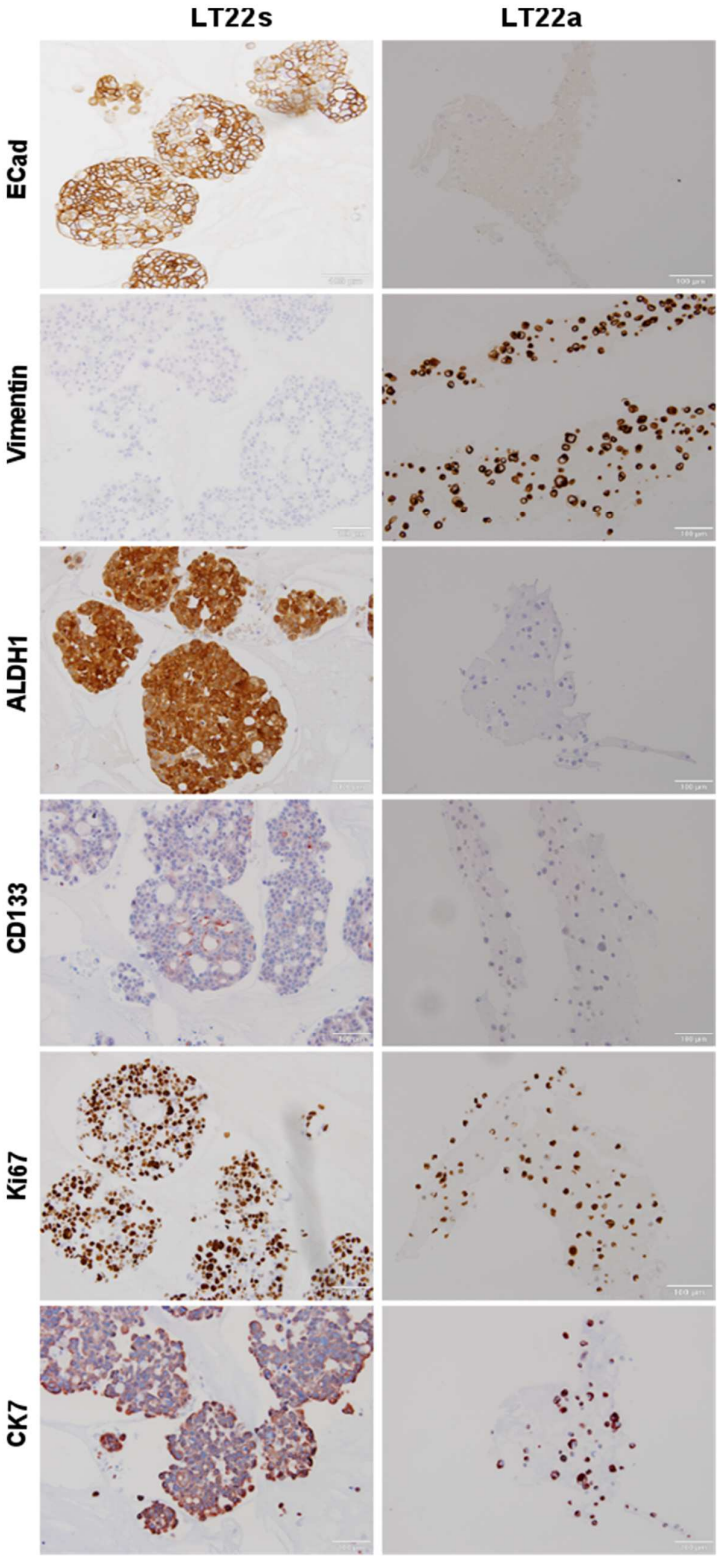

Suppl. figure 1. Representative pictures of of LT22s and LT22a cells in FFPE. Immunohistochemical staining of CSC and EMT markers including ECad, Vimentin, ALDH1, CD133, Ki67 and CK7. Red/brown color indicated positive expression. Measuring bar 100 µm.

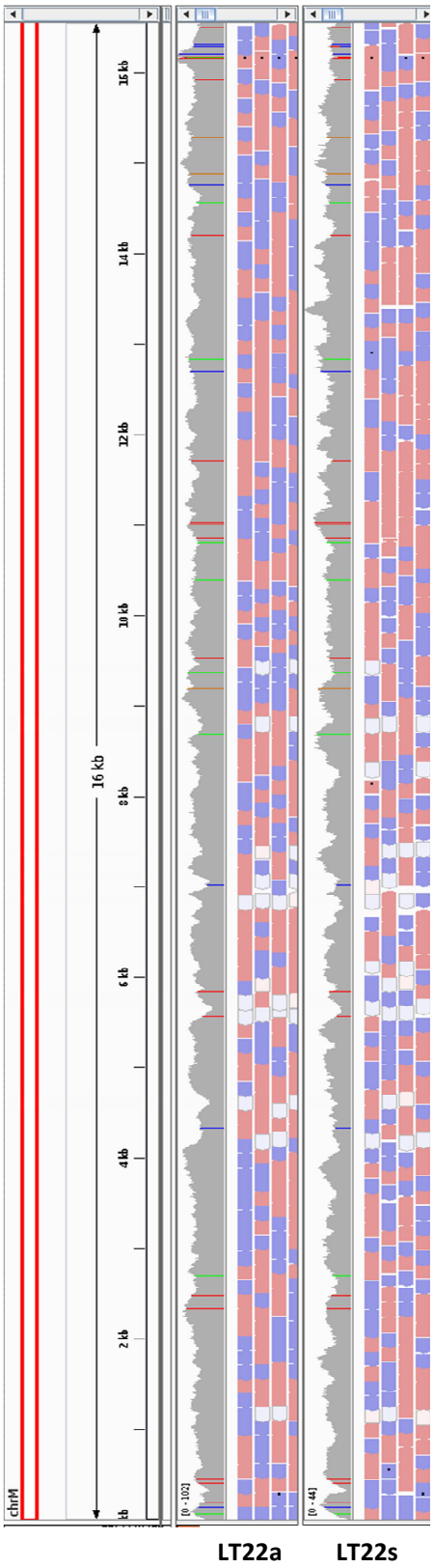

Suppl. figure 2. mtDNA Profile of LT22: Depicted is the mitochondrial chromosome of LT22a (left panel) and LT22s (right panel). The focus lies on the thin colored lines, which indicate mutations of the sequence. Mutations in the mtDNA occur in a constant rate and can clearly asses the genetic relation.

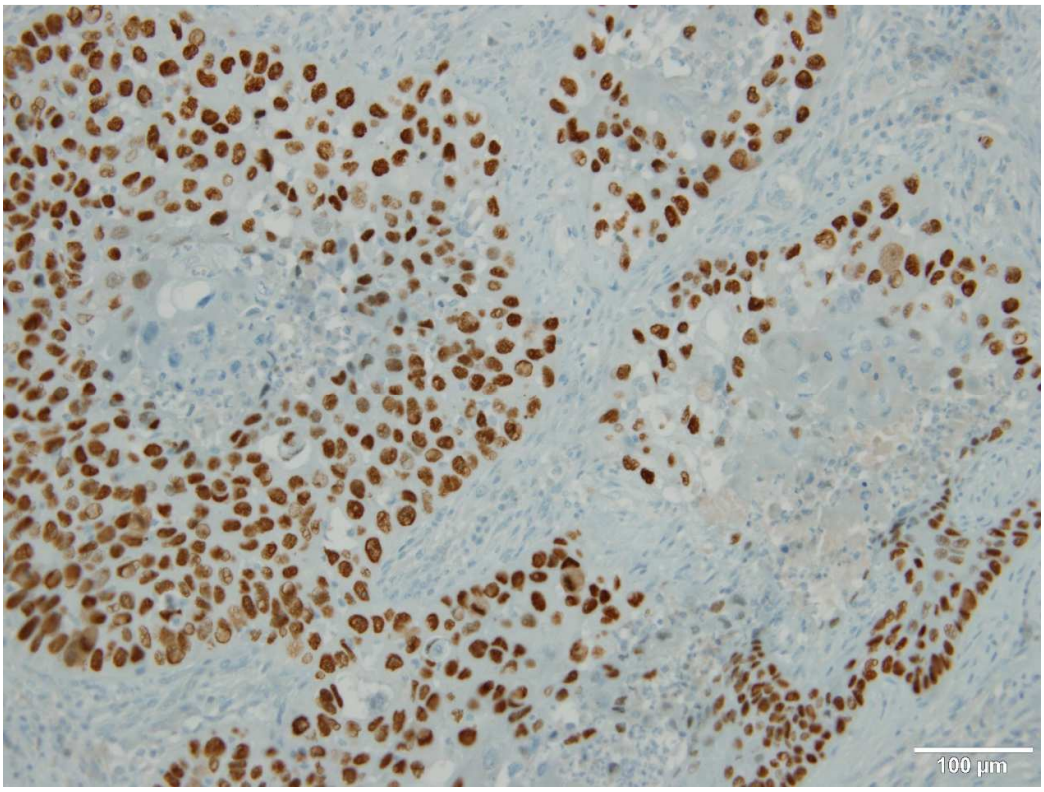

Suppl. figure 3. Immunohistochemical staining of LT67 primary tumor with p40 antibody. Brown color indicates expression of p40. Measuring bar 100 µm.